UNIVERSITY OF CALIFORNIA,
IRVINE

Neurodegeneration and altered brain network organization in preclinical and clinical Alzheimer's disease in people with Down syndrome

DISSERTATION

submitted in partial satisfaction of the requirements
for the degree of

DOCTOR OF PHILOSOPHY

in Biological Sciences

by

Natalie Danielle DiProspero

Dissertation Committee:
Professor Michael A. Yassa, Chair
Associate Professor Jorge A. Busciglio
Professor Mark E. Mapstone

2023

DEDICATION

To Noël Duvall and Michael DiProspero.

To Robert Duvall, Marie Duvall, and Vincenza DiProspero.

To Kevin Rothi.

TABLE OF CONTENTS

	Page
LIST OF FIGURES	v
LIST OF TABLES	vii
LIST OF KEY ABBREVIATIONS	viii
ACKNOWLEDGMENTS	ix
VITA	xi
ABSTRACT OF THE DISSERTATION	xvi
CHAPTER 1: BACKGROUND AND SIGNIFICANCE	1
1.1. BACKGROUND AND PUBLIC HEALTH RELEVANCE OF ALZHEIMER'S DISEASE	1
1.1.1. CLINICAL DESCRIPTION OF ALZHEIMER'S DISEASE	1
1.1.2. ALZHEIMER'S DISEASE PATHOLOGY	2
1.1.3. NEURODEGENERATION AND FUNCTIONAL BRAIN NETWORKS	3
1.1.4. GENETICS OF ALZHEIMER'S DISEASE	7
1.2. BACKGROUND AND PUBLIC HEALTH RELEVANCE OF DOWN SYNDROME	7
1.2.1. CLINICAL DESCRIPTION OF DOWN SYNDROME	7
1.2.2. DEVELOPMENTAL NEUROBIOLOGY OF DOWN SYNDROME	8
1.3. NEUROBIOLOGY OF ALZHEIMER'S DISEASE IN DOWN SYNDROME	9
1.3.1. PATHOLOGY AND SPATIOTEMPORAL SPREAD	9
1.3.2. STRUCTURAL NEUROIMAGING OF NEURODEGENERATION	11
1.3.3. FUNCTIONAL NEOCORTICAL NETWORKS	11
1.3.3.1. DEFAULT MODE NETWORK	11
1.3.3.2. MEDIAL TEMPORAL NETWORK	12
1.4. CURRENT STATE OF KNOWLEDGE AND OPEN QUESTIONS	12
CHAPTER 2: NEUROFILAMENT LIGHT CHAIN CONCENTRATION MEDIATES THE ASSOCIATION BETWEEN REGIONAL MEDIAL TEMPORAL LOBE STRUCTURE AND MEMORY IN PEOPLE WITH DOWN SYNDROME	14
2.1. INTRODUCTION	14
2.2. MATERIALS AND METHODS	15
2.3. RESULTS	19
2.4. DISCUSSION	26
CHAPTER 3: SELECTIVE IMPAIRMENT OF LONG-RANGE DEFAULT MODE NETWORK FUNCTIONAL CONNECTIVITY PRIOR TO CLINICAL ALZHEIMER'S DISEASE IN PEOPLE WITH DOWN SYNDROME	29

3.1. INTRODUCTION 29
3.2. MATERIALS AND METHODS 29
3.3. RESULTS 35
3.4. DISCUSSION 42

CHAPTER 4: MEDIAL TEMPORAL LOBE FUNCTIONAL CONNECTIVITY CHANGES DURING CLINICAL PROGRESSION OF AD IN PEOPLE WITH DS 44
4.1. INTRODUCTION 44
4.2. MATERIALS AND METHODS 44
4.3. RESULTS 49
4.4. DISCUSSION 53

CHAPTER 5: SYNTHESIS AND FUTURE DIRECTIONS 54
5.1. GENERAL SUMMARY 54
5.2. FUTURE DIRECTIONS 58

REFERENCES 61

APPENDIX A 90

APPENDIX B 101

LIST OF FIGURES

Page

CHAPTER 1

Figure 1.1. Hypothesized model of Alzheimer's disease pathological cascade 3

Figure 1.2. Default mode network intrinsic connectivity 5

Figure 1.3. Medial temporal lobe segmentation 6

Figure 1.4. Hypothesized inverse U-shaped curve of medial temporal lobe hyperexcitability during Alzheimer's disease progression 6

Figure 1.5. Cumulative frequency of Alzheimer's disease pathology in Down syndrome 10

CHAPTER 2

Figure 2.1. Regions of interest and MCI/AD diagnosis group differences 21

Figure 2.2. Plasma NfL concentration was negatively associated with hippocampus volume and left alEC thickness 23

Figure 2.3. Hippocampus volume and alEC thickness were positively associated with Memory 24

Figure 2.4. Plasma NfL concentration was negatively associated with memory 25

Figure 2.5. Plasma NfL concentration mediated the relationship between left alEC thickness and FRS 26

CHAPTER 3

Figure 3.1. Differences in DMN functional connectivity between the UCI transitioned and non-transitioned groups 38

Figure 3.2. Reduced long-range functional connectivity was associated with greater cognitive decline 39

Figure 3.3. Reduced ACC-IPC functional connectivity was associated with greater Aβ accumulation in IPC 40

Figure 3.4. Distribution of mean functional connectivity values 40

Figure 3.5. Decision tree classifier results for long-range DMN functional connectivity 42

CHAPTER 4

Figure 4.1. Greater MTL functional connectivity in MCI-DS relative to CS individuals with DS 51

Figure 4.2. Greater right pmEC-right PRC functional connectivity is associated with lower mCRT total recall score 52

Figure 4.3. Trending positive association between right pmEC-right PRC and hippocampus tau 52

LIST OF TABLES

Page

CHAPTER 2

Table 2.1. Participant demographics and neuropsychological assessments for individuals with both MRI and mCRT data 20

CHAPTER 3

Table 3.1. UCI participant demographics and neuropsychological test scores 36

Table 3.2. UCI and UKY participant demographics and neuropsychological test scores 37

Table 3.3. Decision tree classifier results 41

CHAPTER 4

Table 4.1. Participant demographics 50

LIST OF KEY ABBREVIATIONS

Aβ: β-amyloid

ABC-DS: Alzheimer Biomarkers Consortium — Down Syndrome

ACC: anterior cingulate cortex

AD: Alzheimer's disease

alEC: anterolateral entorhinal cortex

CS: cognitively stable

DMN: default mode network

DS: Down syndrome

EC: entorhinal cortex

ICV: intracranial volume

ICC: isthmus of the cingulate cortex, also known as the retrosplenial cortex

IPC: inferior parietal cortex

MCI-DS: mild cognitive impairment in Down syndrome

mCRT: modified Cued Recall Test

MTL: medial temporal lobe

NfL: neurofilament light chain protein

PCC: posterior cingulate cortex

pmEC: posteromedial entorhinal cortex

PRC: perirhinal cortex

ROI: region of interest

rsfMRI: resting state functional magnetic resonance imaging

ACKNOWLEDGMENTS

I thank my mentor and advisor, Dr. Michael Yassa, for seeing my potential and never giving up on me. He challenged me and taught me how to build resilience to make me a better scientist. He understood how to support me as a whole person, not just as a researcher. I will be forever grateful for his contributions to my professional growth and the countless opportunities he made possible for me.

I thank the past and present members of my committee, Drs. Jorge Busciglio, Mark Mapstone, Elizabeth Head, and Craig Stark, for giving me valuable feedback and sharing their expertise. I am humbled to stand on the shoulders of such giants in the field.

I thank the past and present members of the Yassa lab for giving me a home for the past six years. It's rare to find a community of scientifically brilliant people who are this deeply invested in the personal well-being of every person in the lab. I thank Zach Reagh for taking me under his wing more than ten years ago. I thank Liz Murray and Liv McMillan for being the glue that holds the lab together. I thank the former staff, including Joren Adams, Anna Smith, Myra Larson, Blake Miranda, Nikki Hatamian, Lea Stith, and Stephanie Doering, for their dedication to research and ability to weave humor into all situations. I thank the senior graduate students, postdocs, and researchers, including Maria Montchal, Rebecca Stevenson, Jessie Yaros, Freddie Márquez, Logan Harriger, Sandra Gattas, Steve Granger, Sarah Kark, Soyun Kim, Jenna Adams, Caro Chwiesko, and Luis Colon-Perez, for their mentorship and guidance. I thank Miranda Chappel-Farley, Laura Ezama, Bianca Leonard, Batool Rizvi, Destiny Berisha, Nazek Queder, Dana Parker, Abbey Houchin, Gimarie Irizarry Martínez, and Ray Villareal for their friendship and advice. I thank Mithra Sathishkumar, Lisa Taylor, and Derek Taylor for their technical expertise and contributions to my work. I thank all the staff and research assistants, including Joshua Nguyen, who made this research possible.

I thank Manuella Yassa for embodying leadership and vision. I thank the Center for the Neurobiology of Learning and Memory Ambassadors for expanding my mind and my heart. I thank my fellow graduate students in the Interdisciplinary Neuroscience Program cohort and the Department of Neurobiology and Behavior, in particular Morgan Coburn, Julian Quintanilla, Miranda Chappel-Farley, Jan Frankowski, Scott Kilianski, Jessica Lingad, Hamsi Radhakrishnan, and Elena Dominguez for giving me unwavering friendship and much-needed distraction.

I thank my friends, including Kimberly Culp, Alyssa Mendoza, and Vidra Maharaj, for surrounding me with love and support when I needed it most. I thank my family for being a perpetual source of encouragement, humor, and perspective. I thank my parents, Noël Duvall and Michael DiProspero, for enriching my life with opportunities to learn and selflessly letting their only child go where her heart led her. I thank my grandparents, Vincenza DiProspero, Marie Duvall, and Robert Duvall, for dreaming big and making my college education possible. I thank my aunts, uncles, and cousins, as well as Gretchen Gerber, Diane Rothi, Megan Rothi, and Robert Lovdahl, for being there for me as though I was their own child or sibling. Finally, I

thank my partner, Kevin Rothi, for believing in me, and my cats, Sylvia, Meepers, and Bimbles, for comforting me during the hard times.

The work described in this dissertation was supported by NIA grants U01 AG051412 (PIs: N. Schupf, I. Lott, W. Silverman) and T32 AG000096 (PIs: C. Cotman, A. Tenner), and NICHD grants R01 HD065160 (PI: I. Lott) and R01 HD064993 (PIs: E. Head, F. Schmitt). I thank the friends of the CNLM for supporting my research through individual awards.

Chapter 2 of this dissertation is a reprint of the material as it appears in Alzheimer's and Dementia: Disease Monitoring and Diagnosis (DiProspero ND, Sathishkumar M, Janecek J, Smith A, McMillan L, Peterson M, Tustison N, Keator DB, Doran E, Hom C, Nguyen D, Andrews H, Krinsky-McHale S, Brickman AM, Rosas HD, Lai F, Head E, Mapstone M, Silverman W, Lott IT, O'Bryant S, Yassa MA. Anterolateral entorhinal cortical thickness, hippocampus volume, and neurofilament light chain as biomarkers for Alzheimer's disease in Down syndrome. Alzheimers Dement (Amst). Forthcoming 2023.), used with permission from John Wiley & Sons Inc. The co-authors listed in this publication are Mithra Sathishkumar, John Janecek, Anna Smith, Liv McMillan, Dr. Melissa Peterson, Dr. Nick Tustison, Dr. David B. Keator, Eric Doran, Dr. Christy Hom, Dana Nguyen, Dr. Howard Andrews, Dr. Sharon Krinsky-McHale, Dr. Adam M. Brickman, Dr. Diana Rosas, Dr. Florence Lai, Dr. Elizabeth Head, Dr. Mark Mapstone, Dr. Wayne Silverman, Dr. Ira T. Lott, Dr. Sid O'Bryant, and Dr. Michael A. Yassa.

Chapter 3 of this dissertation is a reprint of the material as it appears in the Journal of Alzheimer's Disease (DiProspero ND, Keator DB, Phelan M, van Erp TGM, Doran E, Powell DK, Van Pelt KL, Schmitt FA, Head E, Lott IT, Yassa MA. Selective impairment of long-range default mode network functional connectivity as a biomarker for preclinical Alzheimer's disease in people with Down syndrome. J Alzheimers Dis. 2022;85(1):153-65. https://doi.org/10.3233/JAD-210572.), used with permission from IOS Press, Inc. The co-authors listed in this publication are Dr. David B. Keator, Dr. Michael Phelan, Dr. Theo G. M. van Erp, Eric Doran, Dr. David K. Powell, Dr. Kathryn Van Pelt, Dr. Frederick A. Schmitt, Dr. Elizabeth Head, Dr. Ira T. Lott, and Dr. Michael A. Yassa.

VITA

Natalie Danielle DiProspero

EDUCATION

Ph.D., Biological Sciences — 2020 - 2023
University of California, Irvine; Irvine, CA

M.S., Biological Sciences — 2017 - 2020
University of California, Irvine; Irvine, CA

B.A., Philosophy-Neuroscience-Psychology and French — 2011 - 2015
Washington University in St. Louis, St. Louis, MO

Semester abroad, Psychology and Philosophy — 2013
University of Edinburgh; Edinburgh, UK

RESEARCH

Graduate Research Fellow — 2018 - 2023
Translational Neurobiology Laboratory
University of California, Irvine; Irvine, CA
Principal Investigator: Michael A. Yassa, PhD

Technical Intramural Research Training Award Fellow — 2015 - 2017
Laboratory of Behavioral Neuroscience
National Institute on Aging; Baltimore, MD
Principal Investigator: Susan M. Resnick, PhD

Research Assistant — 2014 - 2015
Research Laboratory for Neural Basis of Cognitive Aging
Washington University in St. Louis; St. Louis, MO
Principal Investigator: Denise Head, PhD

Research Assistant — 2013
Neuroscience of Memory in Aging and Dementia Laboratory
Johns Hopkins University, Baltimore, MD
Principal Investigator: Michael A. Yassa, PhD

Research Assistant — 2012 - 2013
Memory and Complex Learning Laboratory
Washington University in St. Louis; St. Louis, MO
Principal Investigator: Mark A. McDaniel, PhD

TEACHING

Teaching Assistant 2020
Course Title: “Human Neuropsychology”
University of California, Irvine; Irvine, CA
Instructor: Michael A. Yassa, PhD

Teaching Assistant 2019
Course Title: “Neurobiology and Behavior Laboratory”
University of California, Irvine; Irvine, CA
Instructor: Audrey C. Lew, PhD

Teaching Assistant 2019
Course Title: “Advanced Neurobiology II”
University of California, Irvine; Irvine, CA
Instructor: Georg F. Striedter, PhD

SCIENCE COMMUNICATION

Courses/Workshops

Activate to Captivate Workshop with Bri McWhorter 2022

Science Policy and Advocacy for STEM Scientists Course 2020

Communication Skills for Academics Certificate Program with Sandra Tsing Loh 2020

Experience

Writer 2021 - 2022
The Loh Down on Science Podcast
National Public Radio

Program Co-Chair 2019 - 2021
K-12 Outreach Chair 2018 - 2019
Member 2017 - 2022
Ambassador Program
Center for the Neurobiology of Learning and Memory
University of California, Irvine; Irvine, CA

K-12 Outreach Mentor 2011 - 2013
Synapse Neuroscience Interest Group
Washington University in St. Louis; St. Louis, MO

AWARDS AND HONORS

Trainee Professional Development Award 2021
Society for Neuroscience

Director's Excellence Award 2021
Center for the Neurobiology of Learning and Memory
University of California, Irvine; Irvine, CA

NIA T32 Training Grant in the Neurobiology of Aging 2019 - 2021
Alzheimer's Disease ($32,000/year stipend)
Institute for Memory Impairments and Neurological Disorders
University of California, Irvine; Irvine, CA

Jared M. Roberts Memorial Graduate Student Award 2019
Center for the Neurobiology of Learning and Memory
University of California, Irvine; Irvine, CA

Outstanding Poster Award, Postbac Poster Day 2017
National Institutes of Health; Bethesda, MD

NIA Scientific Director's Award, NIA Scientific Retreat 2017
National Institute on Aging; Baltimore, MD

Outstanding Poster Award, Postbac Poster Day 2016
National Institutes of Health; Bethesda, MD

College Honors 2015
Washington University in St. Louis; St. Louis, MO

Summer Undergraduate Research Award 2012
Washington University in St. Louis; St. Louis, MO

Dean's List 2011 - 2014
Washington University in St. Louis; St. Louis, MO

PROFESSIONAL MEMBERSHIPS AND ACTIVITIES

Memberships

Alzheimer's Association ISTAART 2019 - 2023

Society for Neuroscience 2018 - 2022

Initiatives

Member 2021
Working group on transforming curricular culture and pedagogical structures
End Racism Initiative
University of California, Irvine; Irvine, CA

Mentorship

Joshua Nguyen 2022 - 2023
Undergraduate research assistant in the Yassa Lab
University of California, Irvine; Irvine, CA

PEER-REVIEWED PUBLICATIONS

DiProspero ND, Sathishkumar M, Janecek J, Smith A, McMillan L, Peterson M, Tustison N, Keator DB, Doran E, Hom C, Nguyen D, Andrews H, Krinsky-McHale S, Brickman AM, Rosas HD, Lai F, Head E, Mapstone M, Silverman W, Lott IT, O'Bryant S, Yassa MA. Anterolateral entorhinal cortical thickness, hippocampus volume, and neurofilament light chain as biomarkers for Alzheimer's disease in Down syndrome. Alzheimers Dement (Amst). Forthcoming 2023.

DiProspero ND, Keator DB, Phelan M, van Erp TGM, Doran E, Powell DK, Van Pelt KL, Schmitt FA, Head E, Lott IT, Yassa MA. Selective impairment of long-range default mode network functional connectivity as a biomarker for preclinical Alzheimer's disease in people with Down syndrome. J Alzheimers Dis. 2022;85(1):153-65. https://doi.org/10.3233/JAD-210572.

DiProspero ND, Kim S, Yassa, M. Magnetic resonance imaging biomarkers for cognitive decline in Down syndrome. In: Head E, Lott I, editors. The neurobiology of aging and Alzheimer disease inDown syndrome. 1st ed. Cambridge (MA): Elsevier Academic Press; 2021. p. 149-172.

Reagh ZM, Roberts JM, Ly M, DiProspero N, Murray E, Yassa MA. Spatial discrimination deficits as a function of mnemonic interference in aged adults with and without memory impairment. Hippocampus. 2014;24(3):303-14. https://doi.org/10.1002/hipo.22224.

INVITED TALKS

DiProspero ND, Queder N, Taylor L, Sathishkumar M, McMillan L, Keator DB, Doran E, Hom C, Nguyen D, Andrews H, Krinsky-McHale S, Head E, Mapstone M, Brickman AM, Rosas HD, Lai F, Silverman W, Schupf N, Lott IT, Yassa MA. Medial temporal lobe functional connectivity, episodic memory, and tau accumulation in individuals with Down syndrome. Symposium presented at: International Conference on Learning and Memory; 2023 Apr 26-30; Huntington Beach, CA.

DiProspero ND, Sathishkumar M, McMillan L, Keator DB, Doran E, Hom C, Nguyen D, Rosas HD, Lai F, Brickman AM, Schupf N, Silverman W, Lott IT, Yassa MA. Functional connectivity in medial temporal lobe and default mode network changes with Alzheimer's disease progression in individuals with Down syndrome. Talk presented at: Trisomy 21 Research Society International Conference; 2022 Jun 9-12; Long Beach, CA.

DiProspero ND, Doran E, Lott IT, Yassa MA. Intrinsic brain network functional connectivity in default mode network during progression of Alzheimer's disease in Down syndrome. Talk presented at: Trisomy 21 Research Society Virtual Conference; 2021 Jun 8-10.

DiProspero ND, Keator DB, van Erp TGM, Doran E, Lott IT, Yassa MA. Lower long-range default mode network connectivity predicts conversion to Alzheimer's disease in older individuals with Down syndrome. Talk presented at: 10th Annual REMIND Emerging Scientists Symposium; 2019 Feb 11; Irvine, CA.

SELECTED POSTER PRESENTATIONS

DiProspero ND, Lingad JN, Chappel-Farley MG, Henningfield CM, Yassa MO. Building a sustainable model of neuroscience education and community outreach. Poster presented at: Annual Meeting of the Society for Neuroscience; 2022 Nov 12-16; San Diego, CA.

DiProspero ND, Sathishkumar M, McMillan L, Keator DB, Doran E, Hom C, Nguyen D, Rosas HD, Lai F, Brickman AM, Schupf N, Silverman W, Lott IT, Yassa MA. Default mode network and medial temporal lobe functional connectivity changes with Alzheimer's disease severity and cognitive impairment in individuals with Down syndrome. Poster presented at: Alzheimer's Association International Conference; 2022 Jul 31 - Aug 4; San Diego, CA.

DiProspero ND, Keator DB, Phelan M, van Erp TGM, Doran E, Lott IT, Yassa MA. Static and dynamic intrinsic brain network functional connectivity during progression of Alzheimer's disease in Down syndrome. Poster presented at: 12th Annual REMIND Emerging Scientists Symposium; 2021 Mar 18; Irvine, CA.

DiProspero ND, Sathishkumar MT, Keator DB, van Erp TGM, McMillan L, Smith AP, Larson MS, Doran E, Lott IT, Yassa MA. Functional connectivity in a Down syndrome model of preclinical Alzheimer's disease. Poster presented at: Annual Meeting of the Society for Neuroscience; 2018 Nov 3-7; San Diego, CA.

DiProspero ND, Beason-Held L, An Y, Shafer A, Gomez G, Pacheco J, Resnick SM. Metabolic syndrome and cortical thinning in older adults. Poster presented at: NIA Scientific Retreat; 2017 Mar 2-3; Baltimore, MD; and NIH Postbac Poster Day; 2017 May 4; Bethesda, MD.

DiProspero ND, Pacheco J, An Y, Kitner-Triolo M, Resnick SM. Cortical thinning: Associations with age, sex, and cognitive status. Poster presented at: NIH Postbac Poster Day; 2016 Apr 20; Bethesda, MD.

DiProspero ND, Meyer A, McDaniel M. Keeping our brains in shape: The exploration of the relationship between aerobic exercise, cognitive training, and cognitive decline. Poster presented at: Washington University Undergraduate Research Symposium; 2012 Oct 27; St. Louis, MO.

ABSTRACT OF THE DISSERTATION

Neurodegeneration and altered brain network organization in preclinical and clinical Alzheimer's disease in people with Down syndrome

By

Natalie Danielle DiProspero

Doctor of Philosophy in Biological Sciences

University of California, Irvine, 2023

Professor Michael A. Yassa, Chair

Virtually all people with Down syndrome (DS) will develop Alzheimer's disease (AD). Most will also develop dementia, which is characterized by memory loss and functional impairment. The presence of a third copy of chromosome 21 appears to cause accelerated accumulation of the two hallmark pathologies of AD: β-amyloid (Aβ) plaques and neurofibrillary tangles of tau protein. Aβ plaques deposit early in regions of the brain that comprise the default mode network (DMN), while tau tangle deposition begins in the medial temporal lobe (MTL) and eventually spreads to the cortex. Widespread neurodegeneration and the onset of mild cognitive impairment (MCI) and dementia follow soon thereafter. This timeline of functional and structural brain changes relative to pathology accumulation and clinical symptoms is generally accepted for sporadic and familial forms of AD. However, it remains unclear whether a similar pattern of disease progression occurs in people with DS due to the limited number of *in vivo* neuroimaging studies, particularly functional MRI, in this population.

We sought to address these gaps in knowledge through the use of neuroimaging studies involving individuals with DS in both preclinical and clinical stages of AD. First, we measured neurodegeneration in the MTL of people with DS and tested whether it was related to MCI/AD clinical diagnosis, episodic memory performance, and plasma neurofilament light chain protein (NfL), which is a peripheral measure of axonal injury. We found that plasma NfL levels mediated the relationship between atrophy in both the anterolateral entorhinal cortex and hippocampus and verbal free recall. Next, we assessed resting state functional connectivity in the DMN in cognitively stable individuals with DS, some of whom were later diagnosed with dementia. We found that lower connectivity between distant hubs of the DMN predicted future dementia diagnosis and faster cognitive decline. Finally, we investigated how MTL functional connectivity was related to MCI/AD clinical diagnosis, memory impairment, and tau accumulation in people with DS. We found that greater MTL connectivity was present in those with MCI-DS and was associated with worse memory and possibly greater tau deposition. Together, these findings highlight the distinct timing of the neurobiological changes occurring in two brain networks uniquely targeted by AD pathology and suggest that altered brain structure and organization may impact the clinical manifestation of this neurodegenerative disease in individuals with DS.

CHAPTER 1: BACKGROUND AND SIGNIFICANCE

1.1. BACKGROUND AND PUBLIC HEALTH RELEVANCE OF ALZHEIMER'S DISEASE

1.1.1. CLINICAL DESCRIPTION OF ALZHEIMER'S DISEASE

Alzheimer's disease (AD) is a progressive neurodegenerative disease and the most common cause of dementia (Alzheimer's disease facts and figures, 2023). Late-onset AD is sporadic and heterogeneous in origin, though age is the greatest risk factor. Currently, an estimated 6.7 million Americans age 65 and older live with AD dementia, and this number is projected to double by the year 2060 without the development of an intervention to slow, cure, or prevent the disease (Alzheimer's disease facts and figures, 2023).

Despite the urgent need for new treatments, AD clinical trials have been relatively unsuccessful, with a failure rate of 99% (Cummings, 2018). Among the six FDA-approved drugs, four may slow the rate of cognitive decline but have no effect on AD neuropathology, while the remaining two reduce the level of AD pathology in the brain without meaningfully improving symptoms and carry the risk of potentially fatal side effects such as edema and hemorrhage (Alhazmi and Albratty, 2022; Honig et al., 2023).

None of these therapeutics are approved for use in presymptomatic individuals with AD. These therapeutics are only indicated for people with symptomatic AD, at which point it may be impossible to slow or stop disease progression. Treatment is needed before clinical symptoms appear, suggesting preclinical biomarkers are the key to early diagnosis and effective intervention (Öhman et al., 2021). Biomarkers are quantifiable measurements of biological processes that are associated with relevant clinical outcomes and thus can serve as surrogate markers of disease pathogenesis and progression. Since AD begins decades before cognitive impairment emerges, there is a window of time during which biomarkers that have a high likelihood of leading to dementia can be discovered and at-risk individuals can be identified. The

same logic led to the public health success story behind cardiovascular disease prevention through the treatment of hypertension (Moser and Roccella, 2013).

1.1.2. ALZHEIMER'S DISEASE PATHOLOGY

The two defining pathologies of AD are extracellular neuritic plaques formed around a core of misfolded β-amyloid (Aβ) protein and intraneuronal neurofibrillary tangles of hyperphosphorylated tau protein (DeTure and Dickson, 2019). Typically, Aβ pathology accumulates in the brain beginning roughly 30 years before symptom onset, followed by tau pathology roughly 15 years before symptom onset (Jack et al., 2013) (**Figure 1.1**). According to the Thal Aβ phase scoring system, Aβ begins depositing in the neocortex, spreading next to the allocortex, then to the diencephalon, then to the brain stem, and finally to the cerebellum (Thal et al., 2002). The order of initial Aβ accumulation in the cortex is variable, though the majority of individuals with AD show earliest accumulation in the medial frontal cortex and precuneus, later extending to other frontal, parietal, and temporal cortical regions (Collij et al., 2022). The spatiotemporal pattern of pathological tau accumulation is relatively predictable. Tau is initially restricted to the transentorhinal cortex, entorhinal cortex (EC), and hippocampus (stage I-II), then spreads to temporal, frontal, and parietal higher-order association cortices (stage III-IV), and finally reaches first-order sensory and premotor areas (stage V-VI) (Braak et al., 2006). Positron emission tomography (PET) imaging, cerebrospinal fluid (CSF), and plasma can detect Aβ and tau *in vivo*. These measures are strongly correlated with post-mortem Aβ and tau, supporting their use as biomarkers of AD neuropathology (Wisch et al., 2023; Ossenkoppele et al., 2021).

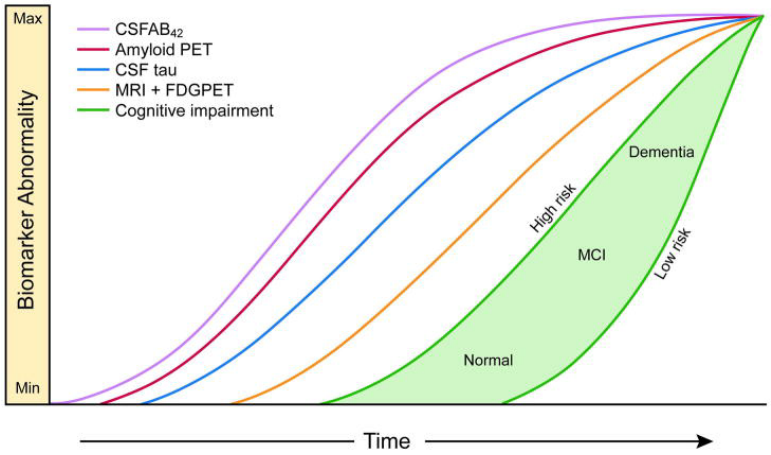

Figure 1.1. Hypothesized model of AD pathological cascade, beginning with Aβ pathology, followed by tau pathology, structural and functional abnormalities, and finally clinical symptoms (Jack et al., 2013).

The National Institute on Aging and Alzheimer's Association recently proposed a novel set of disease classification and staging criteria called the ATN research framework (Jack et al., 2016). Its three biomarker categories are binary, representing the presence or absence of Aβ ("A") measured by Aβ PET or CSF Aβ42, tau ("T") measured by tau PET or CSF phosphorylated tau, and neurodegeneration ("N") measured by [18F]-fluorodeoxyglucose (FDG) PET, structural magnetic resonance imaging (MRI), or CSF total tau. This scheme is independent of cognitive status, though clinical symptoms can be interpreted in combination with ATN classification in order to make a differential diagnosis.

1.1.3. NEURODEGENERATION AND FUNCTIONAL BRAIN NETWORKS

MRI is a non-invasive *in vivo* tool that can be used to derive biomarkers of neurodegeneration and circuit function that may precede and predict clinical symptoms of AD. T1-weighted structural MRI sequences utilize short repetition time (TR, <1000ms) and echo time (TE, <30ms) to generate high-resolution (i.e., 0.5-1mm isotropic) images that distinguish between gray and white matter and capture anatomical details. T1-weighted scans are used to measure brain volume or cortical thickness, which can reflect synaptic and neuronal loss.

In the presence of AD pathology, a distinct pattern of neurodegeneration emerges. The earliest neurodegenerative changes occur in regions susceptible to pathology accumulation such as the hippocampus (Planche et al., 2022) and EC (Gómez-Isla et al., 1996; Holbrook et al., 2020). The hippocampus is also subject to age-related neurodegeneration (Bettio et al., 2017), though no age-related neuron loss is observed within EC (Gómez-Isla et al., 1996). Additionally medial temporal, inferior temporal, temporal pole, inferior parietal, superior frontal, inferior frontal, precuneus, and superior parietal cortex are susceptible to thinning in sporadic AD (Dickerson et al., 2009).

T2*-weighted gradient echo functional MRI (fMRI) sequences utilize a longer TR and TE to measure brain activity via changes in blood flow, called the hemodynamic response, which depends on the coupling of cerebral blood flow, neuronal activation, and energy consumption by brain cells. As neurons become active, they recruit energy and oxygen from the local blood supply, which leads to a differential in oxygenation level. The difference in the magnetic properties of deoxyhemoglobin and oxyhemoglobin allows for a blood oxygen level-dependent (BOLD) contrast to be generated, which can inform on the spatial localization of neural activity. Resting state fMRI (rsfMRI) measures task-independent low-frequency (<0.1 Hz) fluctuations in the spontaneous BOLD signal (Biswal et al., 1995). Fluctuations in a given region tend to be correlated in time with fluctuations in functionally interrelated brain regions. This suggests that regions of the brain are actively communicating with one another in the absence of conscious engagement. In other words, they are intrinsically functionally interconnected.

The default mode network (DMN) comprises several brain regions that are intrinsically functionally connected at rest in healthy individuals (Raichle et al., 2001) (**Figure 1.2**). The medial prefrontal cortex (mPFC), posterior cingulate cortex (PCC), and precuneus are the most commonly identified regions within the DMN (Raichle et al., 2001). However, the retrosplenial

cortex (RSC) (Buckner et al., 2008), angular gyrus (Whitfield-Gabrieli and Ford, 2012), and anterior cingulate cortex (ACC) (Xu et al., 2016) are frequently included in the DMN as well. DMN connectivity is reduced due to age- and AD-related pathology in neurotypical individuals, particularly Aβ accumulation (Raichle et al., 2001; Greicius et al., 2003; Mevel et al., 2011).

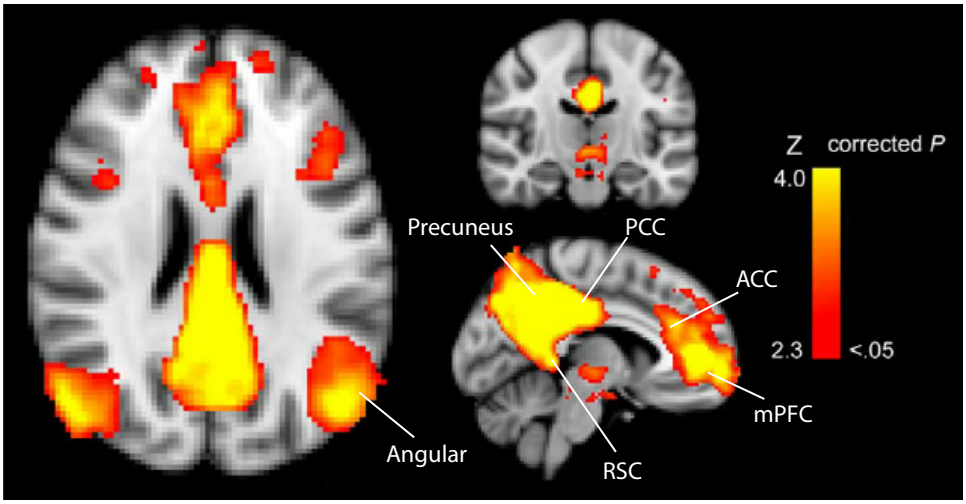

Figure 1.2. DMN intrinsic connectivity. The regions that make up the DMN include the medial prefrontal cortex (mPFC), anterior cingulate cortex (ACC), posterior cingulate cortex (PCC), retrosplenial cortex (RSC), precuneus, and angular gyrus (Adapted from Wojtowicz et al., 2014).

The medial temporal lobe (MTL) network comprises the hippocampus, EC, perirhinal cortex (PRC), and parahippocampal cortex (PHC) (Berron et al., 2021) (**Figure 1.3**). Increased MTL intrinsic connectivity and memory task-related activity is observed in mild cognitive impairment (MCI) (Das et al., 2013; Grajski et al., 2019; Hrybouski et al., 2023, Preprint) and is associated with worse episodic memory in neurotypical older adults with MCI and those with preclinical AD (Pasquini et al., 2015; Salami et al., 2016). This initial increase in MTL connectivity and activity is followed by a decrease during dementia, creating an inverse U-shaped pattern across AD clinical stages (Pasquini et al., 2019; Putcha et al., 2011; Bakker et al., 2012) (**Figure 1.4**). MTL hyperconnectivity may distinguish MCI from cognitively normal individuals, whereas MTL hypoconnectivity may distinguish dementia from MCI. The MTL is vulnerable to age- and AD-related neurodegeneration and tau accumulation (Buckner et al., 2008; La Joie et al., 2012;

Grothe et al., 2016). Hyperexcitability in this region may in turn accelerate local tau deposition and spread to other cortical regions (Pasquini et al., 2019, Adams et al., 2019).

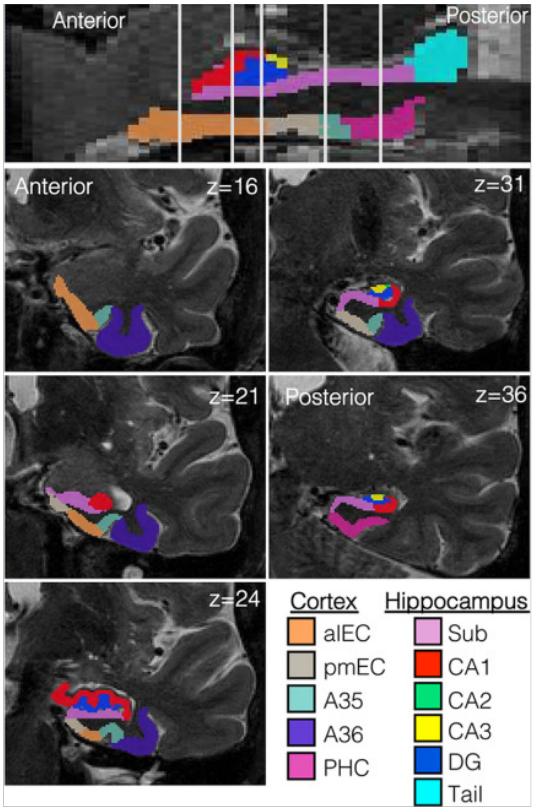

Figure 1.3. MTL segmentation. The hippocampus is divided into its constituent subfields. The entorhinal cortex is divided into anterolateral (alEC) and posteromedial (pmEC) subregions. Brodmann areas 35 and 36 comprise the perirhinal cortex (PRC). Together, the alEC, pmEC, PRC, and parahippocampal cortex (PHC) constitute the MTL cortex (Adapted from Adams et al., 2021).

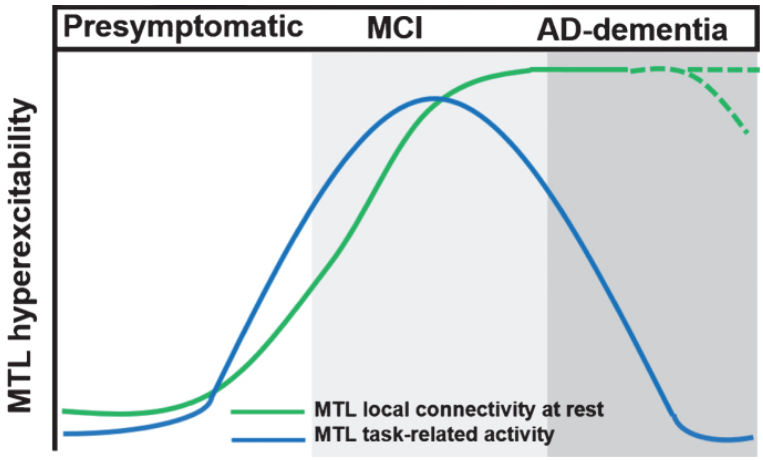

Figure 1.4. Hypothesized inverse U-shaped curve of MTL hyperexcitability during AD progression. MTL functional connectivity increases prior to and throughout MCI then may drop off following dementia onset (Adapted from Pasquini et al., 2019).

1.1.4. GENETICS OF ALZHEIMER'S DISEASE

The Dominantly Inherited Alzheimer Network (DIAN) was formed in an effort to investigate the autosomal dominant form of AD (ADAD) arising from mutations in one of three genes that increase in the production of Aβ: amyloid precursor protein (*APP*), presenilin 1 (*PSEN1*), or presenilin 2 (*PSEN2*) (Moulder et al., 2013). These three mutations are exceedingly rare, accounting for less than 1% of the total prevalence of AD in the U.S. (Sirkis et al., 2022). In contrast, Down syndrome (DS), which affects more than 250,000 Americans (Presson et al., 2013), is considered the strongest genetic risk factor for early onset AD (Gomez et al., 2020). Trisomy 21, or the triplication of chromosome 21, is present in 90-95% of people with DS, while partial trisomy 21 and mosaicism each account for 2-4% of DS cases (Pangalos et al., 1994; Hamerton et al., 1965; Richards, 1969; Mikkelsen, 1977; Hook, 1981). *APP* is located on chromosome 21 (Glenner and Wong, 1984), so people with DS who have three copies of *APP* experience lifelong overproduction of APP. Additional genes on chromosome 21, including *DYRK1A*, *BACE2*, *SOD1*, *RCAN1*, *S100B*, *SYNJ1*, *EST2*, and *CSTB*, are linked to AD pathology, neuroinflammation, and dysfunction of mitochondria, endosomes, and lysosomes (Gomez et al., 2020). Modeled after DIAN, the Alzheimer Biomarkers Consortium — Down Syndrome (ABC-DS) was created to study the genetic vulnerability to AD exhibited by people with DS (Handen et al., 2020).

1.2. BACKGROUND AND PUBLIC HEALTH RELEVANCE OF DOWN SYNDROME

1.2.1. CLINICAL DESCRIPTION OF DOWN SYNDROME

DS is the most common genetic condition in humans, occurring in roughly 1 in 700 live births in the U.S. (Mai et al., 2019). DS manifests in a characteristic phenotype affecting multiple organ systems, including but not limited to the neurological, musculoskeletal, cardiovascular, respiratory, and immune systems (Antonarakis et al., 2020). Consequently, individuals with DS have increased risk of developing comorbid health conditions such as hypothyroidism, epilepsy,

obstructive sleep apnea, obesity, and congenital heart defects, in addition to AD (Antonarakis et al., 2020; Bull et al., 2011). AD is the primary cause of neurodegeneration, dementia, and mortality in people with DS (Strydom et al., 2018; Landes et al., 2020). Age is the biggest risk factor for dementia in this population (Lott and Head, 2019), with an estimated prevalence of 23% at age 50, 45% at age 55, and 88% at age 65 (McCarron et al., 2017). There is an urgent public health need to develop therapeutics to treat AD in people with DS, yet the majority of AD clinical trials exclude people with DS from participation (DeCormier Plosky et al., 2022). Research on AD pathogenesis and progression in individuals with DS is critical to address the disproportionate disease burden carried by people with DS.

1.2.2. DEVELOPMENTAL NEUROBIOLOGY OF DOWN SYNDROME

From a young age, people with DS experience intellectual disability and undergo slower cognitive development, particularly in the domains of episodic memory and expressive language. However, the severity of intellectual impairment can vary among individuals, ranging from mild to moderate to severe (Antonarakis et al., 2020). Differences in neurobiological development begin prenatally (Edgin et al., 2015) and include reduced neurogenesis in the hippocampus and frontal and temporal cortices (Guidi et al., 2008), delayed myelination of fronto-temporal and association fibers (Wisniewski and Schmidt-Sidor, 1989), and impaired synaptogenesis (Schmidt-Sidor et al., 1990). People with DS have a smaller hippocampus and reduced regional cortical volumes, primarily in anterior cingulate, temporal, frontal, and parietal cortices, as well as a smaller cerebellum and larger ventricles compared to their neurotypical peers (Hamner et al., 2018; Kesslak et al., 1994; Raz et al., 1995; Pinter et al., 2001). However, the PHC is larger in people with DS, indicative of potential developmental differences in neurogenesis in this region (Kesslak et al., 1994).

1.3. NEUROBIOLOGY OF ALZHEIMER'S DISEASE IN DOWN SYNDROME

1.3.1. PATHOLOGY AND SPATIOTEMPORAL SPREAD

AD pathology progresses in an age-dependent manner in this population. By age 40, virtually all people with DS have accumulated sufficient Aβ plaques and neurofibrillary tangles to be given a neuropathological diagnosis of AD (Wisniewski et al., 1985; Lott and Head, 2019) (**Figure 1.5**). The overexpression of APP contributes to the accumulation of soluble Aβ beginning *in utero* in DS (Teller et al., 1996). Diffuse plaques are detectable in the late teens and early 20s, beginning in the neocortex then spreading to subcortical regions and the cerebellum by the late 40s (Snyder et al., 2020; Gomez et al., 2020). The striatum is thought to be the first site of Aβ accumulation in DS, beginning around age 35, though this phenomenon is only observed using the Pittsburgh compound B (PiB) PET tracer (Annus et al., 2016; Tudorascu et al., 2019). A similar pattern is observed in ADAD (Lott and Head, 2019). Studies using other Aβ PET tracers, such as florbetapir and 18F-FDDNP, do not replicate these findings, instead showing earliest Aβ deposition in frontal, parietal, and temporal cortical regions prior to the striatum, following the Thal phase staging observed in sporadic AD (Davidson et al., 2018; Keator et al., 2020b). This inconsistency could be due to the ligands having different affinities for different types of Aβ, as the striatum accumulates a larger amount of diffuse plaques than neocortical areas and has a notable absence of fibrillar plaques until later stages of AD in DS (Mann and Iwatsubo, 1996). People with DS have greater PET-detectable Aβ burden and higher concentrations of plasma Aβ40 and Aβ42 compared to neurotypical individuals with AD (Gomez et al., 2020). The increased plaque density in DS mirrors genetic forms of AD (Head et al., 2018). However, like in sporadic AD, Aβ positivity precedes cognitive impairment by roughly two decades in DS (Snyder et al., 2020).

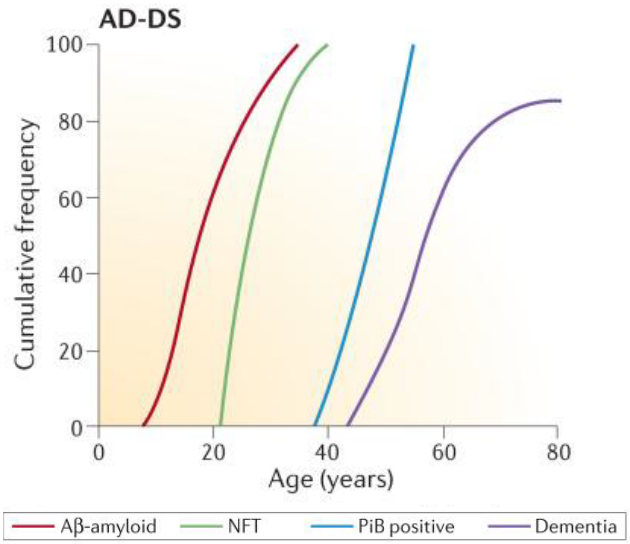

Figure 1.5. Cumulative frequency of Aβ plaque and neurofibrillary tangle (NFT) deposition (measured using histology), PiB binding (measured using PET), and dementia in people with DS (Adapted from Wiseman et al., 2015).

Elevated levels of DYRK1A contribute to the hyperphosphorylation of tau protein (Liu et al, 2008). APP may also play a role in tau phosphorylation as Aβ42 upregulates DYRK1A (Kimura et al., 2007). Tau pathology begins in the outer molecular layer of the hippocampus in the fourth decade of life, after which neurofibrillary tangles appear in layer II of the EC and spread to the hippocampus and then the neocortex generally following Braak staging, though tangle density is higher in AD in DS compared to sporadic AD (Head et al., 2003; Hof et al., 1995). Tau progression can be observed *in vivo* using the tau PET tracers [18F]AV-1451 and [18F]MK-6240. Tau tangles have not been reported in the absence of dense-core Aβ plaques in DS (Wiseman et al., 2015), and individuals with DS who have elevated Aβ PET binding also have greater tau burden across all Braak stage regions (Hartley et al., 2022; Zammit et al., 2021), suggesting Aβ is essential for the development of tau pathology. But as in sporadic AD, tau is more strongly correlated with cognitive impairment, particularly in the domain of memory, than Aβ in people with DS at various stages of clinical AD (Brier et al., 2016; Grigorova et al., 2022; Hartley et al., 2022). This correlation appears to be independent of Aβ.

1.3.2. STRUCTURAL NEUROIMAGING OF NEURODEGENERATION

Trisomy 21 causes developmental neuroanatomical differences that may contribute to regional vulnerability to neurodegeneration later in life. These initial differences are exacerbated with age (Kesslak et al., 1994; Krasuski et al., 2002; Teipel et al., 2004; Beacher et al., 2010; Fortea et al., 2020), making aging individuals with DS susceptible to more extensive neurodegeneration than neurotypical individuals. The earliest AD-related neurodegenerative changes occur in the hippocampus and EC (Beacher et al., 2009; Sadowski et al., 1999; Mak et al., 2019; Hof et al., 1995) and are associated with memory loss prior to MCI or AD diagnosis (Krasuski et al., 2002; Teipel et al., 2004), comparable to sporadic AD. However, neurodegeneration beyond the MTL, including frontal, lateral parietal, and precuneus cortices, follows Aβ and tau accumulation and coincides with the onset of clinical impairment (Padilla et al., 2022; Sabbagh et al., 2015).

1.3.3. FUNCTIONAL NEOCORTICAL NETWORKS

1.3.3.1. DEFAULT MODE NETWORK

People with DS show different patterns of DMN functional connectivity compared to neurotypical individuals. The DMN exhibits greater connectivity with other networks, including the limbic network, in people with DS (Vega et al., 2015; Cañete-Massé et al., 2023). Within-DMN connectivity may be increased as well (Wilson et al., 2019), though this difference could be restricted to the anterior DMN (Rosas et al., 2021; Koenig et al., 2021a; Csumitta et al., 2022), with anterior-posterior DMN node pairings demonstrating lower connectivity in individuals with DS (Cañete-Massé et al., 2023; Rosas et al., 2021; Koenig et al., 2021a). However, these developmental differences do not account for the reduced DMN functional connectivity observed during preclinical AD in DS (Wilson et al., 2019), which mirrors findings in sporadic AD and ADAD.

1.3.3.2. MEDIAL TEMPORAL NETWORK

Little is known about the intrinsic connectivity of the MTL in people with DS, particularly as it relates to age and AD. There may be some developmental differences in MTL connectivity between young adults with DS and age-matched typically developing individuals, though results are mixed (Vega et al., 2015; Cañete-Massé et al., 2023; Koenig et al., 2021b).

FDG PET provides a quantitative measure of neuronal activity based on cerebral glucose metabolic rate, and it tends to overlap spatially with functional connectivity maps derived from rsfMRI (Jiao et al., 2019). Hypometabolism in the temporal cortex is observed in people with DS with AD relative to their cognitively stable (CS) peers (Sabbagh et al., 2015; Deinde et al., 2022) and is associated with older age, cognitive decline, neurodegeneration, and increased Aβ and tau deposition (Lao et al., 2018; Haier et al., 2008; Rafii et al., 2019; Matthews et al., 2016; Rafii et al., 2017). Temporal cortex hypometabolism is preceded by a brief period of hypermetabolism, particularly in the EC, in middle-aged CS individuals with DS, which could reflect increased local neural activity as a compensatory response to preclinical AD processes (Haier et al., 2008; Head et al., 2012; Deinde et al., 2022). This phenomenon of temporary MTL hypermetabolism during the early stages of AD in DS followed by MTL hypometabolism in more advanced stages is consistent with functional connectivity findings in sporadic AD (Pasquini et al., 2019).

1.4. CURRENT STATE OF KNOWLEDGE AND OPEN QUESTIONS

The predicted exponential increase in AD and dementia in the coming decades represents a looming global public health crisis. Improvements in diagnosis, disease monitoring, treatment, and prevention are all essential to managing this silent pandemic. To this end, one urgent goal of biomedical research is to track the neurobiological changes preceding and coinciding with AD-related cognitive decline.

There is substantial evidence supporting the ATN pattern of disease progression in sporadic AD and ADAD. The “A” and “T” components of this framework appear to overlap significantly with AD-DS, albeit on an accelerated timescale. However, it is not fully understood what role neurodegeneration and additional factors play in the development of clinical AD in people with DS. Though Aβ and tau pathology are both necessary for AD, they are not sufficient for dementia diagnosis (Erten-Lyons et al., 2009). An estimated 10-20% of people with DS live to age 60 and beyond without developing cognitive impairment despite the presence of AD pathology (Lott and Head, 2019), comparable to estimates of 20-30% in sporadic AD (Jansen et al., 2015). One possible explanation is that additional neurobiological consequences of AD, such as neurodegeneration and aberrant organization of key brain networks, may contribute to the clinical manifestation of the disease. Identifying the brain changes that predict dementia in individuals with DS would enable earlier diagnosis, more precise staging, and investigation of potential disease-modifying mechanisms that could translate to other forms of AD.

The predictable, age-dependent progression of AD in people with DS creates a unique opportunity to characterize the neurobiological indicators beyond Aβ plaques and tau tangles that are present during the preclinical and early phases of AD-DS. In **Chapter 2**, we aim to show that MTL neurodegeneration coincides with dementia-related memory impairment in DS. The content of this chapter was recently accepted for publication in a preprint by DiProspero et al. (2023, Forthcoming). In **Chapter 3**, our goal is to determine whether DMN intrinsic connectivity predicts the development of dementia in people with DS. The findings of this chapter were published in a paper by DiProspero et al. (2022). In **Chapter 4**, we intend to investigate whether MTL functional connectivity differs across clinical progression of AD-DS and how it relates to memory and tau accumulation. In **Chapter 5**, we summarize the results of the three previous chapters, discuss the conclusions in light of the current state of knowledge in the field, and propose additional avenues for future research.

CHAPTER 2: NEUROFILAMENT LIGHT CHAIN CONCENTRATION MEDIATES THE ASSOCIATION BETWEEN REGIONAL MEDIAL TEMPORAL LOBE STRUCTURE AND MEMORY IN PEOPLE WITH DOWN SYNDROME

2.1. INTRODUCTION

Neurofilament light chain protein (NfL) is released into the extracellular space of the brain following axonal damage. Trace amounts of NfL are detectable in CSF and plasma (Hampel et al., 2018). CSF and plasma concentrations of NfL are strongly correlated (Mattsson et al., 2017). Although the release of NfL is age-related (Khalil et al., 2020) and not specific to AD (Hansson et al., 2022), it is an emerging, minimally invasive biomarker of neurodegeneration in people with DS.

The association between EC thickness, AD pathology, and cognitive decline is driven by the anterolateral subregion of the EC (alEC) (Holbrook et al., 2020). This observation is consistent with neuropathological evidence of alEC vulnerability to early tau pathology (Khan et al., 2014).

The EC and hippocampus are key brain regions that enable episodic memory (Dickerson and Eichenbaum, 2010). The modified Cued Recall Test (mCRT) is used to assess verbal episodic memory in people with DS while accounting for developmental differences in cognitive ability (Krinsky-McHale et al., 2022). We hypothesized that MRI-based measures of hippocampus and EC, in particular alEC, gray matter and plasma NfL concentration would be associated with each other as well as MCI/AD clinical status and memory in people with DS. In order to disentangle these hypothesized relationships, we performed a mediation analysis to explore the contributions of both neurodegenerative indicators to memory impairment.

2.2. MATERIALS AND METHODS

Participants

Participants enrolled in the Alzheimer's Disease in Down Syndrome (ADDS) study, which aims to characterize the evolution of AD in people with DS using neuropsychological assessments, blood, and neuroimaging biomarkers. ADDS enrolled over 200 people with DS age 40 and older at three sites: Columbia University (CU), Massachusetts General Hospital (MGH), and the University of California, Irvine (UCI). The current analyses included participants who completed an MRI scan. Some participants additionally completed memory assessments and had plasma samples collected. All research procedures were reviewed and approved by the Institutional Review Boards of all collaborating institutions, and informed consent, as well as assent, was obtained from all participants and their legally authorized representatives. All participants were reimbursed for their participation.

Memory assessment

Episodic memory was assessed using a modified version of the Cued Recall Test (mCRT) validated for use in people with intellectual disability. The mCRT is sensitive to preclinical and clinical AD in people with DS (Hartley et al., 2020; Benejam et al., 2020). Stimuli were arranged on three cards, each with four line drawings of everyday objects from unique semantic categories, totaling 12 items. During encoding, participants were shown one card at a time and asked to identify which item was a member of a cued category. The card was removed, and participants were asked to recall the item. This was repeated for the remaining 11 items. During retrieval, participants were asked to freely recall all 12 items. This was followed by cued recall of any forgotten items using the category cue. Correct responses were recorded as the free recall score (FRS) and cued recall score (CRS), respectively. Free and cued recall were repeated for two additional trials. The total recall score (TRS) was the sum of FRS and CRS across the three

trials, resulting in a maximum score of 36. Due to the dependence of CRS on FRS, only FRS and TRS were used as memory outcome measures.

Determination of MCI/AD clinical status

Each participant's MCI/AD clinical status was evaluated with a standardized assessment battery (see **Appendix A, Supplementary Methods**). Following data collection, MCI/AD clinical status of each participant was assigned at a consensus case conference conducted without knowledge of mCRT, neuroimaging, or fluid measures (Krinsky-McHale et al., 2013). Consensus diagnosis was performed in accordance with International Classification of Diseases 10th edition (ICD-10) and Diagnostic and Statistical Manual of Mental Disorders 4th edition Text Revision (DSM-IV-TR) criteria described in Sheehan et al. (2015). MCI/AD clinical status was classified into the following categories: *(a) cognitively stable (CS),* indicating with reasonable certainty that clinically significant declines beyond those to be expected with normal aging were absent, *(b) mild cognitive impairment (MCI-DS),* indicating that there was some mild cognitive and/or functional decline greater than would be expected with aging but not severe enough to meet criteria for dementia, *(c) possible dementia,* indicating significant decline over six months or more that suggested dementia was likely, but additional information was needed to establish certainty, *(d) definite dementia,* indicating a high degree of confidence that dementia was present, or *(e) status uncertain due to complications,* indicating that the evidence of decline was present but one or more factors unrelated to an aging-associated neuropathology might be the cause, usually a medical condition or traumatic life event. In most cases, a consensus determination was straightforward (see **Appendix A, Supplementary Methods**). For the purposes of analysis, participants with possible and definite dementia were collapsed into a single dementia (DEM) group.

MR image acquisition

Data were collected on Siemens Prisma 3T MRI scanners at all three institutions, in addition to a Philips Achieva 3T scanner at UCI, which was used until UCI transitioned to the Siemens scanner mid-way through data collection. All scanners were equipped with 32-channel coils. A T1-weighted MPRAGE anatomical sequence based on the Alzheimer's Disease Neuroimaging Initiative (ADNI) 3 parameters was collected on all participants (Siemens: TR=2300ms, TE=2.96ms, flip angle=9°, voxel resolution=1×1×1mm^3, FOV=256×240×208mm; Philips: TR=7.800ms, TE=3.59, flip angle=7°, voxel resolution=1×1×1mm^3, FOV=256×256×176mm).

MR image processing

MTL cortex subregional segmentation was performed with a consensus labeling approach based on a set of 17 T2-weighted images acquired with an optimized MTL-specific acquisition protocol (image resolution: 0.47×0.47mm^2 in-plane, 2.0mm slice thickness) from cognitively normal neurotypical participants that were manually labeled using a highly reliable anatomical protocol used in prior published work (Yassa et al., 2010; Yassa et al., 2011). Anatomical labeling of the atlas set comprises separate labels for left and right EC, alEC, and posteromedial EC (pmEC). The alEC and pmEC boundaries were based on segmentations used in Reagh et al. (2018). Scans were paired with corresponding T1-weighted images (image resolution: 0.75×0.75×0.75mm^3) acquired for multi-spectral atlas-based registration. Spatial normalization and registration of the images to the atlas were performed (see **Appendix A, Supplementary Methods**). Visual quality assessment was performed to exclude participants with excessive motion artifacts or errors in registration or segmentation (see **Appendix A, Supplementary Methods**).

Voxels within bilateral EC, alEC, and pmEC were counted and multiplied by voxel resolution to calculate volumes in cubic millimeters. Cortical thickness of left and right alEC and pmEC was

calculated by dividing volume by surface area for all regions. Cortical reconstruction was performed using Freesurfer 6.0 (Dale et al., 1999) to obtain whole hippocampus volume as well as total intracranial volume (ICV). All volumes were normalized by dividing each participant's measure by their ICV. Regions of interest are shown in **Figure 2.1a**.

Blood sample collection and plasma NfL processing

The participants were not required to fast before blood draw. Blood samples were collected with a butterfly catheter. Within 30 minutes of blood collection, the tubes were centrifuged at the appropriate speed and temperature to separate out plasma, stored in separate 250µL polypropylene aliquots and frozen at -80°C. NfL concentrations were determined with the Single Molecule Array (Simoa) technology using the Human NF-Light Advantage kit (Simoa; Quanterix, Lexington, MA, USA) completed at the University of North Texas Health Science Center, Institute for Translational Research. Further information regarding NfL sample processing and performance parameters can be found in Petersen et al. (2021).

Statistical analysis

All statistical tests were conducted using R (R Core Team, 2022; v3.5.1) and RStudio (RStudio Team, 2022; v1.1.447) software. Normality was assessed visually using quantile-quantile plots and statistically using the Shapiro-Wilk test. All variables of interest were normally distributed except for TRS, right pmEC thickness, and plasma NfL. TRS could not be transformed to approximate a normal distribution, but it is included as an outcome variable based on the recommendation by Krinsky-McHale et al. (2022). When right pmEC thickness and plasma NfL were log-transformed, the results were similar to the untransformed variables (see **Appendix A, Supplementary Results**) so the latter were used during analysis. All models included age, sex, and site as covariates. Differences in demographic and neuropsychological variables among the diagnosis groups (CS, MCI-DS, and DEM) were tested using one-way ANOVA with post-hoc

Tukey test or chi-square test for continuous and categorical measures, respectively. Diagnosis group differences in MRI measures and plasma NfL concentration were tested using multiple linear regression and pairwise contrasts. Effect size for regressions was calculated using the *emmeans* package in R (Lenth, 2022; v1.7.5). Associations between MRI measures, plasma NfL concentration, and memory performance were tested using Pearson partial correlation. Reported results were considered significant at $\alpha<0.05$, after correcting for multiple comparisons using the Holm method (Holm, 1979). Two participants in the DEM group had plasma NfL concentrations >3 standard deviations above the mean. Sensitivity analyses excluding these participants were conducted for all statistical tests involving plasma NfL, and the results remained the same. Causal mediation analysis was performed using the *mediation* package in R (Tingley et al., 2014; v4.5.0). 1000 bootstrap samples were used to calculate bias-corrected and accelerated confidence intervals (CIs) at 2.5th and 97.5th percentiles.

2.3. RESULTS

Demographic and neuropsychological data

A total sample of 101 participants had MRI data after excluding participants who had uncertain diagnoses (*n*=11), whose scans had excessive motion (*n*=26), and whose scans did not pass processing quality control procedures (*n*=11). Demographic information for this sample is summarized in **Supplementary Table A1**. Of those 101 participants, 92 had mCRT data. Demographic information and neuropsychological testing results for this primary sample are summarized in **Table 2.1**. The distribution of participants across sites was as follows: CU *n*=23; MGH *n*=29; UCI *n*=40. Participants from each diagnosis group were proportionately distributed across the three sites (χ^2=3.390, *p*=0.4947). SNR and other quality control measures across sites were comparable. Among the 101 participants with MRI data, 86 had plasma NfL data. Their demographic information is summarized in **Supplementary Table A2**. A total of 77

participants had MRI, plasma NfL, and mCRT. Their demographic information and neuropsychological testing results are summarized in **Supplementary Table A3**.

Table 2.1. Participant demographics and neuropsychological assessments for individuals with both MRI and mCRT data

Variable	CS	MCI-DS	DEM	Test Statistic (*F* value or χ^2)	Group Differences
n	64	18	10	n/a	n/a
Age (mean ± SD)	48.7 ± 5.8	52.2 ± 5.2	54.9 ± 7.5	6.3	B
Sex, female (%)	25 (37.5%)	5 (27.8%)	5 (50.0%)	1.4	n.s.
mCRT FRS	16.9 ± 5.8	10.8 ± 5.7	5.8 ± 6.8	20.0	AB
mCRT TRS	31.0 ± 6.9	22.7 ± 10.5	10.6 ± 10.2	30.7	ABC

Significant pairwise group differences, $p<0.05$: A: CS vs. MCI-DS; B: CS vs. DEM; C: MCI-DS vs. DEM.

Increased plasma NfL concentration in dementia group

Among participants with MRI and plasma NfL data, plasma NfL concentration was higher in the DEM group compared with the MCI-DS ($t(78)=-4.709$, $p<0.0001$, effect size=-1.922) and CS groups ($t(78)=-5.907$, $p<0.0001$, effect size=-2.034) (**Figure 2.1b**). There was no difference in plasma NfL concentration between CS and MCI-DS groups ($t(78)=-0.370$, $p=0.7128$, effect size=-0.112).

Reduced EC and hippocampus volume in dementia group

Left EC volume was lower in the DEM group compared with the MCI-DS ($t(93)=3.746$, $p=0.0003$, effect size=1.391) and CS groups ($t(93)=4.628$, $p<0.0001$, effect size=1.518) (**Figure 2.1c**). There was no difference in left EC volume between CS and MCI-DS groups ($t(93)=0.477$, $p=0.6344$, effect size=0.128). Right EC volume was lower in the DEM group compared with the CS group ($t(93)=2.354$, $p=0.0207$, effect size=0.772), but there was no difference in right EC volume between DEM and MCI-DS groups ($t(93)=1.203$, $p=0.2322$, effect size=0.447) or between MCI-DS and CS groups ($t(93)=1.219$, $p=0.2261$, effect size=0.326) (**Figure 2.1d**).

The DEM group had lower left and right hippocampus volume than the MCI-DS (left: $t(93)=2.704$, $p=0.0082$, effect size=1.004; right: $t(93)=2.596$, $p=0.0109$, effect size=0.964) and CS groups (left: $t(93)=3.827$, $p=0.0002$, effect size=1.256; right: $t(93)=3.884$, $p=0.0002$, effect size=1.274) (**Figure 2.1e,f**). There was no difference in hippocampus volume between CS and MCI-DS groups (left: $t(93)=0.942$, $p=0.3488$, effect size=0.252; right: $t(93)=1.160$, $p=0.2490$, effect size=0.310).

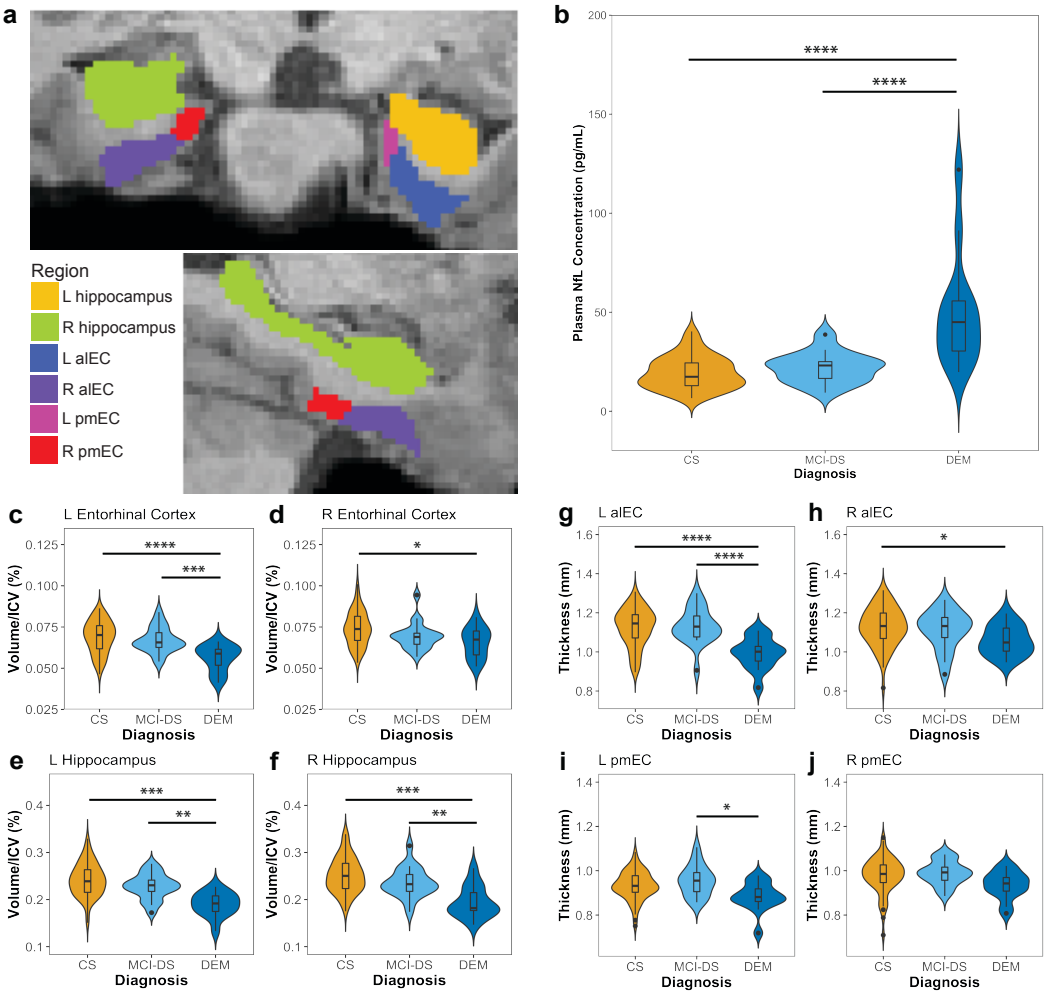

Figure 2.1. (a) Regions of interest. (b) Plasma NfL concentration was significantly higher in the DEM group compared with the CS and MCI-DS groups. (c) The DEM group had lower left EC volume than the MCI-DS and CS groups. (d) The DEM group also had lower right EC volume than the CS group but not the MCI-DS group). (e,f) Left and right hippocampus volume were lower in the DEM group compared with the MCI-DS and CS groups. (g) The DEM group had lower left alEC thickness than the MCI-DS and CS groups. (h) The DEM group also had lower right alEC thickness than the CS group but not the MCI-DS group. (i) The DEM group had lower left pmEC thickness than the CS group. (j) Right pmEC thickness did not differ between the three groups. NfL=neurofilament light, ICV=intracranial volume. *p<0.05, **p<0.01, ***p<0.001, ****p<0.0001

Reduced alEC and pmEC thickness in dementia group

Following our recent work in ADNI[15], we sought to determine whether the EC volumetric differences across diagnosis groups may be driven by its anterolateral or posteromedial segments. Left alEC thickness was lower in the DEM group compared with the MCI-DS (t(93)=4.532, p<0.0001, effect size=1.683) and CS groups (t(93)=4.939, p<0.0001, effect size=0.618) (**Figure 2.1g**). There was no difference in left alEC thickness between CS and MCI-DS groups (t(93)=-0.242, p=0.8094, effect size=-0.065). Right alEC thickness was lower in the DEM group compared with the CS group (t(93)=2.190, p=0.0311, effect size=0.718) (**Figure 2.1h**). There were no differences in right alEC thickness between the DEM and MCI-DS groups (t(93)=1.504, p=0.1359, effect size=0.559) or between the MCI-DS and CS groups (t(93)=0.598, p=0.5515, effect size=0.160).

Left pmEC thickness was lower in the DEM group compared with the MCI-DS group (t(93)=2.176, p=0.0321, effect size=0.808) (**Figure 2.1i**). The difference in left pmEC thickness between the DEM and CS groups was trending toward significant (t(93)=1.685, p=0.0953, effect size=0.553), while the difference between the MCI-DS and CS groups was not significant (t(93)=-0.954, p=0.3425, effect size=-0.255). Right pmEC thickness showed no differences between any of the groups (all p-values >0.1) (**Figure 2.1j**).

Left alEC thickness and bilateral hippocampus volume are associated with plasma NfL concentration

Among participants with MRI and plasma NfL data, there was an inverse relationship between plasma NfL concentration and left hippocampus volume (r=-0.337, p=0.0037), right hippocampus volume (r=-0.432, p=0.0002), and left alEC thickness (r=-0.403, p=0.0005) but not right alEC thickness (r=-0.178, p=0.1067) (**Figure 2.2**). There was no significant partial

correlation between plasma NfL concentration and left or right pmEC thickness, even after excluding the two outliers (all p-values >0.2) (**Supplementary Figure A1**).

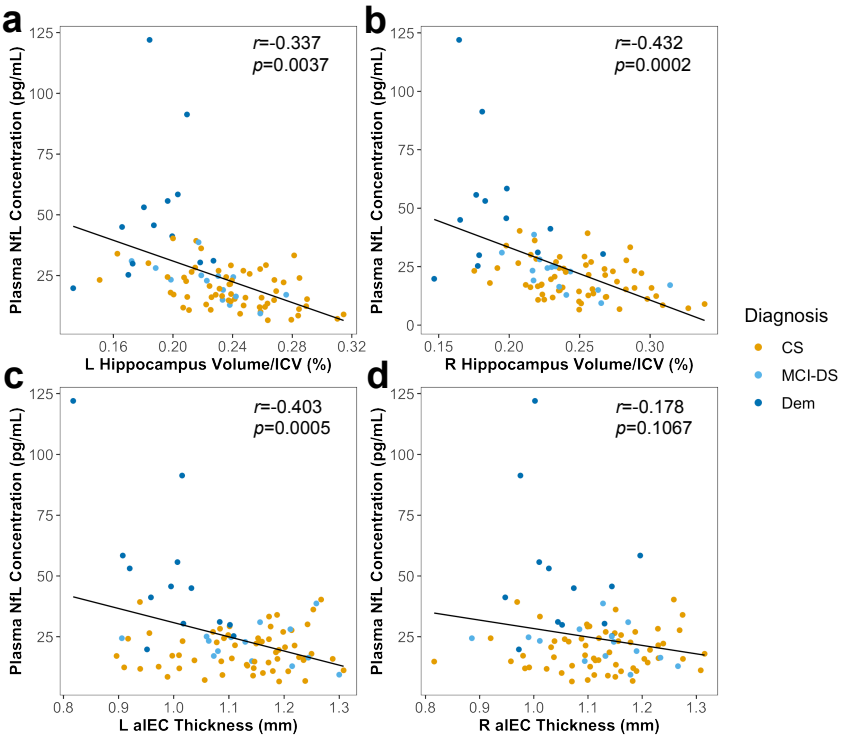

Figure 2.2. (a,b,c) Plasma NfL concentration was negatively associated with bilateral hippocampus volume/ICV percentage and left aIEC thickness. (d) Plasma NfL levels were not associated with right aIEC thickness. Pearson's r is the partial correlation coefficient after controlling for age, sex, and site covariates. The plots include the two outliers with high plasma NfL concentration since their exclusion did not meaningfully alter the results.

Hippocampus volume, aIEC thickness, and plasma NfL concentration are associated with memory recall

Among participants with MRI and mCRT data, there were significant positive partial correlations between both memory scores and left hippocampus volume (FRS: r=0.352, p=0.0021; TRS: r=0.393, p=0.0006) and right hippocampus volume (FRS: r=0.380, p=0.0010; TRS: r=0.377, p=0.0008), as well as trending correlations for left aIEC thickness (FRS: r=0.211, p=0.0944; TRS: r=0.234, p=0.0540) and right aIEC thickness (FRS: r=0.196, p=0.0944; TRS: r=0.193, p=0.0704) (**Figure 2.3**). There were no significant partial correlations between either memory score and bilateral pmEC thickness (all p-values >0.2) (**Supplementary Figure A2**).

Among participants with MRI, plasma NfL, and mCRT data, there were significant negative partial correlations between plasma NfL and FRS (r=-0.438, p<0.0001) and TRS (r=-0.475, p<0.0001) (**Figure 2.4**).

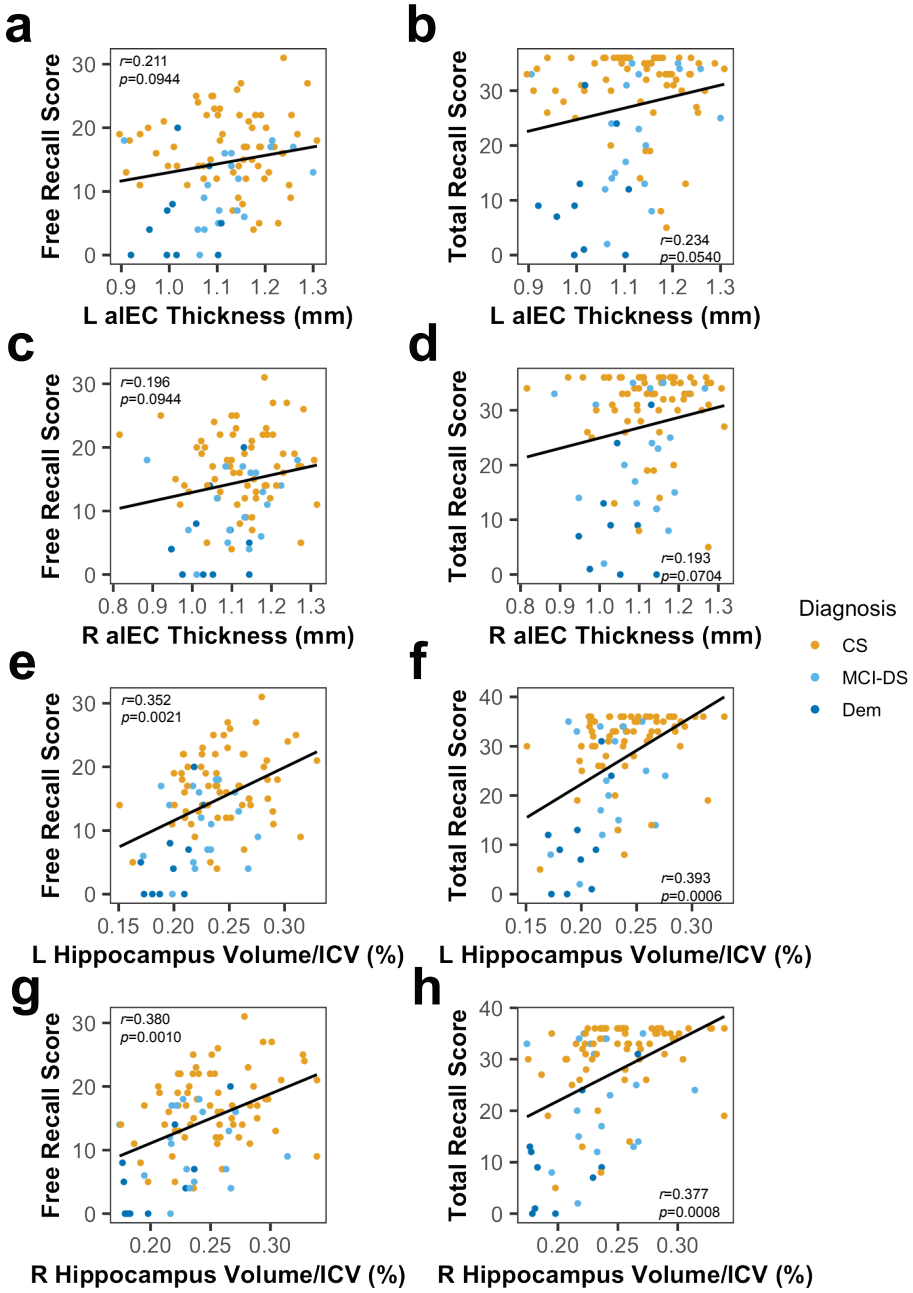

Figure 2.3 Hippocampus volume/ICV percentage and alEC thickness were positively associated with FRS and TRS. Pearson's r is the partial correlation coefficient after controlling for age, sex, and site covariates. (a,b,c,d) Positive partial correlations between FRS and TRS and left and right hippocampus volume were significant. (e,f,g,h) Positive partial correlations between the two memory scores and alEC thickness were trending toward significant.

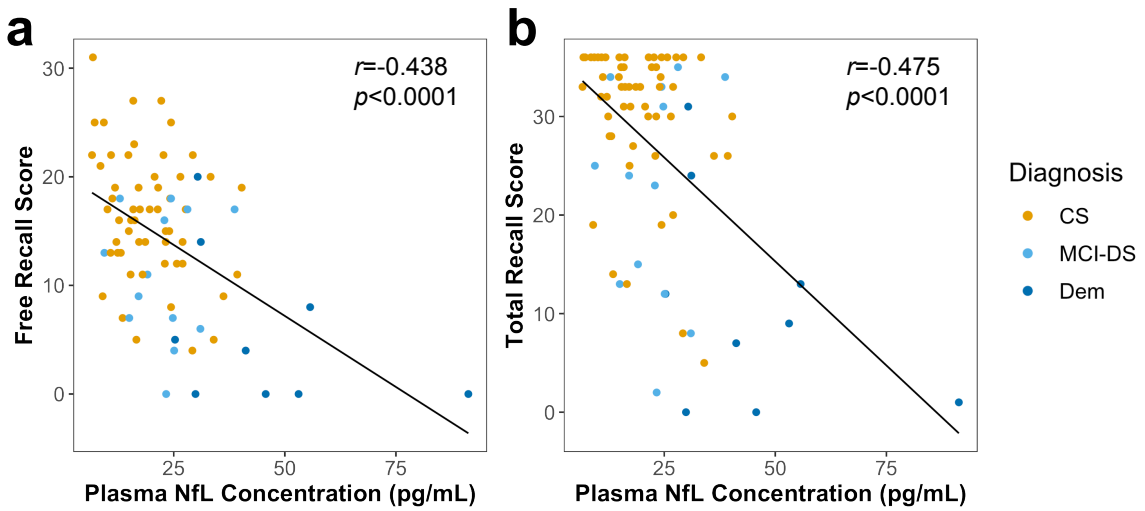

Figure 2.4. Plasma NfL concentration was negatively associated with FRS (a) and TRS (b). Pearson's r is the partial correlation coefficient after controlling for age, sex, and site covariates. The plots include the outlier with high plasma NfL concentration since the exclusion of this participant did not meaningfully alter the results.

Plasma NfL mediates the relationships between left alEC thickness and memory recall

To further understand the potential directional relationships among left alEC thickness and bilateral hippocampus volume, plasma NfL, and memory performance, we used a mediation analysis and reduced our sample to participants who had all of these measures (*n*=77). Since FRS and TRS are highly correlated, we chose to test only FRS as an outcome variable.

Thinner left alEC was associated with greater plasma NfL concentration (*a*=-34.551, *t*(72)=-2.507, *p*=0.0144), which in turn was associated with worse FRS (*b*=-0.216, *t*(71)=-3.534, *p*=0.0007). There was an indirect effect of plasma NfL on the relationship between left alEC thickness and FRS (*ab*=7.464, 95% CI=[0.902,16.9], *p*=0.024) (**Figure 2.5**). After adjusting for plasma NfL, the direct effect of left alEC thickness on FRS was not significant (*c'*=6.397, 95% CI=[-6.363,20.6], *p*=0.384). Plasma NfL mediated 54% of the relationship between left alEC thickness and FRS.

When the reverse mediation was run, with left alEC thickness as the mediator between plasma NfL and FRS, there was no indirect effect of left alEC thickness on the relationship between plasma NfL and FRS (*ab*=-0.0149, 95% CI=[-0.0551,0.01], *p*=0.352), with left alEC thickness mediating only 6% of the relationship between plasma NfL and FRS (**Supplementary Figure A3**).

We repeated the mediation analyses described above for left and right hippocampus volume (**Supplementary Figure A4**). Plasma NfL partially mediated the relationship between left and right hippocampus volume on FRS, but left and right hippocampus volume also partially mediated the relationship between plasma NfL and FRS.

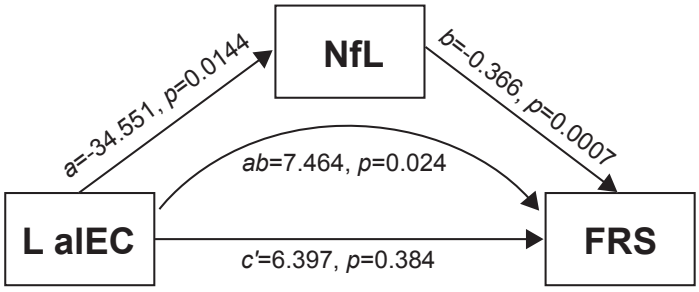

Figure 2.5. Plasma NfL concentration mediated the relationship between left alEC thickness and FRS. The indirect effect of plasma NfL on the relationship between left alEC thickness and FRS represented by ab, was significant. The direct effect of left alEC thickness on FRS, represented by c′, was not significant after accounting for plasma NfL.

2.4. DISCUSSION

We hypothesized that plasma NfL concentration and EC and hippocampus gray matter atrophy would be associated with dementia and memory in people with DS. Individuals with dementia had higher plasma NfL concentrations, lower bilateral hippocampus volume, and lower left alEC thickness than CS and MCI-DS individuals. No differences in plasma NfL levels or MRI measures were observed between CS and MCI-DS individuals. Our findings replicate previous work showing that plasma NfL differentiates asymptomatic individuals with DS from those with clinical AD (Janelidze et al., 2022). Lower hippocampus volume has been observed in CS individuals with DS who are Aβ-positive (Annus et al., 2017) and in those who convert to MCI-

DS (Pujol et al., 2018). We did not observe these early changes in hippocampus volume. Notably, there are age-related differences in hippocampus volume and cortical thickness in people with DS, though the EC shows no such difference (Fortea et al., 2020; Romano et al., 2016). Removing age as a covariate had a negligible effect on the results of our analysis (see **Appendix A, Supplementary Results**). Our findings suggest that the hippocampus and EC are vulnerable to neurodegeneration related to symptomatic AD, rather than aging, in people with DS. We believe our study is the first to demonstrate differential susceptibility to EC thinning in the left hemisphere and along its anterolateral/posteromedial axis in people with DS with dementia.

Left alEC thickness, bilateral hippocampus volume, and plasma NfL concentration were associated with free and total recall. These results are consistent with studies showing that verbal episodic memory is positively associated with hippocampus volume (Pujol et al., 2018) and EC thickness (Benejam et al., 2022) and negatively associated with plasma NfL levels (Janelidze et al., 2022) in individuals with DS across the AD spectrum. Plasma NfL levels were negatively correlated with bilateral hippocampus volume and left alEC thickness but not with other EC subregions, in line with findings in neurotypical individuals with and without symptomatic AD (Mattsson et al., 2017; Mattsson et al., 2019; Mielke et al., 2019; Chen et al., 2021). Our findings show that focal neurodegeneration in the hippocampus and left alEC is linked to impaired episodic memory in older individuals with DS. Despite being a peripheral measure, plasma NfL concentration has a strong, anatomically specific relationship with hippocampus and left alEC neurodegeneration and tracks with episodic memory. The present study is among the first to establish a relationship between plasma NfL and MRI-based measures of neurodegeneration in people with DS.

Plasma NfL levels mediated the relationship between left alEC thickness and memory. Surprisingly left alEC thickness did not mediate the relationship between plasma NfL and memory. In contrast, plasma NfL partially mediated the relationship between bilateral hippocampus volume and memory and vice versa. This suggests that the impact of left alEC thickness on verbal episodic memory may be indirect and mediated by the production and release of NfL, while hippocampus volume and NfL each have a direct impact on memory.

Our findings reveal that left alEC thickness and hippocampus volume reductions measured using MRI and increased levels of plasma NfL contribute to memory impairment in DS through shared neurodegenerative pathways. We highlight the left alEC as a brain region that is equally vulnerable to AD-related neurodegeneration as its better-studied hippocampal counterpart. Taken together, these data further our understanding of the pathophysiology underlying clinically relevant region-specific neurodegeneration in people with DS.

CHAPTER 3: SELECTIVE IMPAIRMENT OF LONG-RANGE DEFAULT MODE NETWORK FUNCTIONAL CONNECTIVITY PRIOR TO CLINICAL ALZHEIMER'S DISEASE IN PEOPLE WITH DOWN SYNDROME

3.1. INTRODUCTION

Aβ-positivity alone is not sufficient to predict dementia in people with DS. It's still unknown whether DMN functional connectivity is a useful biomarker of clinical onset of AD in DS. In this two-cohort study, we hypothesized that lower DMN resting state functional connectivity predicted conversion to dementia in people with DS. In addition, we investigated whether lower DMN functional connectivity was associated with greater cognitive decline as measured by longitudinal neuropsychological assessments and greater regional Aβ burden as measured using PET. Finally, we investigated whether lower DMN functional connectivity was age-related or whether it was related to the clinical onset of AD.

3.2. MATERIALS AND METHODS

Participants

Two cohorts were included in the study. Research procedures were carried out in accordance with the Declaration of Helsinki, and Institutional Review Board approval was obtained at the two participating institutions, UCI and the University of Kentucky (UKY). Informed consent/assent was obtained from all participants and their legal representatives prior to enrollment in the study. The first cohort consisted of 22 CS people with DS recruited at UCI. Participants received an MRI scan. Four participants ended their MRI scan session early and an rsfMRI scan was not acquired for them. One participant was excluded because their rsfMRI scan was corrupted and unusable. Finally, two participants were excluded due to excess motion in the scanner (see **MR image processing**). The remaining 15 people with DS (7 female, mean age=51.66 years, SD=5.34 years, range=42-59 years) comprise the final UCI sample included in the MRI analyses. Thirteen participants received a florbetapir (18F-AV-45) PET scan nine

months before their MRI scan, on average. The remaining two participants received a PiB PET scan and were excluded from the PET analysis. Participants were clinically evaluated every nine months for up to four years following the baseline MRI scan. During the study, four of the 15 participants transitioned to dementia based on clinical impressions evaluations. Importantly, one of those four participants transitioned to dementia two months before their MRI scan. Considering the limited availability of neuroimaging data in this population, this participant was included in the analyses. However, prospective neuroimaging biomarker studies should ideally only include participants who are cognitively normal at baseline so that any changes observed in the data can be confirmed to be preclinical in nature.

The second cohort consisted of 15 CS people with DS who were recruited for a longitudinal study of aging and AD at UKY. Participants received an MRI scan. One participant was excluded because they had a severe traumatic brain injury and possible mosaic DS. No participants needed to be excluded due to excessive motion. The remaining 14 people with DS (9 female, mean age=44.63 years, SD=7.99 years, range=38-61 years) comprise the final UKY sample included in the MRI analysis. No PET data were acquired for UKY participants. Participants were clinically evaluated annually for up to 10 years. During the study, none of the 14 participants transitioned to dementia based on clinical evaluations.

Diagnosis of transition to dementia

For UCI participants, dementia was diagnosed in accordance with ICD-10 and DSM-IV-TR criteria (Sheehan et al., 2015), described in detail in **Chapter 2** (see 2.2. Materials and methods, **Determination of MCI/AD clinical status**). Transition classification followed comprehensive baseline and longitudinal assessments including history, neurological examination, and consideration of previous studies in the medical record. Transition to dementia was decided at a consensus conference by three neurologists as well as the neuropsychologist

who administered the cognitive assessments for the given participant. They were blinded to the MRI scans, PET scans, and neuropsychological assessments. Participants with confounding conditions, such as sensory deficit, untreated thyroid dysfunction, and major depression, that might mimic the symptoms of dementia, were excluded. See Keator et al. (2020a, Supplement S2) for clinical vignettes describing transition symptoms of individual participants. For transitioned participants, the transition times corresponded to the clinical visit at which a new diagnosis was given. The diagnosis of dementia was confirmed at subsequent visits for the transitioned participants, while the non-transitioned participants were confirmed to be CS.

For each UKY participant, an expert consensus review determined dementia diagnosis. The NINCDS-ADRDA criteria for dementia (McKhann et al., 1984) were used. Diagnosis was determined through consensus review by three neurologists, one neuropsychologist, and one psychologist. All data from medical history, medical and neurologic examinations, laboratory tests, mental status measures, and informant reports of any changes in functional status and activities of daily living were used for dementia determination.

Neuropsychological assessments

To evaluate cognitive changes in the UCI participants over time, the Rapid Assessment for Developmental Disabilities (RADD) (Walsh et al., 2007), Severe Impairment Battery (SIB) (Saxton et al., 1990), Fuld Object Memory Evaluation (FOME) (Fuld, 1978), Dementia Questionnaire for People with Learning Disabilities (DLD), formerly known as Dementia Questionnaire for Persons with Mental Retardation, Sum of Cognitive Scores (SCS) and Sum of Social Scores (SOS) (Prasher, 1997) neuropsychological assessments were collected at baseline, nine, 18, and 27 months on participants completing the study. All 15 participants had at least two visits (i.e. baseline and nine months), with some participants completing a maximum of four visits. The RADD assesses language, orientation/attention, short-term memory, general

knowledge, arithmetic, and sensorimotor function. The SIB assesses social interaction, short-term memory, orientation/attention, language/reading, general knowledge, and praxis/construction. The FOME assesses naming skills, learning, and short-term memory. The DLD-SCS assesses short-term memory, long-term memory, and spatial and temporal orientation, and the DLD-SOS assesses speech, practical skills, mood, activity and interest, and behavioral disturbance.

The UKY participants completed the SIB, the DLD-SCS and DLD-SOS, as well as the Brief Praxis Test (BPT) (Dalton and Fedor, 1997), which assesses the planning and executing of new motor actions.

MR image acquisition

For the UCI cohort, MRI data were collected using a Philips Achieva 3T scanner at the baseline visit. RsfMRI data were obtained using a T2*-weighted gradient echo echo planar imaging (EPI) sequence with the following parameters: TR=3000 ms, TE=30 ms, flip angle=80°, voxel resolution=3.3×3.3×3.3mm^3, FOV=212x198.75×158.88mm, volumes=200, duration=10.15min. Participants were instructed to keep their eyes open and fixate on a crosshair. Structural MRI data were obtained using a T1-weighted MPRAGE sequence with the following parameters: TR=6.765 ms, TE=3.19 ms, flip angle=9°, voxel resolution=0.94×0.94×1.20mm^3, FOV=270×204×252.295mm.

For the UKY cohort, MRI data were collected using a Siemens TIM 3T scanner at the baseline visit. RsfMRI data were obtained using a T2*-weighted gradient echo EPI sequence with the following parameters: TR=2190ms, TE=27ms, flip angle=77°, voxel resolution=3.5×3.5×3.5mm^3, FOV=224×224×133mm, volumes=182, duration=6.72min. Participants were instructed to keep their eyes open during the scan, though they were not shown a fixation cross. Structural MRI

data were obtained using a T1-weighted MPRAGE sequence with the following parameters: TR=2530ms, TE=2.26ms, flip angle=7°, voxel resolution=1×1×1mm^3, FOV=256×256×256mm.

MR image processing

MRI data were preprocessed using Analysis of Functional NeuroImages (version 19.2.26) (Cox, 1996). UCI and UKY MRI data were preprocessed separately to account for their specific scanning parameters. The standardized afni_proc.py pipeline was used with some minor changes. EPIs were despiked (3dDespike), corrected for slice timing (3dTshift) and motion (3dvolreg), aligned to each subject's skull-stripped MPRAGE (align_epi_anat.py), masked to exclude voxels outside the brain (3dautomask), and smoothed (3dmerge) using a 2mm FWHM Gaussian kernel. Motion correction parameters were saved into text files for later use in linear regression (see Data Analysis). Advanced Normalization Tools (Avants et al., 2011) non-linear registration (antsRegistrationSyN.sh) was used to warp each participant's MPRAGE into the Desikan-Killiany FreeSurfer atlas (Desikan et al., 2006) that was warped to Montreal Neurological Institute (MNI) space. The parameters from these warps were used to warp each participant's EPI to the template space (WarpImageMultiTransform) for group region of interest (ROI) analyses (see Data Analysis).

Extraction of the functional correlations in hemodynamic signals was done using the following as regressors: bandpass filtering between 0.01 and 0.1 Hz, six motion vectors (x, y, z, pitch, roll, yaw) and their derivatives, and first-, second-, third-, and fourth-order polynomials to model temporal drift (3dDeconvolve). Volumes with motion exceeding 1mm of Euclidean norm displacement were censored from analyses as well as the immediately preceding TRs. Motion, both before and after censoring, did not differ between UCI transitioned and non-transitioned participants (**Supplementary Figure B1**). Additionally, global signal from ventricles and white matter was excluded from gray matter voxels using ANATICOR (Jo et al., 2010).

ROI-based functional connectivity analysis was performed using Analysis of Functional NeuroImages (Cox, 1996) for both the UCI and the UKY cohorts. ROIs were defined by the Desikan-Killiany atlas and computed using FreeSurfer (version 6.0; RRID:SCR_001847). The following six Desikan-Killiany ROIs were used as seeds for the six DMN regions: medial orbitofrontal cortex (mOFC), which covers the same anatomical area as the mPFC; ACC, which was created by combining the rostral ACC and caudal ACC ROIs; PCC; isthmus of the cingulate cortex (ICC), also known as the RSC; precuneus; and inferior parietal cortex (IPC), also known as the angular gyrus. Left and right ROIs were averaged to create bilateral ROIs. Time courses were extracted from each ROI (3dmaskave). Pearson correlation coefficients between the residual BOLD time-series of each seed ROI and that of each remaining ROI were calculated (3dTcorr1D) then normalized using the Fisher z-transformation, resulting in a correlation map for each participant.

PET image acquisition and processing

18F-AV-45 PET scans were acquired for 13 of the 15 UCI participants on a High Resolution Research Tomograph (orientation=axial, voxel size=1.2mm^3, matrix size=256×256×207, reconstruction=OP-OSEM3D). Image acquisition followed the ADNI protocol (Landau et al., 2013): 4×5 minute frames collected 50-70 minutes after injection. PET reconstructions were performed with attenuation and scatter correction. Image processing followed the methods described in Keator et al. (2020b), briefly consisting of PET frame realignment and averaging prior to co-registration with their respective MRI scans. The same six bilateral ROIs used in the functional connectivity analysis were used for the PET analysis to detect concurrent Aβ pathology and altered functional connectivity. MRI-derived voxel-weighted standard uptake value ratio (SUVR) averages for each ROI were computed using the cerebellum-cortex

reference region. Partial volume corrected SUVR averages were then computed using PETSurfer (Greve et al., 2016; Greve et al., 2014).

Statistical analysis

All statistical tests were conducted using R (R Core Team, 2022; v3.5.1) and RStudio (RStudio Team, 2022; v1.1.447) software. Results were corrected for multiple comparisons using the false discovery rate (FDR) at $p<0.05$ level of significance. Longitudinal change in neuropsychological measures was calculated for each UCI participant, resulting in a slope that represents the annual change in score. One participant had missing data at one intermediate visit for three of the measures (RADD, SIB, and FOME). These missing data were interpolated based on the participant's scores for these measures from the visits preceding and following the missing visit.

To evaluate the predictive value of baseline DMN functional connectivity on dementia transition in the UCI cohort, decision tree classifiers were trained using scikit-learn, a Python machine learning library. Two-fold stratified cross validation was performed.

3.3. RESULTS

Demographic and neuropsychological data

The UCI transitioned and non-transitioned groups did not differ in mean age at scan, sex, or baseline neuropsychological assessments (**Table 3.1**). However, the transitioned group participants had more visits on average ($t(13)=2.265$, $p=0.041$). The UCI participants, combined across transitioned and non-transitioned groups, were significantly older than the UKY participants ($t(22)=2.767$, $p=0.011$) (**Table 3.2**). The UCI and UKY participants did not differ in sex or baseline neuropsychological assessments.

Table 3.1. UCI participant demographics and neuropsychological test scores

Measure	UCI transitioned group	UCI non-transitioned group	Difference (*p*-value from *t*-test or *z*-test)
n	4	11	n/a
Age at MRI scan, years (SD)	53.03 (6.17)	51.16 (5.24)	0.616
Time between PET scan and MRI scan, years (SD)	1.23 (0.51)	0.91 (0.78)	0.402
Time between MRI scan and transition, years (SD)	0.98 (0.74)	n/a	n/a
Number of visits per participant (SD)	3.50 (0.58)	2.64 (0.67)	**0.041**
Interval between visits, years (SD)	0.84 (0.23)	1.08 (0.42)	0.054
Sex, female (%)	2 (50%)	5 (45%)	1
APOE ε4 (%)	2 (50%)	1 (9%)	0.307
Baseline RADD, total (SD)	56.00 (12.36)	51.00 (13.33)	0.524
Baseline SIB, total (SD)	91.00 (6.16)	89.09 (12.70)	0.705
Baseline FOME, delayed (SD)	8.25 (1.50)	8.55 (1.51)	0.749
Baseline DLD-SCS (SD)	5.50 (5.92)	6.09 (8.70)	0.885
Baseline DLD-SOS (SD)	4.25 (3.59)	4.00 (2.57)	0.904

Table 3.2. UCI and UKY participant demographics and neuropsychological test scores

Measure	UCI cohort	UKY cohort	Difference (*p*-value from *t*-test or *z*-test)
n	15	14	n/a
Age at MRI scan, years (SD)	51.66 (5.34)	44.63 (7.99)	**0.011**
Sex, female (%)	7 (46.67%)	9 (64.29%)	0.562
Baseline SIB (SD)	89.60 (11.14)	88.43 (13.04)	0.798
Baseline DLD-SCS (SD)	5.93 (7.85)	3.57 (5.68)	0.360
Baseline DLD-SOS (SD)	4.07 (2.74)	2.57 (1.74)	0.090

Lower long- but not short-range DMN functional connectivity predicted transition to dementia in DS

The UCI transitioned group had significantly lower functional connectivity between several DMN regions relative to the non-transitioned group (**Figure 3.1**). After correcting for multiple comparisons, three pairs of ROIs remained significant: ACC-IPC ($t(9)=5.185$, $p=0.0085$), ACC-ICC ($t(7)=5.429$, $p=0.0092$), and ACC-Precuneus ($t(8)=3.454$, $p=0.0474$) (**Supplementary Table B1**). All three of these pairs represent connections between distal DMN regions. In contrast, there were no significant group differences in functional connectivity between proximal DMN regions. Motion does not explain group differences in functional connectivity (**Supplementary Figure B2**). A sensitivity analysis excluding the participant who transitioned to dementia two months before their MRI scan was performed, and the same pattern of selectively lower long-range DMN functional connectivity was found in the transitioned group (**Supplementary Table B2**), albeit with a different rank order and with most of the pairs now trending in significance.

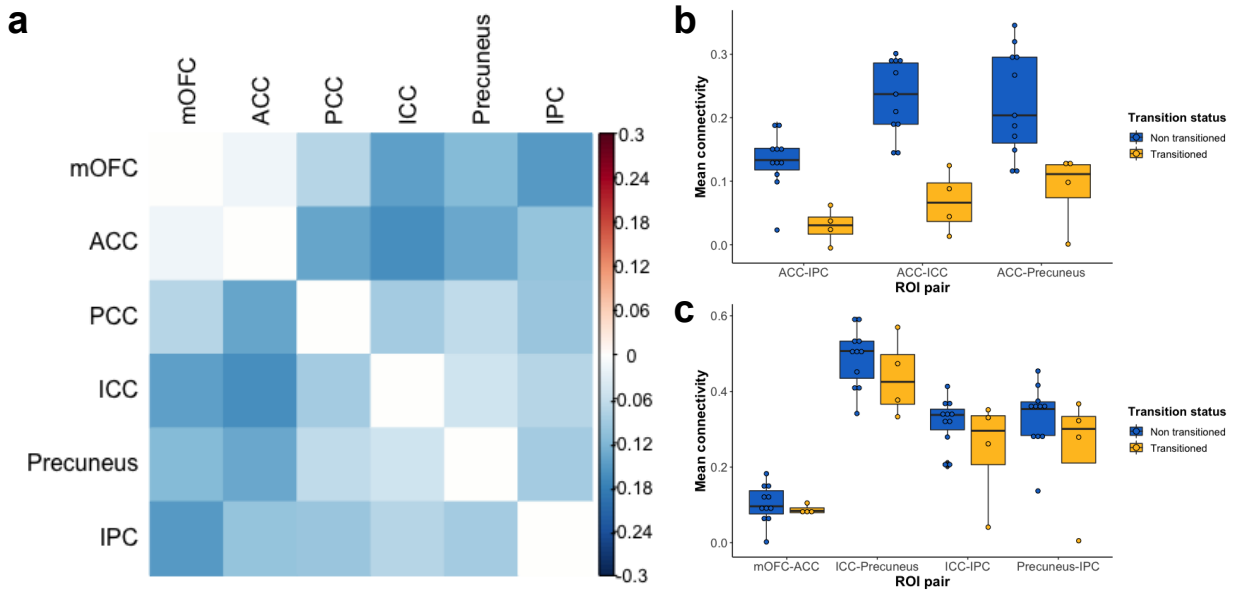

Figure 3.1. Differences in DMN functional connectivity between the UCI transitioned and non-transitioned groups. a) Correlation matrix showing reduced DMN functional connectivity in the transitioned group. Values represented in the matrix are Fisher's z transformed Pearson correlation coefficients between two ROIs. Warmer colors indicate ROI pairs with greater connectivity in the transitioned group, and cooler colors indicate ROI pairs with lower connectivity in the transitioned group. b) Those in the transitioned group have reduced functional connectivity between ACC-IPC, ACC-ICC, and ACC-Precuneus. c) There are no group differences in functional connectivity between short-range pairs of ROIs.

Lower long-range DMN functional connectivity predicted steeper longitudinal cognitive decline in DS

Functional connectivity between ROI pairs that predicted clinical onset of AD in the UCI cohort was significantly associated with longitudinal cognitive decline after adjusting for age and sex. Specifically, lower functional connectivity between ACC-IPC and between ACC-ICC was associated with steeper decline in performance on the SIB across all UCI participants ($F(1,13)=7.728$, $p=0.0156$, and $F(1,13)=7.215$, $p=0.0187$, respectively) (**Figure 3.2**). In addition, there was a trending relationship between lower ACC-Precuneus functional connectivity and steeper decline on the SIB ($F(1,13)=4.455$, $p=0.0547$) (**Figure 3.2**). Additional significant and trending relationships are reported in **Appendix B**, all of which involve long-range pairs of DMN regions (**Supplementary Figure B3, Supplementary Figure B4**). There was no association between baseline cognition and DMN functional connectivity with one exception. Greater PCC-

IPC connectivity was associated with worse performance on the DLD-SOS at baseline, but this association did not differ based on transition status (**Supplementary Table B3**).

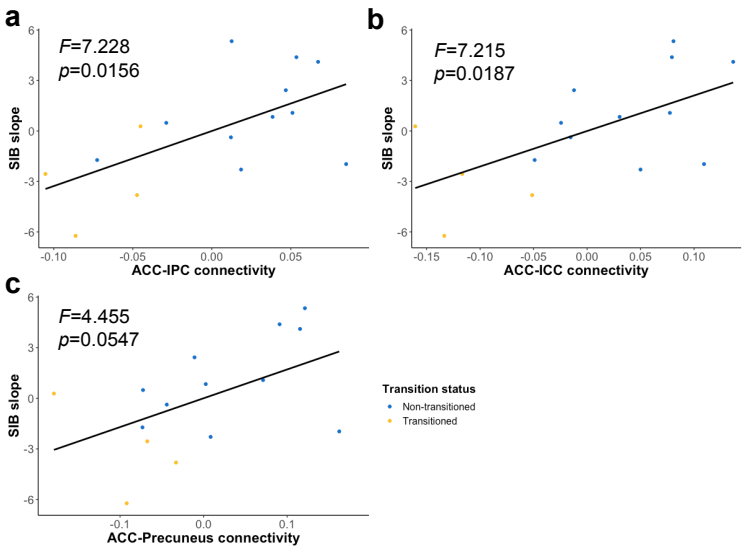

Figure 3.2. Reduced long-range functional connectivity is associated with greater cognitive decline in UCI cohort, as indicated by steeper decline in SIB score during follow-up.

Lower long-range DMN functional connectivity was associated with greater regional Aβ accumulation in inferior parietal cortex

IPC SUVR was negatively associated with functional connectivity between ACC-IPC in the UCI cohort (r=−0.591, p=0.0334) (**Figure 3.3**). There was a marginally significant negative relationship between IPC SUVR and mOFC-IPC functional connectivity (r=−0.544, p=0.0545). ACC SUVR was not associated with ACC-IPC functional connectivity (r=−0.384, p=0.1949), nor was mOFC SUVR associated with mOFC-IPC functional connectivity (r=−0.315, p=0.2946). Regional SUVR averages for each group are reported in **Appendix B** (**Supplementary Table B4).**

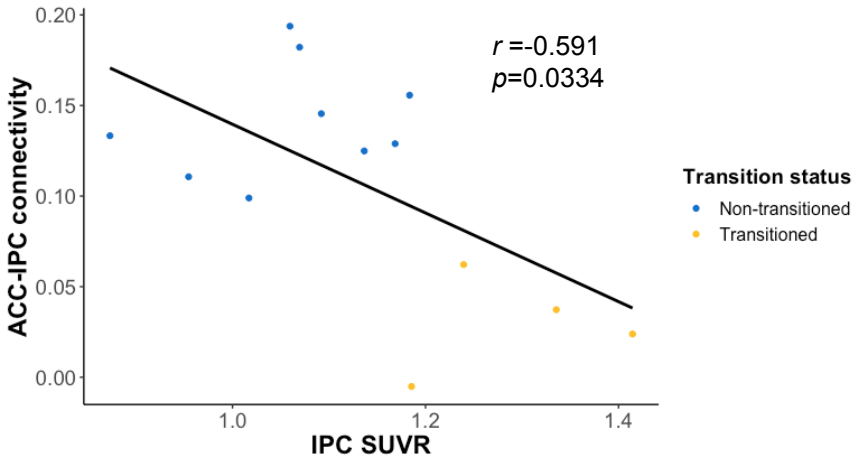

Figure 3.3. In the UCI cohort, reduced functional connectivity between ACC-IPC is associated with greater Aβ accumulation in IPC, as indicated by greater IPC SUVR.

Lower long-range DMN functional connectivity was not explained by age differences

DMN functional connectivity in two cohorts that differed in participant age were compared, with the UKY cohort being significantly younger than the UCI cohort (**Table 3.2**). For long-range functional connectivity, UCI transitioned participants fell outside of the distribution of the UKY participants, but UCI non-transitioned participants fell primarily within the UKY distribution (**Figure 3.4a, Supplementary Table B5, Supplementary Table B6**). However, for short-range functional connectivity, both transitioned and non-transitioned participants fell within the UKY distribution (**Figure 3.4b, Supplementary Table B5, Supplementary Table B6**).

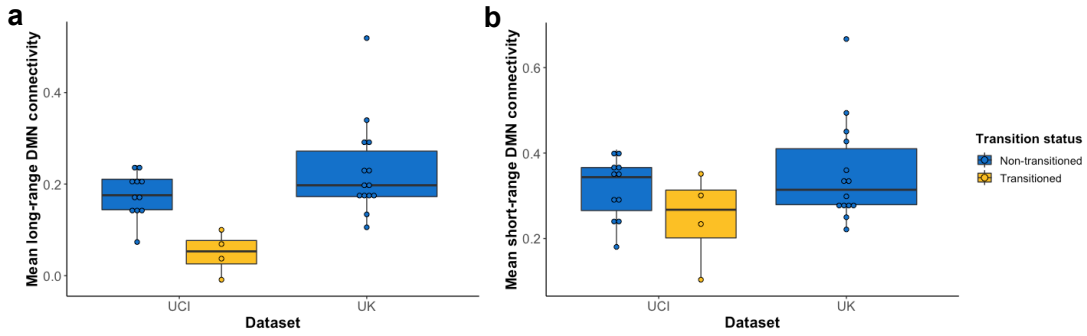

Figure 3.4. Distribution of mean functional connectivity values separated by dataset and transition status. a) Long-range DMN functional connectivity values of those in the transitioned group fall outside the distributions of the non-transitioned group and the younger UKY cohort. However, the non-transitioned group falls within the UKY cohort's distribution of functional connectivity values. b) Short-range DMN functional connectivity values of those in the transitioned group fall within the distributions of the non-transitioned group and the younger UKY cohort.

Classification of future transition to dementia using long-range DMN functional connectivity

We evaluated whether the trained decision tree classifiers could discriminate between UCI participants who transitioned to dementia and UCI participants who remained CS using the three long-range DMN pairs individually as well as combined in one model (**Table 3.3**). We found that functional connectivity between all three pairs (ACC-IPC, ACC-ICC, ACC-Precuneus) performed reasonably well across all four metrics (i.e. sensitivity, specificity, accuracy, area under the receiver operating characteristic [AUC]) when evaluated individually (AUC=0.79-0.96). Classifier performance was comparable when these three variables were evaluated together (AUC=0.79), and after the linear effects of age were removed, the combined model performance improved across all metrics (AUC=0.83) (**Table 3.3, Figure 3.5**).

Table 3.3. Decision tree classifier results

Pairwise functional connectivity	Sensitivity	Specificity	Accuracy	AUC
ACC-IPC	0.94	0.83	0.94	0.96
ACC-ICC	0.80	0.75	0.80	0.79
ACC-Precuneus	0.88	0.75	0.88	0.91
ACC-IPC + ACC-ICC + ACC-Precuneus	0.80	0.75	0.80	0.79
ACC-IPC + ACC-ICC + ACC-Precuneus (+ age as a nuisance variable)	0.87	0.83	0.87	0.83

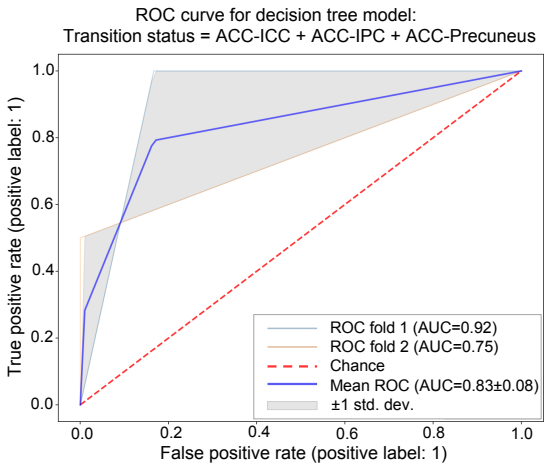

Figure 3.5. Mean ROC curve for a decision tree classifier model that includes all three long-range DMN pairs (ACC-ICC, ACC-IPC, ACC-Precuneus) as independent variables as well as age as a nuisance variable.

3.4. DISCUSSION

The present study investigated whether preclinical changes to resting state functional connectivity within the DMN predicted future conversion to dementia in people with DS. Lower connectivity between long-range but not short-range pairs of DMN regions predicted clinical onset of dementia, predicted steeper cognitive decline, and was associated with greater regional Aβ accumulation in the IPC. People with DS who did not transition to dementia maintained a degree of long-range DMN connectivity comparable to a younger group of CS people with DS. This lack of difference in long-range DMN functional connectivity in older versus younger CS individuals with DS supports our interpretation that the lower long-range DMN connectivity in AD-DS transitioners is associated with AD and not aging.

Results from the present study demonstrate that loss of long-range DMN functional connectivity precedes clinical onset of AD by at least one year and predicts global cognitive decline in people with DS. The results are generally consistent with previous studies in neurotypical older adults at risk for AD showing reduced DMN functional connectivity (Mormino et al., 2011; Chhatwal et al., 2013; Lim et al., 2014; Thomas et al., 2014). However, one study reported increased connectivity between anterior and posterior DMN in individuals with sporadic AD

(Jones et al., 2016). This lack of agreement could reflect dynamic changes in long-range DMN connectivity depending on disease stage and may highlight divergence in AD-DS compared to sporadic AD. Given that lower functional connectivity between anterior-posterior DMN regions has previously been observed in CS individuals with DS relative to age-matched neurotypical controls (Rosas et al., 2021), the findings suggest that AD further lowers long-range DMN functional connectivity beyond its typical level in DS. Additionally, a recent study reported that individuals with DS diagnosed with AD had decreased alpha coherence, an EEG-based metric of functional connectivity, in fronto-parietal connections compared to similarly-aged CS individuals with DS (Musaeus et al., 2021). This could serve as additional evidence of decreased long-range connectivity in clinical AD-DS, though it is unclear whether this observed activity originated in DMN brain regions per se due to the limited spatial resolution of EEG.

The finding that loss of ACC-IPC connectivity is associated with greater Aβ PET SUVR in the IPC is in line with previous work showing that Aβ accumulation in DS mirrors findings in sporadic AD, affecting frontal, temporal, parietal, and cingulate cortices, and precuneus, though binding in the striatum is unique to DS and ADAD (Hartley et al., 2017; Keator et al., 2020a; Keator et al., 2020b; Sabbagh et al., 2015; Annus et al., 2016). Increased Aβ is also associated with regional hypometabolism (Sabbagh et al., 2015; Lao et al., 2018) and reduced memory and executive functioning (Hartley et al., 2017; Keator et al., 2020a; Keator et al., 2020b). In the present study, the SUVRs in all of the DMN regions studied, with the exception of the IPC, were elevated for participants in both groups, greater than the standard SUVR threshold of 1.1 for Aβ positivity (Joshi et al., 2012). This suggests that Aβ accumulation in the DMN occurs at an earlier preclinical stage than changes to resting state functional connectivity.

Taken together, these findings suggest that disruption to functional connectivity between distal nodes of the DMN can indicate imminent progression to clinical AD in CS individuals with DS.

CHAPTER 4: MEDIAL TEMPORAL LOBE FUNCTIONAL CONNECTIVITY CHANGES DURING CLINICAL PROGRESSION OF AD IN PEOPLE WITH DS

4.1. INTRODUCTION

Hyperphosphorylated tau protein is hypothesized to spread in an activity-dependent "prion-like" manner along neuronal connections (Franzmeier et al., 2019). In sporadic AD, there is evidence that tau pathology propagates along intrinsic functional networks of the brain, particularly the MTL, and that hyperexcitability within the MTL may be related to increased local tau deposition (Pasquini et al., 2019, Adams et al., 2019). MTL hyperconnectivity is observed during MCI, is associated with impaired episodic memory, and is followed by hypoconnectivity in dementia (Pasquini et al., 2019; Pasquini et al., 2015). However, MTL intrinsic connectivity at different clinical stages of AD and its relationship to memory has not yet been investigated in DS. We hypothesized that increased MTL functional connectivity would coincide with MCI-DS onset, memory loss, and tau PET binding in early Braak stage regions in people with DS.

4.2. MATERIALS AND METHODS

Participants

As in **Chapter 2**, the present study included ADDS participants age 40 and older who completed an MRI scan at their baseline visit (see 2.2. Materials and methods, **Participants**). Data were collected at CU, MGH, and UCI. Some participants additionally completed memory assessments at their baseline visit and had tau PET data collected at their second visit, approximately 16 months after their baseline visit. All research procedures were reviewed and approved by the Institutional Review Boards of all collaborating institutions, and informed consent, as well as assent, was obtained from all participants and their legally authorized representatives. All participants were reimbursed for their participation.

Determination of MCI/AD clinical status

Each participant's MCI/AD clinical status was determined using the same approach described in **Chapter 2** (see 2.2. Materials and methods, **Determination of MCI/AD clinical status**). The three diagnosis groups included in the sample were CS, MCI-DS, and DEM. The DEM group includes participants with possible and definite dementia, which were combined for the purposes of analysis.

Memory assessments

Episodic memory was assessed using the mCRT, described in **Chapter 2** (see 2.2. Materials and methods, **Memory assessment**), and a modified version of the Selective Reminding Test (mSRT) validated for use in people with intellectual disability. Like the mCRT, the mSRT is sensitive to preclinical AD in people with DS (Krinsky-McHale et al., 2002; Kittler et al., 2006). Participants were given one of two versions of the mSRT, one involving animals or one involving food. During encoding, eight items from one of these categories were read aloud to the participant. For immediate recall, participants were asked to freely recall all eight items in any order. This was repeated for three trials for a maximum score of 24. Items not recalled on the immediately preceding trial were read aloud before the next trial of immediate recall began. After a ten minute delay, participants were asked to freely recall all eight items in any order, for a maximum delayed recall score of 8. Both immediate and delayed recall were used as memory outcome measures from the mSRT. Due to the dependence of CRS on FRS, only FRS and TRS were used as memory outcome measures from the mCRT.

MR image acquisition

Four protocols were used to collect MRI data: initially each site used its own protocol, then all sites transitioned to a harmonized protocol mid-way through data collection. Scanners at all sites were equipped with 32-channel coils, and both T1-weighted MPRAGE and T2*-weighted

gradient echo EPI sequences were collected. At all sites participants were instructed to keep their eyes open and fixate on a crosshair during the rsfMRI sequence.

Data from the unique CU protocol were collected on a Philips Achieva 3T scanner. The parameters for the structural MRI sequence were: TR=6.8ms, TE=3ms, flip angle=9°, voxel resolution=1×1×1.2mm^3, FOV=256×256×170mm. The parameters for the rsfMRI sequence were: TR=3000ms, TE=30ms, flip angle=80°, voxel resolution=3.3×3.3×3.3mm^3, FOV=256×256×192mm, volumes=150, duration=7.5min.

Data from the unique MGH protocol were collected on a Siemens Prisma 3T scanner. The parameters for the structural MRI sequence were: TR=2510ms, TE=1.69/3.55/5.71/7.27ms, flip angle=7°, voxel resolution=1×1×1mm^3, FOV=256×256×176mm. The parameters for the rsfMRI sequence were: TR=5000ms, TE=31ms, flip angle=90°, voxel resolution=2×2×2mm^3, FOV=256×256×150mm, volumes=82, duration=7.37min.

Data from the unique UCI protocol were collected on a Philips Achieva 3T scanner. The parameters for the structural MRI sequence were: TR=7.8ms, TE=3.6ms, flip angle=7°, voxel resolution=1×1×1mm^3, FOV=256×256×176mm. The parameters for the rsfMRI sequence were: TR=5000ms, TE=30ms, flip angle=90°, voxel resolution=2×2×2mm^3, FOV=256×256×140mm, volumes=150, duration=12.75min.

Data from the harmonized protocol were collected on a Siemens Prisma 3T scanner. The parameters for the structural MRI sequence were: TR=2300ms, TE=2.96ms, flip angle=9°, voxel resolution=1×1×1mm^3, FOV=256×240×208mm. The parameters for the rsfMRI sequence were: TR=1250ms, TE=30ms, flip angle=90°, voxel resolution=2.4×2.4×2.4mm^3, FOV=216×216×136.8mm, volumes=408, duration=8.5min.

MR image processing

MRI data were processed using the CONN Toolbox (v.20.b) (Whitfield-Gabrieli and Nieto-Castanon, 2012) implemented in MATLAB 2018a and SPM12. The default MNI preprocessing pipeline was used: slice time correction=interleaved bottom-up, global signal z-value threshold=3, motion threshold=0.5 mm, initial dummy scans dropped=4, tissue probability map=default, structural target resolution=1mm^3, functional target resolution=2mm^3, bounding box=[-90 -126 -72;90 90 108], Gaussian smoothing kernel=5mm full width at half maximum). The MPRAGE was skull-stripped, masked to exclude voxels outside the brain, centered, normalized to MNI space, and segmented into gray matter, white matter, and CSF. After initial dummy scans were discarded, the EPI was centered, slice-time corrected, realigned to the MPRAGE and unwarped, segmented, normalized to MNI space, and smoothed. First-order derivatives (i.e., scan-to-scan differences) were used to determine participants' global signal and movement values. A single composite motion measure based on the three translation (i.e., x, y, z) and three rotation parameters (i.e., roll, pitch, yaw) was used to calculate framewise displacement. Timepoints exceeding the global signal z-value or motion thresholds were removed. Participants whose EPI scans had the same TR (i.e., 1250ms, 3000ms, 5000ms) were preprocessed together, and the resulting files for all participants across sites and protocols were concatenated for initial quality control, denoising, post-denoising quality control, and first-level analysis.

Quality assurance plots were generated and visually inspected to ensure proper normalization and registration of structural and functional scans and to determine whether a sufficient number of volumes (equivalent to 3.5 minutes) remained following global signal z-value and motion scrubbing. Participants who did not meet these criteria were excluded. The selection of 3.5 minutes as the threshold was data-driven with the intention of maximizing the number of eligible participants while minimizing the impact of head motion. Denoising of preprocessed signals was

done using despiking, bandpass filtering (0.01-0.1Hz), and linearly detrending. The CONN Toolbox Anatomical aCompCor method was used to remove noise sources from white matter and CSF. Associations between functional connectivity and both global signal and motion had a minimum of 95% match with the null hypothesis, indicating no relationship between connectivity and quality control measures.

The ROIs were left and right alEC, pmEC, PHC, and PRC (Reagh et al., 2018). Time courses were extracted from each ROI. Pearson correlation coefficients between the residual BOLD time-series of each seed ROI and that of each remaining ROI were calculated then normalized using the Fisher z-transformation, resulting in a correlation map for each participant. Diagnosis group differences in ROI-to-ROI functional connectivity was calculated using multivariate parametric general linear model analysis. The CONN standard criterion for thresholding ROI-to-ROI parametric maps was used, which is a FDR-corrected $p<0.05$ cluster-level threshold and a post-hoc uncorrected $p<0.05$ connection-level threshold.

PET image acquisition and processing

18F-AV-1451 PET scans were acquired at the second visit on a Siemens HR+ scanner at CU and MGH (voxel size=5mm^3) and a High Resolution Research Tomograph scanner at UCI (voxel size=3mm^3). UCI PET scans underwent 2mm of smoothing to match the other sites' scan resolution. 5-minute frames were collected for 80-100 minutes after injection. Data were reconstructed using iterative methods and corrected for deadtime, normalization, attenuation, scatter, and radioactive decay. PET data images were examined, and if necessary, corrected on a frame-by-frame basis for motion. The multi-frame images were then averaged to produce a single frame image representing uptake over the post-injection time. T1-weighted MR images were manually reoriented along the anterior-posterior commissure. The single-frame PET images were then registered to the reoriented MRI using PMOD software via maximization of

normalized mutual information. MRI-derived voxel-weighted SUVR averages for six regions corresponding to Braak stages I-VI were computed using cerebellar gray matter as the reference region. The Braak regions were defined as follows: I) EC, II) hippocampus, III) PHC, fusiform gyrus, lingual gyrus, and amygdala, IV) inferior temporal gyrus, middle temporal gyrus, temporal pole, thalamus, ACC, ICC, PCC, and insula, V) inferior frontal gyrus, middle frontal gyrus, superior frontal gyrus, inferior parietal gyrus, superior parietal gyrus, supramarginal gyrus, lateral occipital cortex, transverse temporal gyrus, superior temporal gyrus, precuneus, banks of the superior temporal sulcus, nucleus accumbens, caudate, putamen, and pallidum, and VI) precentral gyrus, postcentral gyrus, paracentral gyrus, cuneus, and pericalcarine cortex. Partial volume corrected SUVR averages were then computed to account for choroid plexus related off-target binding and extra cortical hotspots (Baker et al., 2017).

Statistical analysis

All statistical tests were conducted using R (R Core Team, 2022; v3.5.1) and RStudio (RStudio Team, 2022; v1.1.447) software. Associations between functional connectivity measures, memory performance, tau PET SUVRs were tested using Pearson partial correlation and were restricted to CS and MCI-DS individuals. Reported results were considered significant at $\alpha<0.05$, after correcting for multiple comparisons using the Holm method (Holm, 1979). All models included age, sex, and site as covariates.

4.3. RESULTS

Demographic and neuropsychological data

An initial sample of 110 participants had MRI data at their baseline visit (CU *n*=11, MGH *n*=51, UCI *n*=48). 31 participants did not pass processing quality control procedures (<3.5 minutes of valid volumes), and 4 participants were missing diagnosis data, leaving a total sample of 75

participants. Demographic information for this sample is summarized in **Table 4.1**. One participant was 31 years old, but all other participants were between 40 and 67 years old. Of those 75 participants, 67 had mCRT and mSRT data at their baseline visit. Of those 75 participants, 29 had tau PET data. The distribution of participants across sites was as follows: CU *n*=7; MGH *n*=37; UCI *n*=31.

Table 4.1. Participant demographics

Variable	CS	MCI-DS	DEM	Total
n	48	16	11	75
Age at scan (SD, range)	48.0 (6.1, 31-66)	50.8 (4.2, 45-59)	57.2 (6.6, 47-67)	50.0 (6.6, 31-67)
Sex, female (%)	20 (42%)	3 (19%)	4 (36%)	27 (36%)
mCRT, *n* (%)	45 (94%)	15 (94%)	7 (64%)	67 (89%)
mSRT, *n* (%)	47 (98%)	15 (94%)	10 (91%)	72 (96%)
Tau PET, *n* (%)	20 (42%)	8 (50%)	1 (9%)	29 (39%)

Greater functional connectivity within the MTL in individuals with MCI-DS compared to CS individuals

We found that individuals with MCI-DS had greater intrinsic connectivity between right pmEC and right PRC as well as between left pmEC and right pmEC compared to CS individuals with DS (**Figure 4.1**). We did not observe a difference in within-MTL connectivity between the MCI-DS and dementia groups or between the CS and dementia groups.

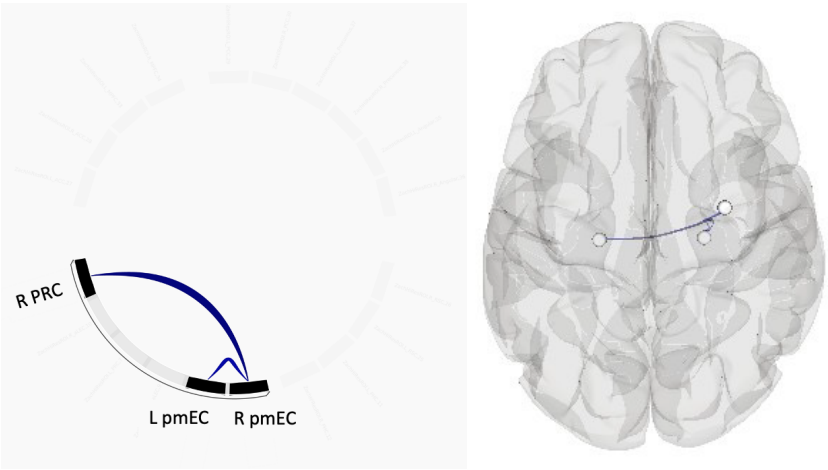

Figure 4.1. Greater MTL functional connectivity in MCI-DS relative to CS individuals with DS.

Greater MTL functional connectivity is associated with worse memory recall

We found a negative association between right pmEC connectivity with right PRC and total recall score on the mCRT (r=-0.26, p=0.049) (**Figure 4.2b**). Right pmEC-right PRC connectivity also had a trending association with delayed recall score on the mSRT (r=-0.25, p=0.059) (**Figure 4.2d**), but had no association with mCRT free recall score (r=-0.19, p=0.152) or mSRT immediate recall score (r=-0.19, p=0.154) (**Figure 4.2a,c**). No associations were observed between left pmEC-right pmEC connectivity and any of the memory measures (all p-values > 0.2).

Greater MTL functional connectivity may be associated with greater tau accumulation in the hippocampus

We observed a trending positive association between right pmEC connectivity with right PRC and tau in Braak stage II, which is the hippocampus (r=0.31, p=0.134) (**Figure 4.3b**). There was no association between right pmEC-right PRC connectivity and Braak stage I or III-VI tau (**Figure 4.3a,c,d,e,f**), or between left pmEC-right pmEC connectivity and Braak stage I-VI tau (all p-values > 0.2).

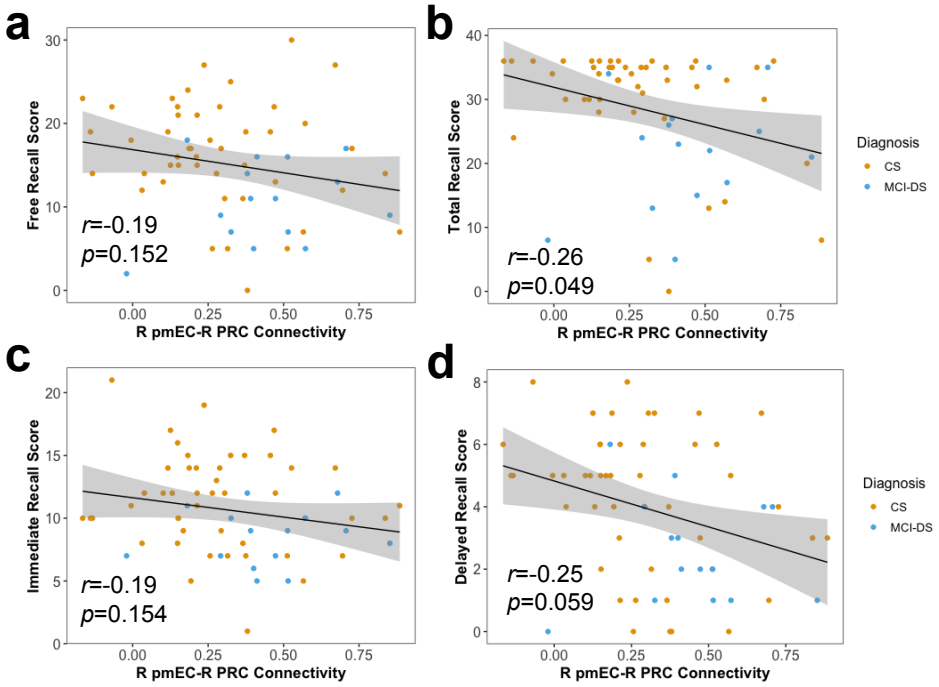

Figure 4.2. (b) Greater right pmEC-right PRC functional connectivity is associated with lower mCRT total recall score. (d) There was a trending relationship with mSRT delayed recall score. (a,c) There was no association with mCRT free recall score or mSRT immediate recall score.

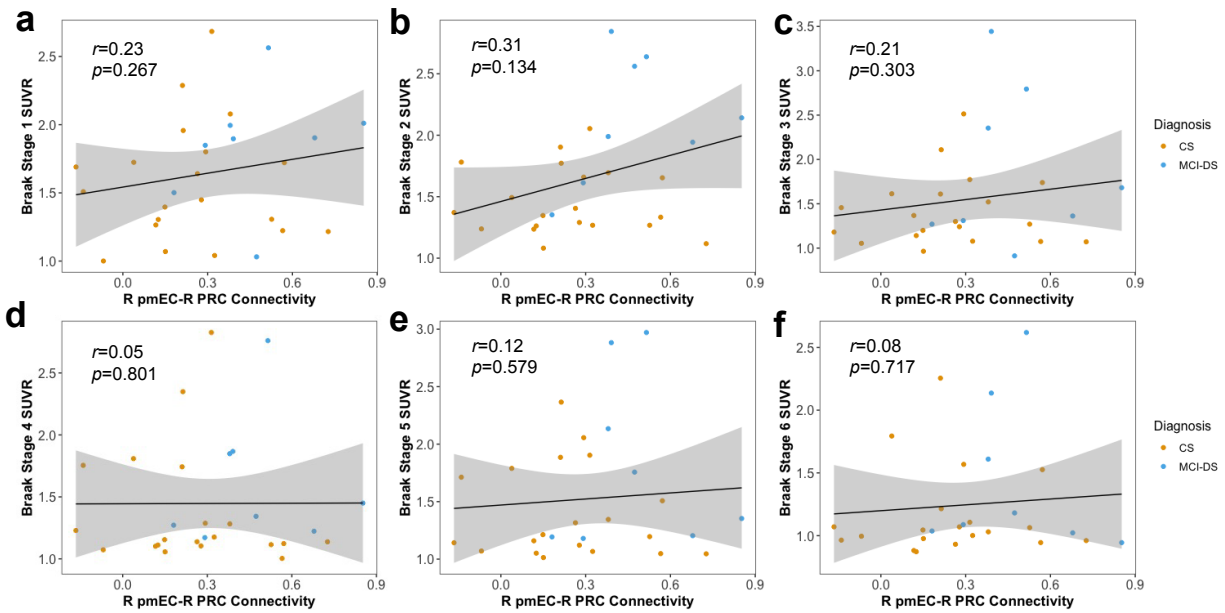

Figure 4.3. (b) Trending positive association between right pmEC-right PRC and hippocampus tau. (a,c,d,e,f) There was no association with tau in any other Braak stage region.

4.4. DISCUSSION

The goal of this study was to test whether the U-shaped pattern of MTL functional connectivity would be present across MCI/AD clinical stages in DS. We hypothesized that MCI-DS individuals would have MTL hyperconnectivity relative to CS individuals, and this hyperconnectivity would be associated with impaired episodic memory and increased tau accumulation in early Braak stage regions. As expected, MCI-DS individuals exhibited greater connectivity between right pmEC and right PRC, as well as between right pmEC and left pmEC, suggesting vulnerability of these MTL regions important for memory during the transition to MCI-DS. We believe this is the first reported observation of MCI-associated MTL hyperconnectivity in people with DS, replicating findings in neurotypical individuals with MCI (Pasquini et al., 2015). There was no difference in MTL intrinsic connectivity between the CS and dementia groups, which could indicate MTL connectivity might begin to decline in dementia in DS, which is observed in sporadic AD (Pasquini et al., 2019).

Right pmEC-right PRC connectivity alone was negatively associated with mCRT total recall score and had a trending positive association with tau in the hippocampus, similar to prior work in neurotypical individuals (Adams et al., 2019). However, these relationships were modest. Due to the nonlinear trajectory of MTL functional connectivity across clinical diagnosis groups, individuals with dementia were excluded from this part of the analysis, further reducing the already undersized sample with memory measures (*n*=60-62) and tau PET measures (*n*=28), thereby limiting statistical power. Taken together, these data provide preliminary evidence in support of MTL functional connectivity as an indicator of AD progression in people with DS.

CHAPTER 5: SYNTHESIS AND FUTURE DIRECTIONS

5.1. GENERAL SUMMARY

The chief goal of this dissertation was to identify the neurobiological indicators other than Aβ and tau, particularly neuroanatomy and brain network organization, that predict and co-occur with clinical AD in people with DS. We undertook a series of investigations to establish relationships among markers of neurodegeneration, functional connectivity, MCI/AD clinical diagnosis, and neuropsychological measures of cognitive impairment and decline. We found that several MRI-based measures of MTL and DMN structure and function are sensitive to preclinical and early clinical stages of AD in DS, demonstrating their potential as relevant biomarkers in this population.

Medial temporal lobe neurodegeneration coincides with clinical memory impairment

In **Chapter 2**, we showed that individuals with DS who have dementia have greater atrophy in the hippocampus and left alEC and greater levels of plasma NfL compared to CS individuals and those with MCI-DS. However, none of these measures differed between CS and MCI-DS individuals, suggesting that MTL neurodegeneration occurs in tandem with, rather than prior to, symptomatic AD in people with DS. Focal neurodegeneration in the hippocampus and left alEC and elevated plasma NfL concentration were associated with impaired episodic memory, adding further support for MTL neurodegeneration taking place around the time of AD clinical manifestation in DS. Although brain atrophy is considered a late manifestation of AD and reflects extensive neurodegeneration, it remains an important AD biomarker and illustrates similarities between AD-DS and sporadic AD (Janelidze et al., 2022; Benejam et al., 2022; Mattsson et al., 2019; Chen et al., 2021).

EC thickness is an emerging AD biomarker (Mielke et al., 2019), though evidence of differential vulnerability along the left/right and anterolateral/posteromedial axes is limited. Here, we

observe a specific relationship between left alEC thickness and clinical outcome measures. In sporadic AD, gray matter loss occurs earlier and progresses faster in the left hemisphere (Lubben et al., 2021), and the alEC is more susceptible to atrophy in the presence of AD pathology (Holbrook et al., 2020; Khan et al., 2014). This asymmetric vulnerability to neurodegeneration within the EC does not appear to be unique to people with DS.

It is not clear whether plasma NfL concentrations increase downstream of gray matter loss. In neurotypical individuals across the AD spectrum, higher baseline plasma NfL predicts faster EC thinning and hippocampal volume loss, but smaller baseline EC thickness and hippocampus volume also predict faster increase in plasma NfL levels (Mattsson et al., 2019). Wallerian degeneration, or anterograde axonal degeneration down the length of the axon, is hypothesized to occur following gray matter loss (Alves et al., 2015). The release of NfL into CSF and blood occurs as a direct result of axon degeneration (Krauss et al., 2020). Given that hippocampus and EC atrophy begin early in AD, initial increases in plasma NfL may serve as a downstream biomarker of AD-related gray matter loss. Our mediation findings involving plasma NfL and MTL atrophy suggest that they are part of a shared neurodegenerative pathway in AD-DS.

Default mode network connectivity declines just prior to dementia

In **Chapter 3**, we provided evidence that diminished long-range DMN intrinsic connectivity was present in CS individuals with DS up to one year before they were diagnosed with dementia and predicted steeper cognitive decline. These findings are consistent with observations of reduced DMN functional connectivity in neurotypical older adults with preclinical AD (Mormino et al., 2011; Lim et al., 2014). In this study, short-range DMN connectivity did not predict dementia diagnosis in people with DS. However, distinctions between long- and short-range connectivity generally have not been reported in sporadic AD. It is possible that connectivity between more proximal DMN hubs is affected later in AD progression in people with DS. Overall, these results

support the potential use of reduced long-range DMN functional connectivity as a preclinical biomarker, enabling more sensitive detection of AD-DS in its earlier stages (Jack et al., 2018).

Loss of long-range DMN functional connectivity, specifically between the ACC and IPC, was linked to greater Aβ deposition in the IPC. Aβ preferentially accumulates in the DMN, and its presence is associated with local hypometabolism and impaired cognition in both AD-DS and sporadic AD (Keator 2020b; Lao et al., 2018; Mevel et al., 2011). Due to the lifelong accumulation of Aβ pathology, nearly all people with DS are expected to be Aβ positive by the age of 40. Given these circumstances, the spatial distribution of Aβ, rather than Aβ positivity, may be more relevant to the development of clinical AD in this population (Keator et al., 2020b). Ultimately, the overlap between regional Aβ deposition and disrupted organization of the DMN reveals that this network is uniquely vulnerable to AD pathology and plays a vital role in AD pathogenesis. Based on our work, we conclude that preclinical loss of resting state functional connectivity within distal hubs of the DMN is a robust predictor of progression to dementia in people with DS.

Clinical AD stage specific pattern of medial temporal lobe connectivity

In **Chapter 4**, we found that transient changes in MTL functional connectivity are present in DS and are related to diagnosis, memory loss, and pathological tau accumulation in DS. These results are consistent with the theory that MTL hyperconnectivity occurs during MCI and then reverts to hypoconnectivity as AD clinical symptoms progressively worsen (Pasquini et al., 2019). Resting state functional connectivity reflects the brain's intrinsic organization rather than task-based activity. Even so, we observed that MTL hyperconnectivity is linked to worse verbal episodic memory across both MCI-DS and CS individuals with DS, both of which may be due to underlying MTL hyperexcitability. Anti-epileptic medication can reverse MTL excitability and rescue memory function in neurotypical individuals with MCI (Bakker et al., 2012), lending

further support to this hypothesis. This hyperexcitability could be driven by neuronal sprouting in hippocampus, which has been posited as a compensatory response to dysfunction and cell loss in the entorhinal cortex (Haier et al., 2003; Head et al., 2007) and may be associated with tau (Head et al., 2003).

The trending positive association between right pmEC-right PRC connectivity and hippocampal tau may hint that MTL connectivity and tau deposition are linked. The EC and PRC are both considered part of Braak stage I, and tau is known to originate in these brain regions and spread out to the cortex via the hippocampus (Braak et al., 2006). One important caveat of these findings is that the [18F]AV-1451 tau PET tracer is known to have off-target binding spill-in from the choroid plexus to the hippocampus due to their proximity (Baker et al., 2017). We attempted to minimize the effects of this binding by using partial volume corrected SUVRs, but it is possible some additional spurious binding remained in the hippocampus. [18F]MK-6240 is considered the preferred tau PET tracer for research on MTL tau since it does not exhibit off-target binding in neighboring regions (Betthauser et al., 2019).

Based on the findings we have presented, we believe that organizational alterations in the MTL network coincide with distinct stages of AD clinical impairment in DS. More evidence is needed to support the theory of network-based tau spread in people with DS. If true, it would underscore functional connectivity as a potential mechanism facilitating the progression of tau pathology in AD-DS.

5.2. FUTURE DIRECTIONS

Limited sample size

The field recognizes the value of data collected in people in DS. However, the sample sizes of the studies presented in this dissertation are relatively small and imbalanced across MCI/AD diagnosis groups due to a number of factors, including missing and low-quality data. Unfortunately, this is a common phenomenon when working with data from a clinical population. A modest sample size limits the statistical tests that can be performed and the number of variables that can be accounted for during analysis. This has consequences for machine learning approaches, which are powerful but rely on sizable training and test datasets for optimal performance. It would be important for future studies to maximize sample size to increase statistical power and enable machine learning models to make robust predictions of disease classification. The ABC-DS study was recently established to collect a rich, standardized, longitudinal dataset of several hundred people with DS (Handen, 2020). This larger dataset can be used to replicate the work presented here.

Longitudinal studies

Cross-sectional analysis cannot be used to establish causation or track an individual's trajectory over time. For instance, we cannot determine which comes first, increased plasma NfL levels or atrophy in the aIEC and/or hippocampus, without the use of longitudinal data. In DS, there is a well-defined ~15-year period that can capture both preclinical pathological changes and the initial onset of clinical symptoms. Future studies should be conducted on longitudinal datasets, such as ABC-DS, to investigate disease-related changes that predict dementia and improve earlier detection of AD.

Aβ and tau biomarkers

Given that the DMN and MTL are the earliest sites of Aβ and tau pathology, respectively, future work should utilize repeated measures of concurrent MRI and PET imaging to determine the spatiotemporal overlap between neurodegeneration, functional connectivity changes, and AD pathology accumulation in these two networks *in vivo*. This will be possible using the ABC-DS dataset, which includes, and FDG PET imaging collected across multiple visits. There should be emphasis on creating composite MRI and PET biomarkers, which will improve diagnostic classification and prediction of cognitive decline in DS.

Vascular and immune contributions

In addition to Aβ and tau pathologies of AD, cerebrovascular pathology, white matter pathology, neuroinflammation, and oxidative damage are also implicated in AD-DS pathophysiology (Lott and Head, 2019). Each of these processes may interact with the neurodegenerative and functional brain network pathways we have reported. Commonly co-occurring medical conditions such hypothyroidism, obesity, and obstructive sleep apnea may contribute to heterogeneity in the age of onset and/or the rate of progression of clinical AD in people with DS. Future work should investigate how vascular and immune dysfunction modifies the AT(N) framework in this population.

Disability and age confounds in DS

We did not adjust for severity of intellectual disability, which could impact cognitive performance independent of dementia (Krinsky-McHale et al., 2020). Future studies should include intellectual disability as a covariate. An additional confound to consider is age. The strong age-dependent progression of AD pathology in DS makes it challenging to separate the effects of AD from those of age alone, as these processes are inherently interrelated. We controlled for age in all of our analyses and even assessed relationships between age and our variables of

interest in some instances. Future work should aim to disentangle age from AD so that disease-specific biomarkers with high diagnostic accuracy can be identified.

Influence of motion on rsfMRI data

It is notoriously difficult to collect high quality neuroimaging data in older people with DS. Inherent characteristics of this population, namely developmental disability, age, and preclinical disease, lead to increased motion in the scanner (Neale et al., 2018), which may render some of the neuroimaging data – particularly the rsfMRI data – unusable by creating spurious yet systematic correlations (Lao et al., 2019; Power et al., 2012). A motion censor threshold of 0.2-0.3mm is generally recommended for young, healthy populations to prevent motion from influencing the resulting functional connectivity maps (Power et al., 2014). However, a more lenient threshold (0.5-1mm), in line with prior rsfMRI studies in DS (Wilson et al., 2019; Koenig et al., 2021a), was chosen as an exclusion criterion for the present work to conserve as much resting state data as possible from this special population on whom limited data are even available. We performed post-hoc tests to determine the relationship between motion that survived the threshold and the variables of interest and found no association. It is possible that this approach did not fully control for motion artifacts, but we are assured by the convergent evidence linking functional connectivity to cognition and AD pathology, both of which lend additional support to our conclusions that the connectivity effects we observed are related to AD rather than head motion. Still, a top priority for research in DS should be to prevent head motion in the first place through the use of MRI head coils with a snug yet comfortable fit.

An additional consequence of motion censoring is that it reduces the number of functional volumes that can be analyzed. Canonical resting state networks such as the DMN can be reliably detected at the group level with a scan as short as 5 minutes (Fox et al., 2005; Van Dijk et al., 2010; O'Connor and Zeffiro, 2019). After motion censoring, the resting state data

presented in **Chapter 3** meet this convention, but the data from **Chapter 4** are just shy of it at 3.5 minutes. Setting the threshold to 5 minutes would have resulted in the exclusion of more than half of the participants in that study. However, we are confident that we captured true MTL functional connectivity in that sample due to its associations with diagnosis and memory performance. Increasing the scan length and sampling at a faster rate (i.e., TR ≤ 1500ms) would increase the likelihood of retaining a sufficient amount of data following scrubbing to ensure accurate estimates of functional connectivity. But there are practical limitations to implementing these changes to an MRI protocol for people with DS, as a scan duration beyond 60 minutes may constitute an undue burden on the participants due to the loud and uncomfortable nature of being scanned. Future studies should consider prioritizing rsfMRI sequences by performing it earlier during the scan session or splitting the various sequences (i.e., rsfMRI, DTI, etc.) across two scan sessions.

REFERENCES

Adams JN, Maass A, Berron D, et al. Reduced repetition suppression in aging is driven by tau-related hyperactivity in medial temporal lobe. *J Neurosci*. 2021;41(17):3917-3931. https://doi.org/10.1523/JNEUROSCI.2504-20.2021.

Adams JN, Maass A, Harrison TM, Baker SL, Jagust WJ. Cortical tau deposition follows patterns of entorhinal functional connectivity in aging. *Elife*. 2019;8:e49132. https://doi.org/10.7554/eLife.49132.

Alhazmi HA, Albratty M. An update on the novel and approved drugs for Alzheimer disease. *Saudi Pharm J*. 2022;30(12):1755-1764. https://doi.org/10.1016/j.jsps.2022.10.004.

Alves GS, Oertel Knöchel V, Knöchel C, et al. Integrating retrogenesis theory to Alzheimer's disease pathology: insight from DTI-TBSS investigation of the white matter microstructural integrity. *Biomed Res Int*. 2015;2015:291658. https://doi.org/10.1155/2015/291658.

Alzheimer's disease facts and figures. *Alzheimers Dement*. 2023;19(4):1598-1695. https://doi.org/10.1002/alz.13016.

Annus T, Wilson LR, Acosta-Cabronero J, et al. The Down syndrome brain in the presence and absence of fibrillar β-amyloidosis. *Neurobiol Aging*. 2017;53:11-19. https://doi.org/10.1016/j.neurobiolaging.2017.01.009.

Annus T, Wilson LR, Hong YT, et al. The pattern of amyloid accumulation in the brains of adults with Down syndrome. *Alzheimers Dement*. 2016;12(5):538-545. https://doi.org/10.1016/j.jalz.2015.07.490.

Antonarakis SE, Skotko BG, Rafii MS, et al. Down syndrome. *Nat Rev Dis Primers*. 2020;6(1):9. https://doi.org/10.1038/s41572-019-0143-7.

Avants BB, Tustison NJ, Song G, Cook PA, Klein A, Gee JC. A reproducible evaluation of ANTs similarity metric performance in brain image registration. *Neuroimage*. 2011;54(3):2033-2044. https://doi.org/10.1016/j.neuroimage.2010.09.025.

Baker SL, Maass A, Jagust WJ. Considerations and code for partial volume correcting [18F]-AV-1451 tau PET data. *Data Brief*. 2017;15:648-657. https://doi.org/10.1016/j.dib.2017.10.024.

Bakker A, Krauss GL, Albert MS, et al. Reduction of hippocampal hyperactivity improves cognition in amnestic mild cognitive impairment. *Neuron*. 2012;74(3):467-474. https://doi.org/10.1016/j.neuron.2012.03.023.

Beacher F, Daly E, Simmons A, et al. Alzheimer's disease and Down's syndrome: an in vivo MRI study. *Psychol Med*. 2009;39(4):675-684. https://doi.org/10.1017/S0033291708004054.

Beacher F, Daly E, Simmons A, et al. Brain anatomy and ageing in non-demented adults with Down's syndrome: an in vivo MRI study. *Psychol Med*. 2010;40(4):611-619. https://doi.org/10.1017/S0033291709990985.

Benejam B, Aranha MR, Videla L, et al. Neural correlates of episodic memory in adults with Down syndrome and Alzheimer's disease. *Alzheimers Res Ther*. 2022;14(1):123. https://doi.org/10.1186/s13195-022-01064-x.

Benejam B, Videla L, Vilaplana E, et al. Diagnosis of prodromal and Alzheimer's disease dementia in adults with Down syndrome using neuropsychological tests. *Alzheimers Dement (Amst)*. 2020;12(1):e12047. https://doi.org/10.1002/dad2.12047.

Berron D, Vogel JW, Insel PS, et al. Early stages of tau pathology and its associations with functional connectivity, atrophy and memory. *Brain*. 2021;144(9):2771-2783. https://doi.org/10.1093/brain/awab114.

Betthauser TJ, Cody KA, Zammit MD, et al. In vivo characterization and quantification of neurofibrillary tau PET radioligand 18F-MK-6240 in humans from Alzheimer disease dementia to young controls. *J Nucl Med*. 2019;60(1):93-99. https://doi.org/10.2967/jnumed.118.209650.

Bettio LEB, Rajendran L, Gil-Mohapel J. The effects of aging in the hippocampus and cognitive decline. *Neurosci Biobehav Rev*. 2017;79:66-86. https://doi.org/10.1016/j.neubiorev.2017.04.030.

Braak H, Alafuzoff I, Arzberger T, Kretzschmar H, Del Tredici K. Staging of Alzheimer disease-associated neurofibrillary pathology using paraffin sections and immunocytochemistry. *Acta Neuropathol*. 2006;112(4):389-404. https://doi.org/10.1007/s00401-006-0127-z.

Brier MR, Gordon B, Friedrichsen K, et al. Tau and Aβ imaging, CSF measures, and cognition in Alzheimer's disease. *Sci Transl Med*. 2016;8(338):338ra66. https://doi.org/10.1126/scitranslmed.aaf2362.

Buckner RL, Andrews-Hanna JR, Schacter DL. The brain's default network: anatomy, function, and relevance to disease. *Ann N Y Acad Sci*. 2008;1124:1-38. https://doi.org/10.1196/annals.1440.011.

Bull MJ, Committee on Genetics. Health supervision for children with Down syndrome. *Pediatrics*. 2011;128(2):393-406. https://doi.org/10.1542/peds.2011-1605.

Cañete-Massé C, Carbó-Carreté M, Peró-Cebollero M, Cui SX, Yan CG, Guàrdia-Olmos J. Abnormal degree centrality and functional connectivity in Down syndrome: a resting-state fMRI study. *Int J Clin Health Psychol*. 2023;23(1):100341. https://doi.org/10.1016/j.ijchp.2022.100341.

Csumitta KD, Gotts SJ, Clasen LS, Martin A, Lee NR. Youth with Down syndrome display widespread increased functional connectivity during rest. *Sci Rep*. 2022;12:9836. https://doi.org/10.1038/s41598-022-13437-1.

Chen Y, Therriault J, Luo J, Ba M, Zhang H; Alzheimer's Disease Neuroimaging Initiative. Neurofilament light as a biomarker of axonal degeneration in patients with mild cognitive impairment and Alzheimer's disease. *J Integr Neurosci*. 2021;20(4):861-870. https://doi.org/10.31083/j.jin2004088.

Chhatwal JP, Schultz AP, Johnson K, et al. Impaired default network functional connectivity in autosomal dominant Alzheimer disease. *Neurology*. 2013;81(8):736-744. https://doi.org/10.1212/WNL.0b013e3182a1aafe.

Collij LE, Salvadó G, Wottschel V, et al. Spatial-temporal patterns of β-amyloid accumulation: a subtype and stage inference model analysis. *Neurology*. 2022;98(17):e1692-e1703. https://doi.org/10.1212/WNL.0000000000200148.

Cox RW. AFNI: software for analysis and visualization of functional magnetic resonance neuroimages. *Comput Biomed Res*. 1996;29(3):162-173. https://doi.org/10.1006/cbmr.1996.0014.

Cummings J. Lessons learned from Alzheimer disease: clinical trials with negative outcomes. *Clin Transl Sci*. 2018;11(2):147-152. https://doi.org/10.1111/cts.12491.

Dale AM, Fischl B, Sereno MI. Cortical surface-based analysis: I. Segmentation and surface reconstruction. *Neuroimage*. 1999;9(2):179-194. https://doi.org/10.1006/nimg.1998.0395.

Dalton A, Fedor B. *DYSPRAXIA Scale for Adults with Down Syndrome*. Staten Island, NY: NYS Institute for Basic Research in Developmental Disabilities; 1997.

Das SR, Pluta J, Mancuso L, et al. Increased functional connectivity within medial temporal lobe in mild cognitive impairment. *Hippocampus*. 2013;23(1):1-6. https://doi.org/10.1002/hipo.22051.

Davidson YS, Robinson A, Prasher VP, Mann DMA. The age of onset and evolution of Braak tangle stage and Thal amyloid pathology of Alzheimer's disease in individuals with Down syndrome. *Acta Neuropathol Commun*. 2018;6(1):56. https://doi.org/10.1186/s40478-018-0559-4.

DeCormier Plosky W, Ne'eman A, Silverman BC, et al. Excluding people with disabilities from clinical research: eligibility criteria lack clarity and justification. *Health Aff (Millwood)*. 2022;41(10):1423-1432. https://doi.org/10.1377/hlthaff.2022.00520.

Deinde F, Kotecha J, Lau LSL, Bhattacharyya S, Velayudhan L. A review of functional neuroimaging in people with Down syndrome with and without dementia. *Dement Geriatr Cogn Disord Extra*. 2022;11(3):324-332. https://doi.org/10.1159/000520880.

Desikan RS, Ségonne F, Fischl B, et al. An automated labeling system for subdividing the human cerebral cortex on MRI scans into gyral based regions of interest. *Neuroimage*. 2006;31(3):968-980. https://doi.org/10.1016/j.neuroimage.2006.01.021.

DeTure MA, Dickson DW. The neuropathological diagnosis of Alzheimer’s disease. *Mol Neurodegener*. 2019;14(1):32. https://doi.org/10.1186/s13024-019-0333-5.

Dickerson BC, Bakkour A, Salat DH, et al. The cortical signature of Alzheimer's disease: regionally specific cortical thinning relates to symptom severity in very mild to mild AD dementia and is detectable in asymptomatic amyloid-positive individuals. *Cereb Cortex*. 2009;19(3):497-510. https://doi.org/10.1093/cercor/bhn113.

Dickerson BC, Eichenbaum H. The episodic memory system: neurocircuitry and disorders. *Neuropsychopharmacology*. 2010;35(1):86-104. https://doi.org/10.1038/npp.2009.126.

DiProspero ND, Keator DB, Phelan M, et al. Selective impairment of long-range default mode network functional connectivity as a biomarker for preclinical Alzheimer's disease in people with Down syndrome. *J Alzheimers Dis*. 2022;85(1):153-165. https://doi.org/10.3233/JAD-210572.

DiProspero ND, Sathishkumar M, Janecek J, et al. Anterolateral entorhinal cortical thickness, hippocampus volume, and neurofilament light chain as biomarkers for Alzheimer’s disease in Down syndrome. *Alzheimers Dement (Amst)*. Forthcoming 2023.

Edgin JO, Clark CA, Massand E, Karmiloff-Smith A. Building an adaptive brain across development: targets for neurorehabilitation must begin in infancy. *Front Behav Neurosci*. 2015;9:232. https://doi.org/10.3389/fnbeh.2015.00232.

Erten-Lyons D, Woltjer RL, Dodge H, et al. Factors associated with resistance to dementia despite high Alzheimer disease pathology. *Neurology*. 2009;72(4):354-360. https://doi.org/10.1212/01.wnl.0000341273.18141.64.

Fortea J, Vilaplana E, Carmona-Iragui M, et al. Clinical and biomarker changes of Alzheimer's disease in adults with Down syndrome: a cross-sectional study. *Lancet*. 2020;395(10242):1988-1997. https://doi.org/10.1016/S0140-6736(20)30689-9.

Fox MD, Snyder AZ, Vincent JL, Corbetta M, Van Essen DC, Raichle ME. The human brain is intrinsically organized into dynamic, anticorrelated functional networks. *Proc Natl Acad Sci U S A*. 2005;102(27):9673-9678. https://doi.org/10.1073/pnas.0504136102.

Franzmeier N, Rubinski A, Neitzel J, et al. Functional connectivity associated with tau levels in ageing, Alzheimer's, and small vessel disease. *Brain*. 2019;142(4):1093-1107. https://doi.org/10.1093/brain/awz026.

Fuld PA. Psychological testing in the differential diagnosis of the dementias. In: Katzman R, Terry RD, Bick KL, eds. *Alzheimer's Disease: Senile Dementia and Related Disorders*. New York, NY: Raven Press; 1978:185-193.

Glenner GG, Wong CW. Alzheimer's disease and Down's syndrome: sharing of a unique cerebrovascular amyloid fibril protein. *Biochem Biophys Res Commun*. 1984;122(3):1131-1135. https://doi.org/10.1016/0006-291x(84)91209-9.

Gomez W, Morales R, Maracaja-Coutinho V, Parra V, Nassif M. Down syndrome and Alzheimer's disease: common molecular traits beyond the amyloid precursor protein. *Aging*. 2020;12(1):1011-1033. https://doi.org/10.18632/aging.102677.

Gómez-Isla T, Price JL, McKeel DW, Morris JC, Growdon JH, Hyman BT. Profound loss of layer II entorhinal cortex neurons occurs in very mild Alzheimer's disease. *J Neurosci*. 1996;16(14):4491-4500. https://doi.org/10.1523/JNEUROSCI.16-14-04491.1996.

Grajski KA, Bressler SL; Alzheimer's Disease Neuroimaging Initiative. Differential medial temporal lobe and default-mode network functional connectivity and morphometric changes in Alzheimer's disease. *Neuroimage Clin*. 2019;23:101860. https://doi.org/10.1016/j.nicl.2019.101860.

Greicius MD, Krasnow B, Reiss AL, Menon V. Functional connectivity in the resting brain: a network analysis of the default mode hypothesis. *Proc Natl Acad Sci U S A*. 2003;100(1):253-258. https://doi.org/10.1073/pnas.0135058100.

Greve DN, Salat DH, Bowen SL, et al. Different partial volume correction methods lead to different conclusions: an (18)F-FDG-PET study of aging. *Neuroimage*. 2016;132:334-343. https://doi.org/10.1016/j.neuroimage.2016.02.042.

Greve DN, Svarer C, Fisher PM, et al. Cortical surface-based analysis reduces bias and variance in kinetic modeling of brain PET data. *Neuroimage*. 2014;92:225-236. https://doi.org/10.1016/j.neuroimage.2013.12.021.

Grigorova M, Mak E, Brown SSG, et al. Amyloid- β and tau deposition influences cognitive and functional decline in Down syndrome. *Neurobiol Aging*. 2022;119:36-45. https://doi.org/10.1016/j.neurobiolaging.2022.07.003.

Grothe MJ, Teipel SJ; Alzheimer's Disease Neuroimaging Initiative. Spatial patterns of atrophy, hypometabolism, and amyloid deposition in Alzheimer's disease correspond to dissociable functional brain networks. *Hum Brain Mapp*. 2016;37(1):35-53. https://doi.org/10.1002/hbm.23018.

Guidi S, Bonasoni P, Ceccarelli C, et al. Neurogenesis impairment and increased cell death reduce total neuron number in the hippocampal region of fetuses with Down syndrome. *Brain Pathol*. 2008;18(2):180-197. https://doi.org/10.1111/j.1750-3639.2007.00113.x.

Haier RJ, Alkire MT, White NS, et al. Temporal cortex hypermetabolism in Down syndrome prior to the onset of dementia. *Neurology*. 2003;61(12):1673-1679. https://doi.org/10.1212/01.wnl.0000098935.36984.25.

Haier RJ, Head K, Head E, Lott IT. Neuroimaging of individuals with Down's syndrome at-risk for dementia: evidence for possible compensatory events. *Neuroimage*. 2008;39(3):1324-1332. https://doi.org/10.1016/j.neuroimage.2007.09.064.

Hamerton JL, Giannelli F, Polani PE. Cytogenetics of Down’s syndrome (Mongolism) I. Data on a consecutive series of patients referred for genetic counseling and diagnosis. *Cytogenetics*. 1965;4(3):171-185. https://doi.org/10.1159/000129853.

Hamner T, Udhnani MD, Osipowicz KZ, Lee NR. Pediatric brain development in Down syndrome: a field in its infancy. *J Int Neuropsychol Soc*. 2018;24(9):966-976. https://doi.org/10.1017/S1355617718000206.

Hampel H, O'Bryant SE, Molinuevo JL, et al. Blood-based biomarkers for Alzheimer disease: mapping the road to the clinic. *Nat Rev Neurol*. 2018;14(11):639-652. https://doi.org/10.1038/s41582-018-0079-7.

Handen BL. The search for biomarkers of Alzheimer's disease in Down syndrome. *Am J Intellect Dev Disabil*. 2020;125(2):97-99. https://doi.org/10.1352/1944-7558-125.2.97.

Handen BL, Lott IT, Christian BT, et al. The Alzheimer's Biomarker Consortium-Down Syndrome: rationale and methodology. *Alzheimers Dement (Amst)*. 2020;12(1):e12065. https://doi.org/10.1002/dad2.12065.

Hansson O, Edelmayer RM, Boxer AL, et al. The Alzheimer's Association appropriate use recommendations for blood biomarkers in Alzheimer's disease. *Alzheimers Dement*. 2022;18(12):2669-2686. https://doi.org/10.1002/alz.12756.

Hartley SL, Handen BL, Devenny D, et al. Cognitive decline and brain amyloid-β accumulation across 3 years in adults with Down syndrome. *Neurobiol Aging*. 2017;58:68-76. https://doi.org/10.1016/j.neurobiolaging.2017.05.019.

Hartley SL, Handen BL, Devenny D, et al. Cognitive indicators of transition to preclinical and prodromal stages of Alzheimer's disease in Down syndrome. *Alzheimers Dement (Amst)*. 2020;12(1):e12096. https://doi.org/10.1002/dad2.12096.

Hartley SL, Handen BL, Tudorascu D, et al. Role of tau deposition in early cognitive decline in Down syndrome. *Alzheimers Dement (Amst)*. 2022;14(1):e12256. https://doi.org/10.1002/dad2.12256.

Head E, Helman AM, Powell D, Schmitt FA. Down syndrome, beta-amyloid and neuroimaging. *Free Radic Biol Med*. 2018;114:102-109. https://doi.org/10.1016/j.freeradbiomed.2017.09.013.

Head E, Lott IT, Hof PR, et al. Parallel compensatory and pathological events associated with tau pathology in middle aged individuals with Down syndrome. *J Neuropathol Exp Neurol*. 2003;62(9):917-926. https://doi.org/10.1093/jnen/62.9.917.

Head E, Lott IT, Patterson D, Doran E, Haier RJ. Possible compensatory events in adult Down syndrome brain prior to the development of Alzheimer disease neuropathology: targets for nonpharmacological intervention. *J Alzheimers Dis*. 2007;11(1):61-76. https://doi.org/10.3233/jad-2007-11110.

Head E, Powell D, Gold BT, Schmitt FA. Alzheimer's disease in Down syndrome. *Eur J Neurodegener Dis*. 2012;1(3):353-364.

Hof PR, Bouras C, Perl DP, Sparks DL, Mehta N, Morrison JH. Age-related distribution of neuropathologic changes in the cerebral cortex of patients with Down's syndrome. Quantitative regional analysis and comparison with Alzheimer's disease. *Arch Neurol*. 1995;52(4):379-391. https://doi.org/10.1001/archneur.1995.00540280065020.

Holbrook AJ, Tustison NJ, Marquez F, et al. Anterolateral entorhinal cortex thickness as a new biomarker for early detection of Alzheimer's disease. *Alzheimers Dement (Amst)*. 2020;12(1):e12068. https://doi.org/10.1002/dad2.12068.

Holm S. A simple sequentially rejective multiple test procedure. *Scand J Stat*. 1979;6(2):65-70.

Honig LS, Barakos J, Dhadda S, et al. ARIA in patients treated with lecanemab (BAN2401) in a phase 2 study in early Alzheimer's disease. *Alzheimers Dement (N Y)*. 2023;9(1):e12377. https://doi.org/10.1002/trc2.12377.

Hook EB. Down syndrome: frequency in human populations and factors pertinent to variation in rates. In: de la Cruz FF, Gerald PS, eds. *Trisomy 21 (Down Syndrome): Research Perspectives*. Baltimore, MD: University Park Press; 1981:3-67.

Hrybouski S, Das SR, Xie L, et al. Aging and Alzheimer's disease have dissociable effects on medial temporal lobe connectivity. *medRxiv* [Preprint]. 2023:2023.01.18.23284749. https://doi.org/10.1101/2023.01.18.23284749.

Jack CR Jr, Bennett DA, Blennow K, et al. NIA-AA Research Framework: toward a biological definition of Alzheimer’s disease. *Alzheimers Dement*. 2018;14(4):535-562. https://doi.org/10.1016/j.jalz.2018.02.018.

Jack CR Jr, Bennett DA, Blennow K, et al. A/T/N: an unbiased descriptive classification scheme for Alzheimer disease biomarkers. *Neurology*. 2016;87(5):539-547. https://doi.org/10.1212/WNL.0000000000002923.

Jack CR Jr, Knopman DS, Jagust WJ, et al. Tracking pathophysiological processes in Alzheimer's disease: an updated hypothetical model of dynamic biomarkers. *Lancet Neurol*. 2013;12(2):207-216. https://doi.org/10.1016/S1474-4422(12)70291-0.

Janelidze S, Christian BT, Price J, et al. Detection of brain tau pathology in Down syndrome using plasma biomarkers. *JAMA Neurol*. 2022;79(8):797-807. https://doi.org/10.1001/jamaneurol.2022.1740.

Jansen WJ, Ossenkoppele R, Knol DL, et al. Prevalence of cerebral amyloid pathology in persons without dementia: a meta-analysis. *JAMA*. 2015;313(19):1924-1938. https://doi.org/10.1001/jama.2015.4668.

Jiao F, Gao Z, Shi K, et al. Frequency-dependent relationship between resting-state fMRI and glucose metabolism in the elderly. *Front Neurol*. 2019;10:566. https://doi.org/10.3389/fneur.2019.00566.

Jo HJ, Saad ZS, Simmons WK, Milbury LA, Cox RW. Mapping sources of correlation in resting state FMRI, with artifact detection and removal. *Neuroimage*. 2010;52(2):571-582. https://doi.org/10.1016/j.neuroimage.2010.04.246.

Jones DT, Knopman DS, Gunter JL, et al. Cascading network failure across the Alzheimer's disease spectrum. *Brain*. 2016;139(2):547-562. https://doi.org/10.1093/brain/awv338.

Joshi AD, Pontecorvo MJ, Clark CM, et al. Performance characteristics of amyloid PET with florbetapir F 18 in patients with Alzheimer's disease and cognitively normal subjects. *J Nucl Med*. 2012;53(3):378-384. https://doi.org/10.2967/jnumed.111.090340.

Keator DB, Doran E, Taylor L, et al. Brain amyloid and the transition to dementia in Down syndrome. *Alzheimers Dement (Amst)*. 2020a;12(1):e12126. https://doi.org/10.1002/dad2.12126.

Keator DB, Phelan MJ, Taylor L, et al. Down syndrome: distribution of brain amyloid in mild cognitive impairment. *Alzheimers Dement (Amst)*. 2020b;12(1):e12013. https://doi.org/10.1002/dad2.12013.

Kesslak JP, Nagata SF, Lott I, Nalcioglu O. Magnetic resonance imaging analysis of age-related changes in the brains of individuals with Down's syndrome. *Neurology*. 1994;44(6):1039-1045. https://doi.org/10.1212/wnl.44.6.1039.

Khalil M, Pirpamer L, Hofer E, et al. Serum neurofilament light levels in normal aging and their association with morphologic brain changes. *Nat Commun*. 2020;11(1):812. https://doi.org/10.1038/s41467-020-14612-6.

Khan UA, Liu L, Provenzano FA, et al. Molecular drivers and cortical spread of lateral entorhinal cortex dysfunction in preclinical Alzheimer's disease. *Nat Neurosci*. 2014;17(2):304. https://doi.org/10.1038/nn.3606.

Kimura R, Kamino K, Yamamoto M, et al. The DYRK1A gene, encoded in chromosome 21 Down syndrome critical region, bridges between beta-amyloid production and tau phosphorylation in Alzheimer disease. *Hum Mol Genet*. 2007;16(1):15-23. https://doi.org/10.1093/hmg/ddl437.

Kittler P, Krinsky-McHale SJ, Devenny DA. Verbal intrusions precede memory decline in adults with Down syndrome. J Intellect Disabil Res. 2006;50(1):1-10. https://doi.org/10.1111/j.1365-2788.2005.00715.x.

Koenig KA, Bekris LM, Ruedrich S, et al. High-resolution functional connectivity of the default mode network in young adults with Down syndrome. *Brain Imaging Behav*. 2021a;15(4):2051-2060. https://doi.org/10.1007/s11682-020-00399-z.

Koenig KA, Oh SH, Stasko MR, et al. High resolution structural and functional MRI of the hippocampus in young adults with Down syndrome. *Brain Commun*. 2021b;3(2):fcab088. https://doi.org/10.1093/braincomms/fcab088.

Krasuski JS, Alexander GE, Horwitz B, Rapoport SI, Schapiro MB. Relation of medial temporal lobe volumes to age and memory function in nondemented adults with Down's syndrome: implications for the prodromal phase of Alzheimer's disease. *Am J Psychiatry*. 2002;159(1):74-81. https://doi.org/10.1176/appi.ajp.159.1.74.

Krauss R, Bosanac T, Devraj R, Engber T, Hughes RO. Axons matter: the promise of treating neurodegenerative disorders by targeting SARM1-mediated axonal degeneration. *Trends Pharmacol Sci*. 2020;41(4):281-293. https://doi.org/10.1016/j.tips.2020.01.006.

Krinsky-McHale SJ, Devenny DA, Silverman WP. Changes in explicit memory associated with early dementia in adults with Down’s syndrome. *J Intellect Disabil Res*. 2002;46(3):198-208. https://doi.org.10.1046/j.1365-2788.2002.00365.x.

Krinsky-McHale SJ, Hartley S, Hom C, et al. A modified Cued Recall Test for detecting prodromal AD in adults with Down syndrome. *Alzheimers Dement (Amst)*. 2022;14(1):e12361. https://doi.org/10.1002/dad2.12361.

Krinsky-McHale SJ, Silverman W. Dementia and mild cognitive impairment in adults with intellectual disability: issues of diagnosis. *Dev Disabil Res Rev*. 2013;18(1):31-42. https://doi.org/10.1002/ddrr.1126.

Krinsky-McHale SJ, Zigman WB, Lee JH, et al. Promising outcome measures of early Alzheimer's dementia in adults with Down syndrome. *Alzheimer's Dement*. 2020;12(1):e12044. https://doi.org/10.1002/dad2.12044.

La Joie R, Perrotin A, Barré L, et al. Region-specific hierarchy between atrophy, hypometabolism, and β-amyloid (Aβ) load in Alzheimer's disease dementia. *J Neurosci*. 2012; 32(46):16265. https://doi.org/10.1523/JNEUROSCI.2170-12.2012.

Landau SM, Breault C, Joshi AD, et al. Amyloid-β imaging with Pittsburgh compound B and florbetapir: comparing radiotracers and quantification methods. *J Nucl Med*. 2013;54(1):70-77. https://doi.org/10.2967/jnumed.112.109009.

Landes SD, Stevens JD, Turk MA. Cause of death in adults with Down syndrome in the United States. *Disabil Health J*. 2020;13(4):100947. https://doi.org/10.1016/j.dhjo.2020.100947.

Lao PJ, Handen BL, Betthauser TJ, et al. Imaging neurodegeneration in Down syndrome: brain templates for amyloid burden and tissue segmentation. *Brain Imaging Behav*. 2019;13(2):345-353. https://doi.org/10.1007/s11682-018-9888-y.

Lao PJ, Handen BL, Betthauser TJ, et al. Alzheimer-like pattern of hypometabolism emerges with elevated amyloid-β burden in Down syndrome. *J Alzheimers Dis*. 2018;61(2):631-644. https://doi.org/10.3233/JAD-170720.

Lenth RV. emmeans: estimated marginal means, aka least-squares means. R package version 1.7.5. 2022. https://CRAN.R-project.org/package=emmeans.

Lim HK, Nebes R, Snitz B, et al. Regional amyloid burden and intrinsic connectivity networks in cognitively normal elderly subjects. *Brain*. 2014;137(12):3327-3338. https://doi.org/10.1093/brain/awu271.

Liu F, Liang Z, Wegiel J, et al. Overexpression of Dyrk1A contributes to neurofibrillary degeneration in Down syndrome. *FASEB J*. 2008;22(9):3224-3233. https://doi.org/10.1096/fj.07-104539.

Lott IT, Head E. Dementia in Down syndrome: unique insights for Alzheimer disease research. *Nat Rev Neurol*. 2019;15(3):135-147. https://doi.org/10.1038/s41582-018-0132-6.

Lubben N, Ensink E, Coetzee GA, Labrie V. The enigma and implications of brain hemispheric asymmetry in neurodegenerative diseases. *Brain Commun*. 2021;3(3):fcab211. https://doi.org/10.1093/braincomms/fcab211.

Mai CT, Isenburg JL, Canfield MA, et al. National population-based estimates for major birth defects, 2010-2014. *Birth Defects Res*. 2019;111(18):1420-1435. https://doi.org/10.1002/bdr2.1589.

Mak E, Padilla C, Annus T, et al. Delineating the topography of amyloid-associated cortical atrophy in Down syndrome. *Neurobiol Aging*. 2019;80:196-202. https://doi.org/10.1016/j.neurobiolaging.2019.02.018.

Mann DM, Iwatsubo T. Diffuse plaques in the cerebellum and corpus striatum in Down's syndrome contain amyloid beta protein (A beta) only in the form of A beta 42(43). *Neurodegeneration*. 1996;5(2):115-120. https://doi.org/10.1006/neur.1996.0017.

Matthews DC, Lukic AS, Andrews RD, et al. Dissociation of Down syndrome and Alzheimer's disease effects with imaging. *Alzheimers Dement (N Y)*. 2016;2(2):69-81. https://doi.org/10.1016/j.trci.2016.02.004.

Mattsson N, Andreasson U, Zetterberg H, Blennow K; Alzheimer's Disease Neuroimaging Initiative. Association of plasma neurofilament light with neurodegeneration in patients with Alzheimer disease. *JAMA Neurol*. 2017;74(5):557-566. https://doi.org/10.1001/jamaneurol.2016.6117.

Mattsson N, Cullen NC, Andreasson U, Zetterberg H, Blennow K. Association between longitudinal plasma neurofilament light and neurodegeneration in patients with Alzheimer disease. *JAMA Neurol*. 2019;76(7):791-799. https://doi.org/10.1001/jamaneurol.2019.0765.

McCarron M, McCallion P, Reilly E, Dunne P, Carroll R, Mulryan N. A prospective 20-year longitudinal follow-up of dementia in persons with Down syndrome. *J Intellect Disabil Res*. 2017;61(9):843-852. https://doi.org/10.1111/jir.12390.

McKhann G, Drachman D, Folstein M, Katzman R, Price D, Stadlan EM. Clinical diagnosis of Alzheimer's disease: report of the NINCDS-ADRDA Work Group under the auspices of Department of Health and Human Services Task Force on Alzheimer's Disease. *Neurology*. 1984;34(7):939-944. https://doi.org/10.1212/wnl.34.7.939.

Mevel K, Chételat G, Eustache F, Desgranges B. The default mode network in healthy aging and Alzheimer's disease. *Int J Alzheimers Dis*. 2011;2011:535816. https://doi.org/10.4061/2011/535816.

Mielke MM, Syrjanen JA, Blennow K, et al. Plasma and CSF neurofilament light. *Neurology*. 2019;93(3):e252-e260. https://doi.org/10.1212/WNL.0000000000007767.

Mikkelsen M. Down syndrome: cytogenetical epidemiology. *Hereditas*. 1977;86(1):45-50. https://doi.org/10.1111/j.1601-5223.1977.tb01211.x

Mormino EC, Smiljic A, Hayenga AO, et al. Relationships between beta-amyloid and functional connectivity in different components of the default mode network in aging. *Cereb Cortex*. 2011;21(10):2399-2407. https://doi.org/10.1093/cercor/bhr025.

Moser M, Roccella EJ. The treatment of hypertension: a remarkable success story. *J Clin Hypertens (Greenwich)*. 2013;15(2):88-91. https://doi.org/10.1111/jch.12033.

Moulder KL, Snider BJ, Mills SL, et al. Dominantly Inherited Alzheimer Network: facilitating research and clinical trials. *Alzheimers Res Ther*. 2013;5(5):48. https://doi.org/10.1186/alzrt213.

Musaeus CS, Salem LC, Kjaer TW, Waldemar G. Electroencephalographic functional connectivity is altered in persons with Down syndrome and Alzheimer's disease. *J Intellect Disabil Res*. 2021;65(3):236-245. https://doi.org/10.1111/jir.12803.

Neale N, Padilla C, Fonseca LM, Holland T, Zaman S. Neuroimaging and other modalities to assess Alzheimer's disease in Down syndrome. *Neuroimage Clin*. 2018;17:263-271. https://doi.org/10.1016/j.nicl.2017.10.022.

O'Connor EE, Zeffiro TA. Why is clinical fMRI in a resting state? *Front Neurol*. 2019;10:420. https://doi.org/10.3389/fneur.2019.00420.

Öhman F, Hassenstab J, Berron D, Schöll M, Papp KV. Current advances in digital cognitive assessment for preclinical Alzheimer's disease. *Alzheimers Dement (Amst)*. 2021;13(1):e12217. https://doi.org/10.1002/dad2.12217.

Ossenkoppele R, Reimand J, Smith R, et al. Tau PET correlates with different Alzheimer's disease-related features compared to CSF and plasma p-tau biomarkers. *EMBO Mol Med*. 2021;13(8):e14398. https://doi.org/10.15252/emmm.202114398.

Padilla C, Montal V, Walpert MJ, et al. Cortical atrophy and amyloid and tau deposition in Down syndrome: a longitudinal study. *Alzheimers Dement (Amst)*. 2022;14(1):e12288. https://doi.org/10.1002/dad2.12288.

Pangalos C, Avramopoulos D, Blouin JL, et al. Understanding the mechanism(s) of mosaic trisomy 21 by using DNA polymorphism analysis. *Am J Hum Genet*. 1994;54(3):473-481.

Pasquini L, Rahmani F, Maleki-Balajoo S, et al. Medial temporal lobe disconnection and hyperexcitability across Alzheimer's disease stages. *J Alzheimers Dis Rep*. 2019;3(1):103-112. https://doi.org/10.3233/ADR-190121.

Pasquini L, Scherr M, Tahmasian M, et al. Link between hippocampus' raised local and eased global intrinsic connectivity in AD. *Alzheimers Dement*. 2015;11(5):475-484. https://doi.org/10.1016/j.jalz.2014.02.007.

Petersen ME, Rafii MS, Zhang F, et al. Plasma total-tau and neurofilament light chain (Nf-L) as diagnostic biomarkers of Alzheimer's disease dementia and mild cognitive impairment in adults with Down syndrome. *J Alzheimers Dis*. 2021;79(2):671. https://doi.org/10.3233/JAD-201167.

Pinter JD, Eliez S, Schmitt JE, Capone GT, Reiss AL. Neuroanatomy of Down's syndrome: a high-resolution MRI study. *Am J Psychiatry*. 2001;158(10):1659-1665. https://doi.org/10.1176/appi.ajp.158.10.1659.

Planche V, Manjon JV, Mansencal B, et al. Structural progression of Alzheimer's disease over decades: the MRI staging scheme. *Brain Commun*. 2022;4(3);fcac109. https://doi.org/10.1093/braincomms/fcac109.

Power JD, Barnes KA, Snyder AZ, Schlaggar BL, Petersen SE. Spurious but systematic correlations in functional connectivity MRI networks arise from subject motion. *Neuroimage*. 2012;59(3):2142-2154. https://doi.org/10.1016/j.neuroimage.2011.10.018.

Power JD, Mitra A, Laumann TO, Snyder AZ, Schlaggar BL, Petersen SE. Methods to detect, characterize, and remove motion artifact in resting state fMRI. *Neuroimage*. 2014;84:320-341. https://doi.org/10.1016/j.neuroimage.2013.08.048.

Prasher VP. Dementia Questionnaire for Persons with Mental Retardation (DMR): modified criteria for adults with Down's syndrome. *J Appl Res Intellect Disabil*. 1997;10(1):54-60. https://doi.org/10.1111/j.1468-3148.1997.tb00006.x.

Presson AP, Partyka G, Jensen KM, et al. Current estimate of Down syndrome population prevalence in the United States. *J Pediatr*. 2013;163(4):1163-1168. https://doi.org/10.1016/j.jpeds.2013.06.013.

Pujol J, Fenoll R, Ribas-Vidal N, et al. A longitudinal study of brain anatomy changes preceding dementia in Down syndrome. *Neuroimage Clin*. 2018;18:160-166. https://doi.org/10.1016/j.nicl.2018.01.024.

Putcha D, Brickhouse M, O'Keefe K, et al. Hippocampal hyperactivation associated with cortical thinning in Alzheimer's disease signature regions in non-demented elderly adults. *J Neurosci*. 2011;31(48):17680-17688. https://doi.org/10.1523/JNEUROSCI.4740-11.2011.

R Core Team. R: a language and environment for statistical computing. R Foundation for Statistical Computing, Vienna, Austria. 2022. https://www.R-project.org/.

Rafii MS, Donohue MC, Matthews DC, et al. Plasma neurofilament light and Alzheimer's disease biomarkers in Down syndrome: results from the Down Syndrome Biomarker Initiative (DSBI). *J Alzheimers Dis*. 2019;70(1):131-138. https://doi.org/10.3233/JAD-190322.

Rafii MS, Lukic AS, Andrews RD, et al. PET imaging of tau pathology and relationship to amyloid, longitudinal MRI, and cognitive change in Down syndrome: results from the Down Syndrome Biomarker Initiative (DSBI). *J Alzheimers Dis*. 2017;60(2):439-450.

https://doi.org/10.3233/JAD-170390.

Raichle ME, MacLeod AM, Snyder AZ, Powers WJ, Gusnard DA, Shulman GL. A default mode of brain function. *Proc Natl Acad Sci U S A.* 2001;98(2):676-682. https://doi.org/10.1073/pnas.98.2.676.

Raz N, Torres IJ, Briggs SD, et al. Selective neuroanatomic abnormalities in Down's syndrome and their cognitive correlates: evidence from MRI morphometry. *Neurology*. 1995;45(2):356-366. https://doi.org/10.1212/wnl.45.2.356.

Reagh ZM, Noche JA, Tustison NJ, Delisle D, Murray EA, Yassa MA. Functional imbalance of anterolateral entorhinal cortex and hippocampal dentate/CA3 underlies age-related object pattern separation deficits. *Neuron*. 2018;97(5):1187-1198.e4. https://doi.org/10.1016/j.neuron.2018.01.039.

Richards BW. Mosaic mongolism. *J Ment Defic Res*. 1969;13(1):66-83. https://doi.org/10.1111/j.1365-2788.1969.tb01067.x.

Romano A, Cornia R, Moraschi M, et al. Age-related cortical thickness reduction in non-demented Down’s syndrome subjects. *J Neuroimaging*. 2016;26(1):95-102. https://doi.org/10.1111/jon.12259.

Rosas HD, Lewis LR, Mercaldo ND, et al. Altered connectivity of the default mode network in cognitively stable adults with Down syndrome: "accelerated aging" or a prelude to Alzheimer's disease?. *Alzheimers Dement (Amst)*. 2021;13:e12105. https://doi.org/10.1002/dad2.12105.

RStudio Team. RStudio: integrated development environment for R. RStudio, PBC, Boston, MA. 2022. https://www.rstudio.com/.

Sabbagh MN, Chen K, Rogers J, et al. Florbetapir PET, FDG PET, and MRI in Down syndrome individuals with and without Alzheimer's dementia. *Alzheimers Dement*. 2015;11(8):994-1004. https://doi.org/10.1016/j.jalz.2015.01.006.

Sadowski M, Wisniewski HM, Tarnawski M, Kozlowski PB, Lach B, Wegiel J. Entorhinal cortex of aged subjects with Down's syndrome shows severe neuronal loss caused by neurofibrillary pathology. *Acta Neuropathol*. 1999;97(2):156-164. https://doi.org/10.1007/s004010050968.

Salami A, Wåhlin A, Kaboodvand N, Lundquist A, Nyberg L. Longitudinal evidence for dissociation of anterior and posterior MTL resting-state connectivity in aging: links to perfusion and memory. *Cereb Cortex*. 2016;26(10):3953-3963. https://doi.org/10.1093/cercor/bhw233.

Saxton J, McGonigle-Gibson KL, Swihart AA, Miller VJ, Boller F. Assessment of the severely impaired patient: description and validation of a new neuropsychological test battery. *Psychol Assess*. 1990;2(3):298-303. https://doi.org/10.1037/1040-3590.2.3.298.

Schmidt-Sidor B, Wisniewski KE, Shepard TH, Sersen EA. Brain growth in Down syndrome subjects 15 to 22 weeks of gestational age and birth to 60 months. *Clin Neuropathol*. 1990;9(4):181-190.

Sheehan R, Sinai A, Bass N, et al. Dementia diagnostic criteria in Down syndrome. *Int J Geriatr Psychiatry*. 2015;30(8):857-863. https://doi.org/10.1002/gps.4228.

Sirkis DW, Bonham LW, Johnson TP, La Joie R, Yokoyama JS. Dissecting the clinical heterogeneity of early-onset Alzheimer's disease. *Mol Psychiatry*. 2022;27(6):2674-2688. https://doi.org/10.1038/s41380-022-01531-9.

Snyder HM, Bain LJ, Brickman AM, et al. Further understanding the connection between Alzheimer's disease and Down syndrome. *Alzheimers Dement*. 2020;16(7):1065-1077. https://doi.org/10.1002/alz.12112.

Strydom A, Heslegrave A, Startin CM, et al. Neurofilament light as a blood biomarker for neurodegeneration in Down syndrome. *Alzheimers Res Ther*. 2018;10(1):39. https://doi.org/10.1186/s13195-018-0367-x.

Teipel SJ, Alexander GE, Schapiro MB, Möller HJ, Rapoport SI, Hampel H. Age-related cortical grey matter reductions in non-demented Down's syndrome adults determined by MRI with voxel-based morphometry. *Brain*. 2004;127(4):811-824. https://doi.org/10.1093/brain/awh101.

Teller JK, Russo C, DeBusk LM, et al. Presence of soluble amyloid beta-peptide precedes amyloid plaque formation in Down's syndrome. *Nat Med*. 1996;2(1):93-95. https://doi.org/10.1038/nm0196-93.

Thal DR, Rüb U, Orantes M, Braak H. Phases of A beta-deposition in the human brain and its relevance for the development of AD. *Neurology*. 2002;58(12):1791-1800. https://doi.org/10.1212/wnl.58.12.1791.

Thomas JB, Brier MR, Bateman RJ, et al. Functional connectivity in autosomal dominant and late-onset Alzheimer disease. *JAMA Neurol*. 2014;71(9):1111-1122. https://doi.org/10.1001/jamaneurol.2014.1654.

Tingley D, Yamamoto T, Hirose K, Keele L, Imai K. mediation: R package for causal mediation Analysis. *J Stat Softw*. 2014;59(5):1-38. https://doi.org/10.18637/jss.v059.i05.

Tudorascu DL, Anderson SJ, Minhas DS, et al. Comparison of longitudinal Aβ in nondemented elderly and Down syndrome. *Neurobiol Aging*. 2019;73:171-176. https://doi.org/10.1016/j.neurobiolaging.2018.09.030.

Van Dijk KR, Hedden T, Venkataraman A, Evans KC, Lazar SW, Buckner RL. Intrinsic functional connectivity as a tool for human connectomics: theory, properties, and optimization. *J Neurophysiol*. 2010;103(1):297-321. https://doi.org/10.1152/jn.00783.2009.

Vega JN, Hohman TJ, Pryweller JR, Dykens EM, Thornton-Wells TA. Resting-state functional connectivity in individuals with Down syndrome and Williams syndrome compared with typically developing controls. *Brain Connect*. 2015;5(8):461-475. https://doi.org/10.1089/brain.2014.0266.

Walsh DM, Finwall J, Touchette PE, et al. Rapid assessment of severe cognitive impairment in individuals with developmental disabilities. *J Intellect Disabil Res*. 2007;51(2):91-100. https://doi.org/10.1111/j.1365-2788.2006.00853.x.

Whitfield-Gabrieli S, Ford JM. Default mode network activity and connectivity in psychopathology. *Annu Rev Clin Psychol*. 2012;8:49-76. https://doi.org/10.1146/annurev-clinpsy-032511-143049.

Whitfield-Gabrieli S, Nieto-Castanon A. Conn: a functional connectivity toolbox for correlated and anticorrelated brain networks. *Brain Connect*. 2012;2(3):125-141. https://doi.org/10.1089/brain.2012.0073.

Wilson LR, Vatansever D, Annus T, et al. Differential effects of Down's syndrome and Alzheimer's neuropathology on default mode connectivity. *Hum Brain Mapp*. 2019;40(15):4551-4563. https://doi.org/10.1002/hbm.24720.

Wisch JK, Gordon BA, Boerwinkle AH, et al. Predicting continuous amyloid PET values with CSF and plasma Aβ42/Aβ40. *Alzheimers Dement (Amst)*. 2023;15(1):e12405. https://doi.org/10.1002/dad2.12405.

Wiseman FK, Al-Janabi T, Hardy J, et al. A genetic cause of Alzheimer disease: mechanistic insights from Down syndrome. *Nat Rev Neurosci*. 2015;16(9):564-574. https://doi.org/10.1038/nrn3983.

Wisniewski KE, Schmidt-Sidor B. Postnatal delay of myelin formation in brains from Down syndrome infants and children. *Clin Neuropathol*. 1989;8(2):55-62.

Wisniewski KE, Wisniewski HM, Wen GY. Occurrence of neuropathological changes and dementia of Alzheimer's disease in Down's syndrome. *Ann Neurol*. 1985;17(3):278-282. https://doi.org/10.1002/ana.410170310.

Wojtowicz M, Mazerolle EL, Bhan V, Fisk JD. Altered functional connectivity and performance variability in relapsing–remitting multiple sclerosis. *Mult Scler*. 2014;20(11):1453-1463. https://doi.org/10.1177/1352458514524997.

Xu X, Yuan H, Lei X. Activation and connectivity within the default mode network contribute independently to future-oriented thought. *Sci Rep*. 2016;6:21001. https://doi.org/10.1038/srep21001.

Yassa MA, Mattfeld AT, Stark SM, Stark CEL. Age-related memory deficits linked to circuit-specific disruptions in the hippocampus. *Pro Nat Acad Sci U S A*. 2011;108(21):8873. https://doi.org/10.1073/pnas.1101567108.

Yassa MA, Stark SM, Bakker A, Albert MS, Gallagher M, Stark CEL. High-resolution structural and functional MRI of hippocampal CA3 and dentate gyrus in patients with amnestic mild cognitive impairment. *Neuroimage*. 2010;51(3):1242. https://doi.org/10.1016/j.neuroimage.2010.03.040.

Zammit MD, Tudorascu DL, Laymon CM, et al. PET measurement of longitudinal amyloid load identifies the earliest stages of amyloid-beta accumulation during Alzheimer's disease progression in Down syndrome. *Neuroimage*. 2021;228:117728. https://doi.org/10.1016/j.neuroimage.2021.117728.

APPENDIX A: SUPPLEMENTARY MATERIAL FOR CHAPTER 2

SUPPLEMENTARY METHODS

Assessments used to determine MCI/AD clinical status

The standard assessment battery included a detailed review of medical records, informant interviews focused on functional and vocational abilities as well as neuropsychiatric concerns, direct assessment of a variety of cognitive abilities, maladaptive behaviors and neuropsychiatric symptoms, and general health status. The following neuropsychological assessments were evaluated during consensus diagnosis: a modified version of the Mini-Mental State Examination for people with Down syndrome (Folstein et al., 1975; Wisniewski and Hill, 1985), the Down Syndrome Mental Status Examination (DSMSE) (Haxby, 1985), the Test for Severe Impairment (Albert and Cohen, 1992), a modified version of the Selective Reminding Test (Buschke, 1973; Krinsky-McHale et al., 2002), the McCarthy Verbal Fluency Test (McCarthy, 1972), the Block Design subtest from the Wechsler Intelligence Scale for Children (Weschler, 1974) supplemented with less complex items from the DSMSE, and the Beery Buktenica Developmental Test of Visual-Motor Integration (Beery and Buktenica, 1989).

Differential diagnosis

In rare cases judged to be at the border of diagnosis categories, a rating was made based upon the majority opinion of the consensus conference group. Further, for any participant who was rated as having possible or definite dementia, findings were expanded to establish a provisional differential diagnosis. These were either AD, AD in combination with possible other pathology, or dementia due to uncertain causes (Heller et al., 2018). All participants with possible or definite dementia who were included in the present study were given a diagnosis of AD without any additional contributing pathology or uncertain causes.

Spatial normalization and registration procedure

To propagate a weighted consensus labeling from the expertly labeled atlas set to the unlabeled T1-weighted images of our study cohort, the atlas set was spatially normalized to the unlabeled participant using the Advanced Normalization Tools package (Avants et al., 2011). The joint label fusion technique (Wang et al., 2013) was used for consensus-based labeling. First, the intra-participant atlas T1/T2 rigid transforms were calculated. To minimize the total number of deformable registrations, a “pseudo-geodesic” approach to align the data was used (Tustison and Avants, 2013). This required construction of an optimal T1-weighted template (Avants et al., 2010) representing the average shape/intensity information of the T1 component of the atlas set. Deformable transformations between each T1-weighted image of the study cohort and the T1 atlas template were calculated. Transformation between the atlas labels and unlabeled study cohort image was then computed by concatenating the T1 atlas/T2 atlas rigid transformation, the T1 atlas/T1 template deformable transformation, and the T1 template/T1 participant deformable transforms. Once the atlas set was normalized to the unlabeled participant, regional labeling was determined using weighted averaging where the weighting takes into account the unique intensity information contributed by each atlas member. This protocol is illustrated in Tustison et al. (2021, Figure 2).

Visual quality assessment

An initial visual quality assessment (QA) of the unprocessed T1-weighted MRI images was performed to exclude scans with indicators of motion such as ringing and low contrast. Next the MRI Quality Control tool (Esteban et al., 2017) was used to calculate the signal-to-noise ratio (SNR) for each remaining image. Following image processing, a second visual QA was performed to exclude participants with errors in atlas registration or region-of-interest segmentation. Usually the latter visual QA corresponded with the SNR of a given image (i.e.,

low visual quality and low SNR), but on occasions when it did not (i.e., low visual quality and high SNR), the decision to exclude was made based on the visual QA.

SUPPLEMENTARY RESULTS

Results using log-transformed plasma NfL

There were non-normal distributions for TRS (W=0.801, p<0.0001), right pmEC thickness (W=0.969, p=0.0185), and plasma NfL (W=0.718, p<0.0001). Right pmEC thickness was transformed using log(2-x) (W=0.983, p=0.2154). Transformed right pmEC thickness showed no differences between any of the MCI/AD clinical status groups (all p-values >0.1), no partial correlation with plasma NfL (p>0.2), and no partial correlation with either FRS or TRS (all p-values >0.3).

Plasma NfL was transformed using log(x) (W=0.983, p=0.3034). Transformed plasma NfL was greater in the DEM group compared with the MCI-DS (t(78)=-3.300, p=0.0015, effect size=-1.347) and CS groups (t(78)=-4.629, p<0.0001, effect size=-1.594), was not different in the MCI-DS group compared with the CS group (t(78)=-0.815, p=0.4173, effect size=-0.247), was negatively associated with bilateral hippocampus volume (left: r=-0.446, p<0.0001; right: r=-0.467, p<0.0001) and left alEC thickness (r=-0.332, p=0.0044) but not right alEC thickness (r=-0.129, p=0.2441) or bilateral pmEC thickness (left: r=-0.120, p=0.5570; right: r=-0.067, p=0.5570), and was negatively associated with FRS (r=-0.408, p=0.0003) and TRS (r=-0.398, p=0.0004).

Using the transformed plasma NfL variable did not meaningfully impact the results of the mediation analysis. There was an indirect effect of transformed plasma NfL on the relationship between left alEC thickness and FRS (ab=8.305, 95% CI=[1.625,19.58], p=0.032). After adjusting for transformed plasma NfL, the direct effect of left alEC thickness on FRS was not

significant (*c'*=4.156, 95% CI=[-10.274,18.64], *p*=0.580). Transformed plasma NfL mediated 67% of the relationship between left alEC thickness and FRS.

When the reverse mediation was run, with left alEC thickness as the mediator between transformed plasma NfL and FRS, there was no indirect effect of left alEC thickness on the relationship between transformed plasma NfL and FRS (*ab*=-0.00845, 95% CI=[-0.04484,0.02], *p*=0.6), with left alEC thickness mediating only 3% of the relationship between transformed plasma NfL and FRS.

Transformed plasma NfL partially mediated the relationship between left (*ab*=35.325, 95% CI=[10.539,65.61], *p*=0.008; *c'*=60.249, 95% CI=[5.208,109.09], *p*=0.030) and right hippocampus volume (*ab*=32.699, 95% CI=[10.603,57.58], *p*<0.0001; *c'*=56.449, 95% CI=[6.993,99.90], *p*=0.026) on FRS, but left (*ab*=-0.0724, 95% CI=[-0.2084,-0.02], *p*=0.034; *c'*=-0.1917, 95% CI=[-0.3240,0.07], *p*=0.006) and right hippocampus volume (*ab*=-0.0754, 95% CI=[-0.1603,-0.02], *p*=0.008; *c'*=-0.1887, 95% CI=[-0.3239,0.09], *p*<0.0001) also partially mediated the relationship between plasma NfL and FRS.

Relationships with age and results using models without age as a covariate

In our sample, the MCI/AD clinical status groups differ in age ($F(2,98)=9.786$, $p=0.0001$). A post-hoc Tukey test indicated that the dementia group was older than the CS group ($p=0.0002$), while the age of the MCI-DS group was trending but not significantly different than that of the other two groups, falling in between them ($0.05<p<0.15$). Age is strongly correlated with bilateral hippocampus volume (left: $r=-0.567$, $p<0.0001$; right: $r=-0.504$, $p<0.0001$), plasma NfL ($r=-0.371$, $p=0.0004$), and memory (FRS: $r=-0.349$, $p=0.0006$; TRS: $r=-0.348$, $p=0.0007$) but not bilateral alEC (left: $r=-0.033$, $p=0.7421$; right: $r=-0.045$, $p=0.6571$) or pmEC thickness (left: $r=-$

0.076, p=0.4525; right: r=-0.095, p=0.3444). These relationships remain when we restrict the sample to only CS individuals.

After removing age as a covariate, there was no change in MCI/AD clinical status group differences for plasma NfL or any MRI measure except bilateral hippocampus volume. Previously no difference was observed between the CS and MCI-DS groups, but without age as a covariate, left and right hippocampus volume were each trending but not significantly lower in the MCI-DS group compared with the CS group (left: t(94)=1.704, p=0.0916, effect size=0.445; right: t(94)=1.773, p=0.0796, effect size=0.463). This is likely due to the strong association between hippocampus volume and age and the older age of the MCI-DS group.

Additionally there was no change in partial correlations between plasma NfL and MRI measures except for right alEC thickness, which was now significantly correlated with plasma NfL (r=-0.226, p=0.0384). There was no change in partial correlations between memory and plasma NfL or memory and MRI measures except FRS and bilateral alEC thickness. Previously left and right alEC thickness had a trending association with FRS, but without age as a covariate the partial correlations were not significant (left: r=0.188, p=0.1490; right: r=0.189, p=0.1490).

Removing age as a covariate did not meaningfully impact the results of the mediation analysis. There was an indirect effect of plasma NfL on the relationship between left alEC thickness and FRS (ab=8.305, 95% CI=[1.625,19.58], p=0.032). After adjusting for plasma NfL, the direct effect of left alEC thickness on FRS was not significant (c'=4.156, 95% CI=[-10.274,18.64], p=0.580). Plasma NfL mediated 67% of the relationship between left alEC thickness and FRS.

When the reverse mediation was run, with left alEC thickness as the mediator between plasma NfL and FRS, there was no indirect effect of left alEC thickness on the relationship between

plasma NfL and FRS (*ab*=-0.00845, 95% CI=[-0.04484,0.02], *p*=0.6), with left alEC thickness mediating only 3% of the relationship between plasma NfL and FRS.

Plasma NfL partially mediated the relationship between left (*ab*=35.325, 95% CI=[10.539,65.61], *p*=0.008; *c'*=60.249, 95% CI=[5.208,109.09], *p*=0.030) and right hippocampus volume (*ab*=32.699, 95% CI=[10.603,57.58], *p*<0.0001; *c'*=56.449, 95% CI=[6.993,99.90], *p*=0.026) on FRS, but left (*ab*=-0.0724, 95% CI=[-0.2084,-0.02], *p*=0.034; *c'*= 0.1917, 95% CI=[-0.3240,0.07], *p*=0.006) and right hippocampus volume (*ab*=-0.0754, 95% CI=[-0.1603,-0.02], *p*=0.008; *c'*=-0.1887, 95% CI=[-0.3239,0.09], *p*<0.0001) also partially mediated the relationship between plasma NfL and FRS. These results are highly similar to the models that included age as a covariate.

Supplementary References

Albert M, Cohen C. The Test for Severe Impairment: an instrument for the assessment of patients with severe cognitive dysfunction. *J Am Geriatr Soc*. 1992;40(5):449-453. https://doi.org/10.1111/j.1532-5415.1992.tb02009.x.

Avants BB, Tustison NJ, Song G, Cook PA, Klein A, Gee JC. A reproducible evaluation of ANTs similarity metric performance in brain image registration. *Neuroimage*. 2011;54:2033. https://doi.org/10.1016/j.neuroimage.2010.09.025.

Avants BB, Yushkevich P, Pluta J, et al. The optimal template effect in hippocampus studies of diseased populations. *Neuroimage*. 2010;49:2457. https://doi.org/10.1016/j.neuroimage.2009.09.062.

Beery KE, Buktenica NA. *Developmental Test of Visual-Motor Integration*. Cleveland: Modern Curriculum Press; 1989.

Buschke H. Selective reminding for analysis of memory and learning. *J Verbal Learning Verbal Behav*. 1973;12(5):534-550.

Esteban O, Birman D, Schaer M, Koyejo OO, Poldrack RA, Gorgolewski KJ. MRIQC: advancing the automatic prediction of image quality in MRI from unseen sites. *PLoS One*. 2017;12(9):e0184661. https://doi.org/10.1371/journal.pone.0184661.

Folstein MF, Folstein SE, McHugh PR. Mini-mental state, a practical method for grading the cognitive state of patients for the clinician. *J Psychiatr Res*. 1975;12(3):189-198.

Haxby JV. Neuropsychological evaluation of adults with Down's syndrome: patterns of selective impairment in non-demented old adults. *J Intellect Disabil Res*. 1989;33(3):193-210. https://doi.org/10.1111/j.1365-2788.1989.tb01467.x.

Heller T, Scott HM, Janicki MP; Pre-Summit Workgroup on Caregiving and Intellectual/Developmental Disabilities. Caregiving, intellectual disability, and dementia: report of the Summit Workgroup on Caregiving and Intellectual and Developmental Disabilities. *Alzheimers Dement (N Y)*. 2018;4:272-282. https://doi.org/10.1016/j.trci.2018.06.002.

Krinsky-McHale S, Devenny D, Silverman W. Changes in explicit memory associated with early dementia in adults with Down's syndrome. *J Intellect Disabil Res*. 2002;46(3):198-208. https://doi.org/10.1046/j.1365-2788.2002.00365.x.

McCarthy DA. *Scales of Children's Abilities*. San Antonio: Psychological Corp; 1972.

Tustison NJ, Avants BB. Explicit B-spline regularization in diffeomorphic image registration. *Front Neuroinform*. 2013;7:39. https://doi.org/10.3389/fninf.2013.00039.

Tustison NJ, Cook PA, Holbrook AJ, et al. The ANTsX ecosystem for quantitative biological and medical imaging. *Sci Rep*. 2021;11:9068. https://doi.org/10.1038/s41598-021-87564-6.

Wang H, Suh JW, Das SR, Pluta JB, Craige C, Yushkevich PA. Multi-atlas segmentation with joint label fusion. *IEEE Trans Pattern Anal Mach Intell*. 2013;35:611-623. https://doi.org/10.1109/TPAMI.2012.143.

Wechsler D. *Wechsler Intelligence Scale for Children-Revised*. New York: Psychological Corp; 1974.

Wisniewski KE, Hill AL. Clinical aspects of dementia in mental retardation and developmental disabilities. In: Wisniewski H, Janicki M, eds. *Aging and Developmental Disabilities: Issues and Approaches*. Baltimore, USA: Brookes; 1985:195-210.

SUPPLEMENTARY FIGURES

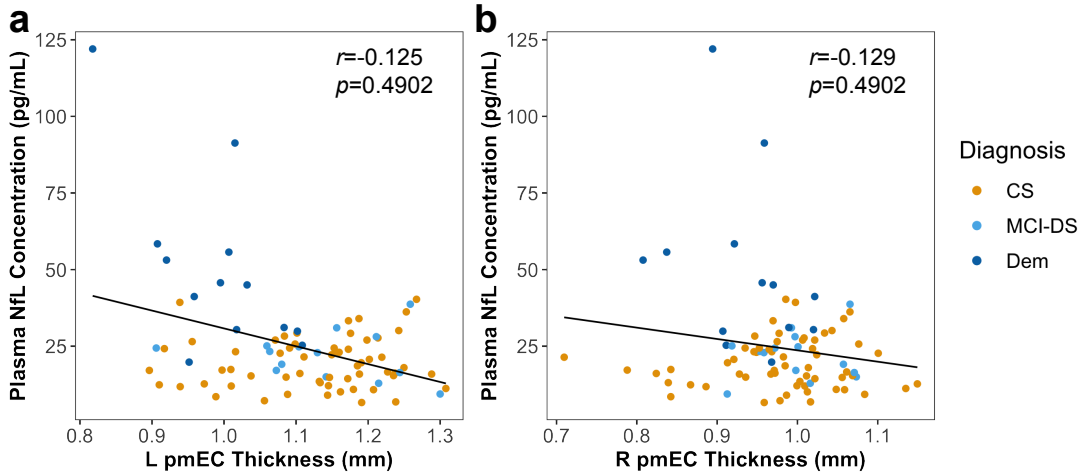

Supplementary Figure A1. Plasma NfL concentration was not associated with bilateral pmEC thickness. The plots include the two outliers with high plasma NfL concentration since their exclusion did not meaningfully alter the results.

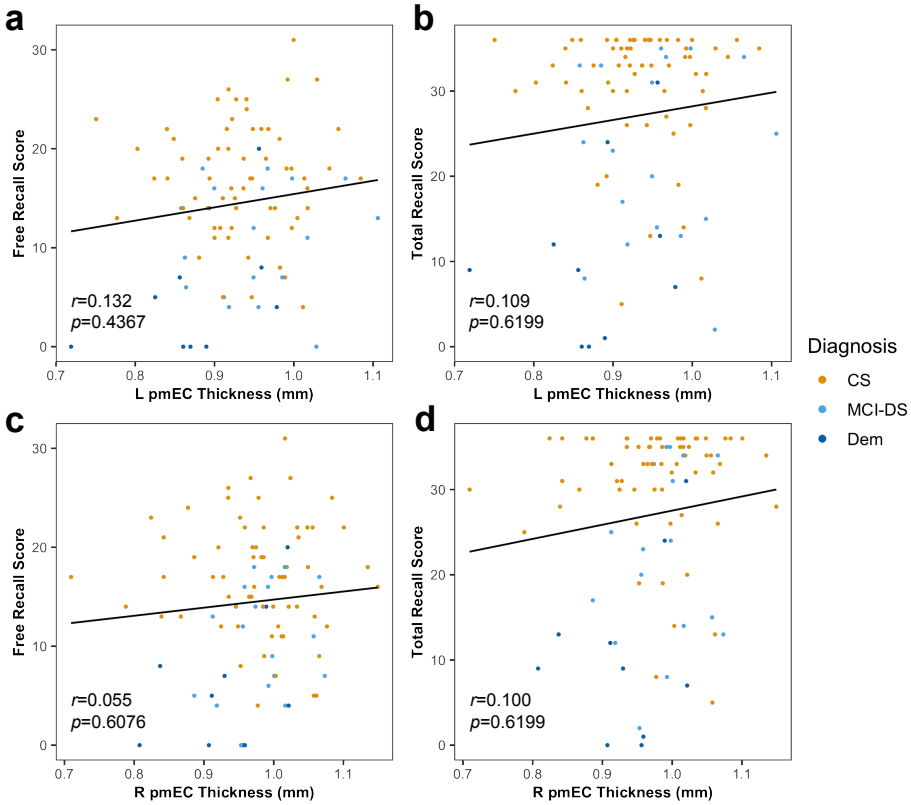

Supplementary Figure A2. Bilateral pmEC thickness was not associated with FRS or TRS.

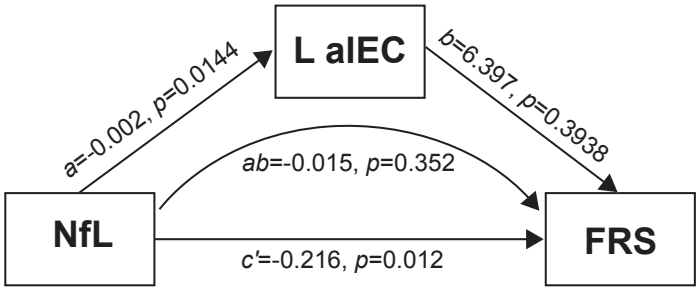

Supplementary Figure A3. Left alEC thickness did not mediate the relationship between plasma NfL concentration and FRS. The indirect effect of left alEC thickness on the relationship between plasma NfL and FRS, represented by *ab*, was not significant. The direct effect of plasma NfL on FRS, represented by *c'*, was significant even after accounting for left alEC thickness.

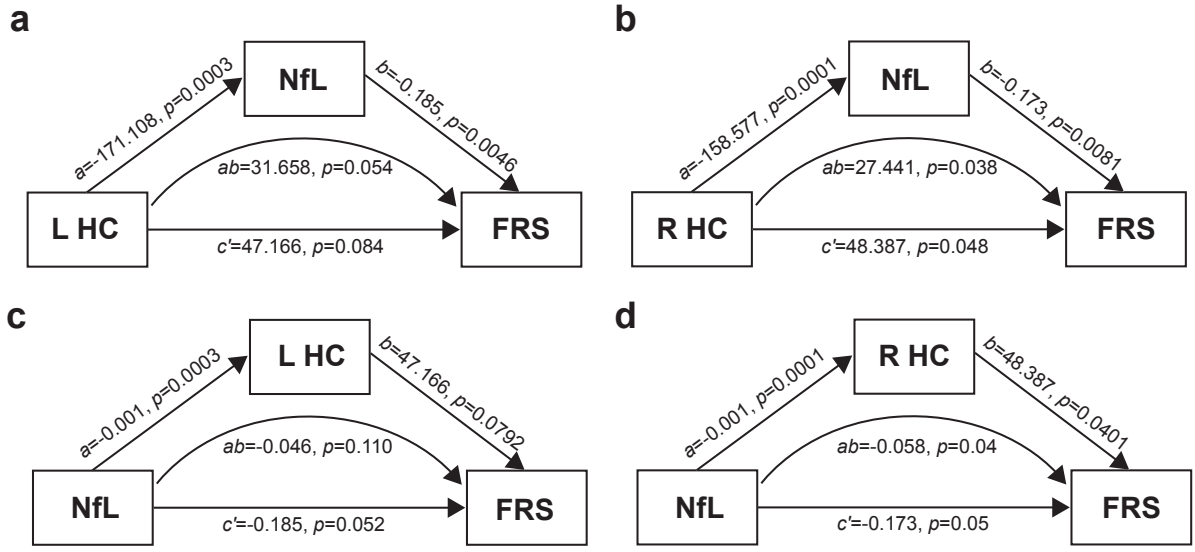

Supplementary Figure A4. (a,b) Plasma NfL partially mediated the relationship between left and right hippocampus volume/ICV percentage and FRS. (c,d) Additionally left and right hippocampus volume/ICV percentage partially mediated the relationship between plasma NfL and FRS.

SUPPLEMENTARY TABLES

Supplementary Table A1. Participant demographics for individuals with MRI data

Variable	CS	MCI-DS	DEM	Test Statistic (*F* value or χ^2)	Group Differences
n	68	19	14	n/a	n/a
Age (mean ± SD)	48.7 ± 5.8	51.9 ± 5.1	56.1 ± 7.6	9.8	B
Sex, female (%)	25 (36.8%)	5 (26.3%)	6 (42.9%)	1.1	n.s.

Significant pairwise group differences, $p<0.05$: A: CS vs. MCI-DS; B: CS vs. DEM; C: MCI-DS vs. DEM.

Supplementary Table A2. Participant demographics for individuals with MRI and plasma NfL data

Variable	CS	MCI-DS	DEM	Test Statistic (*F* value or χ^2)	Group Differences
n	59	14	13	n/a	n/a
Age (mean ± SD)	48.7 ± 5.5	51.0 ± 3.8	55.2 ± 7.2	7.5	B
Sex, female (%)	21 (35.6%)	4 (28.6%)	6 (46.2%)	1.0	n.s.

Significant pairwise group differences, $p<0.05$: A: CS vs. MCI-DS; B: CS vs. DEM; C: MCI-DS vs. DEM.

Supplementary Table A3. Participant demographics and neuropsychological assessments for individuals with MRI, plasma NfL, and mCRT data

Variable	CS	MCI-DS	DEM	Test Statistic (*F* value or χ^2)	Group Differences
n	55	13	9	n/a	n/a
Age (mean ± SD)	48.7 ± 5.5	51.2 ± 3.8	53.6 ± 6.5	3.8	B
Sex, female (%)	20 (36.4%)	4 (30.8%)	5 (55.6%)	1.5	n.s.
mCRT FRS	16.5 ± 5.9	11.0 ± 6.0	5.7 ± 7.2	14.7	AB
mCRT TRS	30.4 ± 7.3	22.2 ± 11.2	10.8 ± 10.8	23.0	ABC

Significant pairwise group differences, $p<0.05$: A: CS vs. MCI-DS; B: CS vs. DEM; C: MCI-DS vs. DEM.

APPENDIX B: SUPPLEMENTARY MATERIAL FOR CHAPTER 3

SUPPLEMENTARY FIGURES

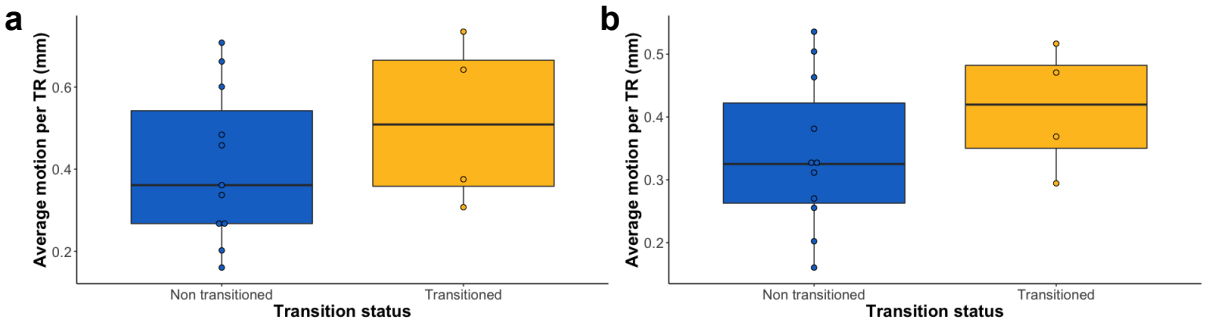

Supplementary Figure B1. Motion censoring in UCI cohort. a) No group difference in motion before motion censoring. b) No group difference in motion after motion censoring.

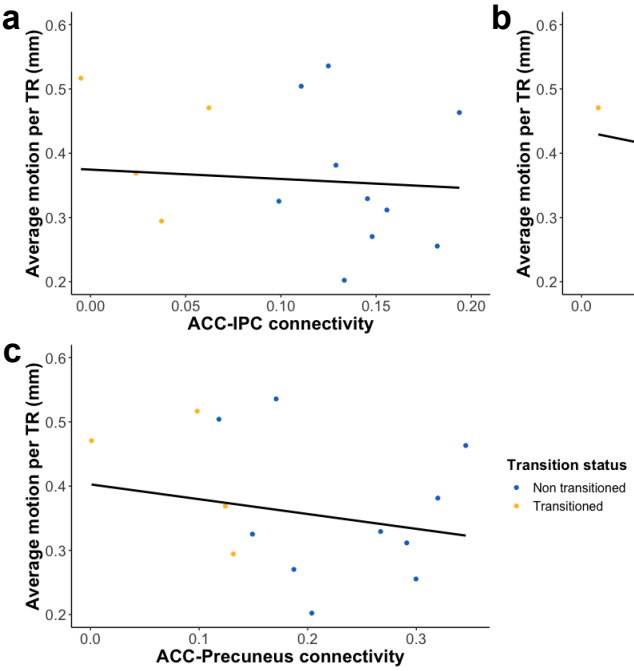

Supplementary Figure B2. Motion was not associated with long-range functional connectivity in ACC-IPC, ACC-ICC, or ACC-Precuneus in UCI cohort

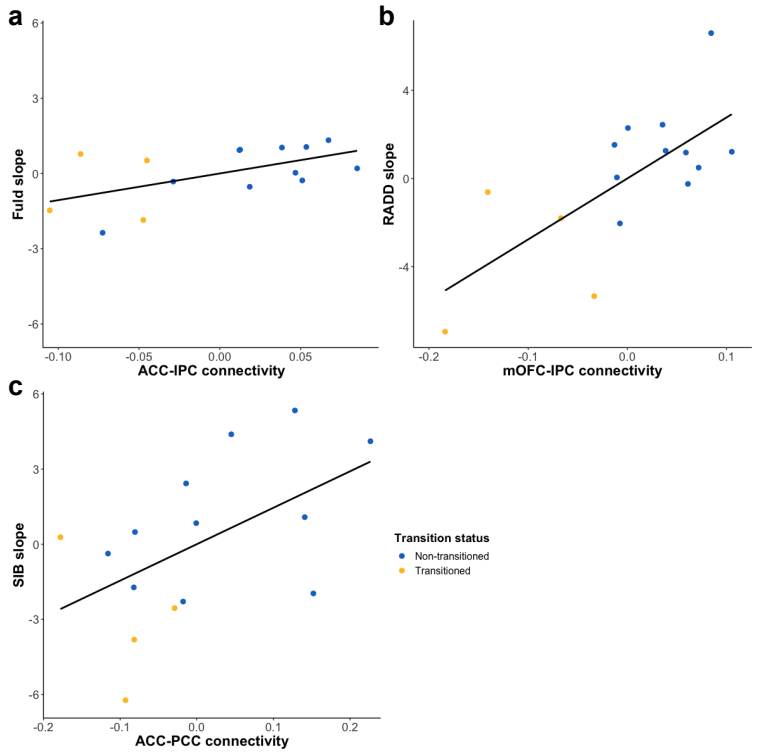

Supplementary Figure B3. Significant positive association between long-range functional connectivity and rate of change of cognitive performance in UCI cohort

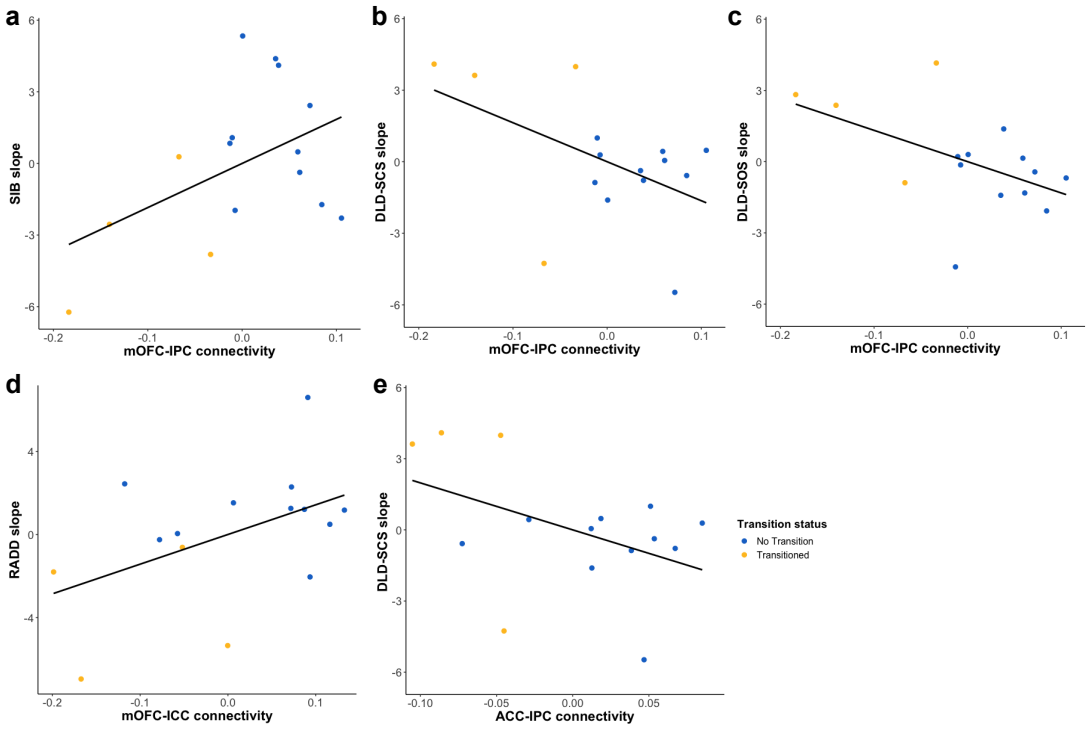

Supplementary Figure B4. Trending positive association between long-range functional connectivity and rate of change of cognitive performance in UCI cohort. Higher scores on DLD-SCS and DLD-SOS indicate worse performance.

SUPPLEMENTARY TABLES

Supplementary Table B1. Group differences in pairwise functional connectivity between UCI transitioned and non-transitioned groups

ROI Pair	*t*	Uncorrected *p*-value	FDR corrected *p*-value
ACC-IPC	5.1847	0.0006	**0.0085****
ACC-ICC	5.4292	0.0012	**0.0092****
ACC-Precuneus	3.4535	0.0095	**0.0474***
mOFC-IPC	3.7723	0.0157	0.0590
ACC-PCC	2.6518	0.0292	0.0876
mOFC-ICC	2.7244	0.0409	0.1025
mOFC-Precuneus	2.5027	0.0582	0.1247
mOFC-PCC	1.7712	0.1093	0.2049
PCC-IPC	1.5975	0.1796	0.2994
PCC-ICC	1.2383	0.2692	0.4038
Precuneus-IPC	1.0428	0.3617	0.4289
mOFC-ACC	0.9184	0.3758	0.4289
ICC-IPC	0.9841	0.3887	0.4289
PCC-Precuneus	0.9009	0.4008	0.4289
ICC-Precuneus	0.8731	0.4289	0.4289

Supplementary Table B2. Group differences in pairwise functional connectivity between UCI transitioned and UCI non-transitioned groups after removing participant who transitioned to dementia prior to MRI

ROI Pair	*t*	Uncorrected *p*-value	FDR corrected *p*-value
ACC-ICC	6.5180	0.0011	**0.0168***
mOFC-IPC	5.1561	0.0097	0.0513
ACC-IPC	4.3766	0.0103	0.0513
mOFC-ICC	3.8053	0.0195	0.0641
mOFC-PCC	2.7294	0.0213	0.0641
ACC-Precuneus	3.1367	0.0291	0.0727

Supplementary Table B3. Greater functional connectivity between PCC-IPC is associated with worse performance on the DLD-SOS at baseline in UCI cohort

ROI Pair	Neuropsychological Test	*r*	*F*	*p*-value
ACC-IPC	RADD	-0.005435558	0.0003841	0.9847
	SIB	0.01200671	0.001874	0.9661
	FOME	0.184822	0.4598	0.5096
	DLD-SCS	0.07164784	0.06708	0.7997
	DLD-SOS	0.1721542	0.397	0.5395
ACC-ICC	RADD	-0.06848571	0.06126	0.8084
	SIB	0.03512807	0.01606	0.9011
	FOME	0.05374908	0.03767	0.8491
	DLD-SCS	-0.0351488	0.01608	0.901
	DLD-SOS	0.1435219	0.2734	0.6098
ACC-Precuneus	RADD	-0.09094888	0.1084	0.7472
	SIB	0.01039248	0.001404	0.9707
	FOME	-0.04649438	0.02816	0.8693
	DLD-SCS	0.02001068	0.005208	0.9436
	DLD-SOS	0.1285445	0.2184	0.648
ACC-PCC	RADD	0.1636834	0.3579	0.56
	SIB	0.2171025	0.643	0.437
	FOME	-0.03067817	0.01225	0.9136
	DLD-SCS	-0.1893261	0.4833	0.4992
	DLD-SOS	0.03747875	0.01829	0.8945
mOFC-IPC	RADD	-0.179561	0.4331	0.522
	SIB	0.04291113	0.02398	0.8793
	FOME	0.1809958	0.4403	0.5186
	DLD-SCS	-0.05424792	0.03837	0.8477
	DLD-SOS	-0.07710939	0.07776	0.7847
mOFC-ICC	RADD	-0.04125716	0.02217	0.8839
	SIB	0.1735701	0.4038	0.5362
	FOME	0.2164332	0.6389	0.4385
	DLD-SCS	-0.1790759	0.4307	0.5231
	DLD-SOS	-0.2826877	1.129	0.3073
mOFC-Precuneus	RADD	-0.1576951	0.3315	0.5746
	SIB	0.05563327	0.04036	0.8439
	FOME	0.1005651	0.1328	0.7214
	DLD-SCS	-0.1064821	0.1491	0.7057
	DLD-SOS	-0.325927	1.545	0.2358
mOFC-PCC	RADD	0.1481049	0.2916	0.5984
	SIB	0.2255689	0.6969	0.4189
	FOME	0.09451324	0.1172	0.7376
	DLD-SCS	-0.1069902	0.1505	0.7043
	DLD-SOS	-0.09411833	0.1162	0.7387
PCC-IPC	RADD	-0.1104726	0.1606	0.6951
	SIB	-0.1316824	0.2294	0.6399
	FOME	-0.0280263	0.01022	0.921
	DLD-SCS	0.2591012	0.9355	0.3511
	DLD-SOS	0.5812183	6.632	**0.02306**
PCC-ICC	RADD	-0.1112807	0.163	0.693
	SIB	-0.1046966	0.1441	0.7104
	FOME	-0.2311933	0.7341	0.4071
	DLD-SCS	0.2633126	0.9685	0.343
	DLD-SOS	0.4944661	4.207	0.06097
Precuneus-IPC	RADD	0.09536509	0.1193	0.7353
	SIB	0.2166727	0.6404	0.438
	FOME	0.1000356	0.1314	0.7228
	DLD-SCS	-0.08428274	0.09301	0.7652
	DLD-SOS	0.308985	1.372	0.2625
mOFC-ACC	RADD	0.04283453	0.0239	0.8795
	SIB	0.02260957	0.006649	0.9363
	FOME	0.05593903	0.04081	0.843
	DLD-SCS	0.05266173	0.03615	0.8521
	DLD-SOS	-0.003051109	0.000121	0.9914
ICC-IPC	RADD	0.03901004	0.01981	0.8902
	SIB	0.1181766	0.1841	0.6749
	FOME	0.1046227	0.1439	0.7106
	DLD-SCS	-0.002777526	0.0001003	0.9922
	DLD-SOS	0.3356347	1.65	0.2213
PCC-Precuneus	RADD	0.04141699	0.02234	0.8835
	SIB	0.05268246	0.03618	0.8521
	FOME	-0.1290501	0.2202	0.6467
	DLD-SCS	0.1481463	0.2917	0.5983
	DLD-SOS	0.445172	3.213	0.09634
ICC-Precuneus	RADD	-0.04156134	0.02249	0.8831
	SIB	0.0315034	0.01291	0.9113
	FOME	-0.01865121	0.004524	0.9474
	DLD-SCS	0.1618578	0.3497	0.5644
	DLD-SOS	0.4860982	4.022	0.06618

Supplementary Table B4. Regional SUVR averages for UCI transitioned and non-transitioned groups

ROI	Group	Average SUVR
mOFC	Transitioned	1.5755
	Non-transitioned	1.2973
ACC	Transitioned	1.6771
	Non-transitioned	1.49
ICC	Transitioned	1.4348
	Non-transitioned	1.5445
PCC	Transitioned	1.8929
	Non-transitioned	1.4192
Precuneus	Transitioned	1.5401
	Non-transitioned	1.3337
IPC	Transitioned	1.2938
	Non-transitioned	1.0616

Supplementary Table B5. Percentile rank of pairwise functional connectivity for UCI participants relative to UKY cohort

Participant	Group	Percentile rank of average functional connectivity for all long-range ROI pairs (%)	Percentile rank of average functional connectivity for all short-range ROI pairs (%)
1	Transitioned	0	7.14
2	Transitioned	0	0
3	Transitioned	0	64.29
4	Transitioned	0	50.00
5	Non-transitioned	21.43	64.29
6	Non-transitioned	0	7.14
7	Non-transitioned	50.00	42.86
8	Non-transitioned	28.57	42.86
9	Non-transitioned	7.14	0
10	Non-transitioned	21.43	71.43
11	Non-transitioned	42.86	71.43
12	Non-transitioned	42.86	71.43
13	Non-transitioned	50.00	71.43
14	Non-transitioned	50.00	64.29
15	Non-transitioned	7.14	7.14

The following are all eight long-range ROI pairs: ACC-IPC, ACC-ICC, ACC-Precuneus, ACC-PCC, mOFC-IPC, mOFC-ICC, mOFC-Precuneus, and mOFC-PCC. The following are all seven short-range ROI pairs: mOFC-ACC, PCC-ICC, PCC-Precuneus, PCC-IPC, ICC-Precuneus, ICC-IPC, and Precuneus-IPC.

Supplementary Table B6. Summary measures of percentile rank of pairwise functional connectivity for UCI transitioned and non-transitioned groups relative to UKY cohort

ROI pairs	Group	Min	1st Q	Median	Mean	3rd Q	Max
All long-range ROI pairs	Transitioned	0	0	0	0	0	0
	Non-transitioned	0	14.29	28.57	29.22	46.43	50.00
All short-range ROI pairs	Transitioned	0	5.36	28.57	30.36	53.57	64.29
	Non-transitioned	0	25.00	64.29	46.75	71.43	71.43

The following are all eight long-range ROI pairs: ACC-IPC, ACC-ICC, ACC-Precuneus, ACC-PCC, mOFC-IPC, mOFC-ICC, mOFC-Precuneus, and mOFC-PCC. The following are all seven short-range ROI pairs: mOFC-ACC, PCC-ICC, PCC-Precuneus, PCC-IPC, ICC-Precuneus, ICC-IPC, and Precuneus-IPC.